UNIVERSITY OF OKLAHOMA

GRADUATE COLLEGE

GEOSPATIAL MODELING OF SURFACE WATER TRENDS USING TIME SERIES AND IMAGE OBSERVATION ANALYSIS

A DISSERTATION

SUBMITTED TO THE GRADUATE FACULTY

in partial fulfillment of the requirements for the

Degree of

DOCTOR OF PHILOSOPHY

By

EMAD HASAN
Norman, Oklahoma
2017

GEOSPATIAL MODELING OF SURFACE WATER TRENDS USING TIME SERIES AND IMAGE OBSERVATION ANALYSIS

A DISSERTATION APPROVED FOR THE GRADUATE COLLEGE

BY

Dr. Yang Hong, Chair

Dr. Naiyu Wang

Dr. Xiangming Xiao

Dr. Aondover Tarhule

Dr. Sadiq Khan

Dedication

To my lovely wife Emy, to my babies Malek, Elleen, and Adam

Acknowledgements

I am grateful to God Almighty for providing the ability and the strength to conduct this research and finalize this dissertation. I feel this great blessing as lucid as I recite “And whatever of blessings and good things you have, it is from Allah” (Nahl, 16:53).

I thank many individuals whose academic knowledge and support allowed me to complete this work on my dissertation. First, I would like to express my deep appreciation and gratitude to my advisor *Dr. Yang Hong,* for his mentorship, instruction, and great support during this research. Despite Dr. Hong’s busy schedule, he always kept his door open providing an excellent scholarly input and feedback, which I am very grateful.
I am also thankful to *Dr. Aondover Tarhule*, who and despite his input, this dissertation would be incomplete. Dr. Tarhule was a great mentor and advisor who never turned away from me or locked down any advice. I learnt so much about Africa and the Nile Basin during many fruitful discussions with him. I believe he knew Africa like a small neighborhood. He is knowledgeable professor and his advices were a great help to me through this research.

My special thanks goes to *Dr. Sadiq Khan* who adjusted my way and helped me a lot to tackle and understand many science issues. I really appreciate his input during several stages of my research, he really embraced me with his advices and I am truly grateful to him so much.

I thank *Dr. Pierre Kirstetter* for providing an excellent scholarly and advise during this research. I was delighted, benefited and learnt a lot during my work with Dr. *Kirstetter*, his knowledge and constructive comments were great support to my work. I appreciate all the time and effort he provided me during my research.

Other special thanks goes to my friends *Dr. Humberto Vergara* and *Dr. Race Clark*, whose provide me with so impressive comments and advices through the time of my research. I appreciate *Dr. Vergara's* help in providing and running the hydrologic model. Moreover, Thanks to *Dr. Clark* for the proofreading and the prolific comments on different parts of my work.

Thanks to *Dr. Ke Zhang* for his guidance and assistance in the ET products and for providing very beneficial comments on my work.

Many thanks goes to *Dr. Valliappa Lakshmanan*, Dr. Lak was my great programming teacher. Without taking his geospatial programing class and his guidelines and discussions, I think I could still search between dropdown menus and toolboxes to execute one by one operation through single clicking, thanks to his effort and support that helped me to become so independent and able to deal professionally with my data sets.

I do thank *Mr. Mano Ratwatte*, my brilliant Java programming language instructor and teacher at the University of Oklahoma. My deep thanks and appreciation goes to him for the excellent learning opportunity he offered to me through his powerful Java programming course. He was a model teacher who introduced the programming logics in very smooth and easy way. I feel whatever I wrote I could not give him the right acknowledgement he really deserves, thanks to him so much.

My thanks go to the Institute for Study of Human Flourishing, University of Oklahoma, and to the Director *Dr. Nancy Snow,* for providing me with the research fund through a dissertation fellowship. I thank *Dr. Snow* so much for being so supportive, encouraging and planting the optimistic seeds that pushing me forward during my work at the institute. Additionally, many thanks to *Dr. Kyle Harper*, the University of

Oklahoma Senior Vice President and Provost, for making this dissertation fellowship possible, I appreciated *Dr. Harper's* support, effort, and his time allowing me to discuss my research.

I also thankful to the *Egyptian Mission sector, Ministry for higher education and scientific research, Egypt* for awarding me the initial PhD scholarship to conduct my research in USA. Thanks also goes to the Advanced Radar Research Center (ARRC), and the Hydrometrology and Remote Sensing Laboratory (HyDROS) lab at University of Oklahoma, for providing me with the research facilities, workspace and the research equipment to accomplish this work.

I would like to thank the data centers that made GRACE, remote sensing, model reanalysis, and land surface model data sets be available and downloadable. Thanks to NASA's GRACE tellus website for providing GRACE data. The Goddard Earth Science Data and Information Service Centers (GES DISCs) that made many satellite products free and accessible. Thanks to the Climatic Research Unit at the University of East Anglia, the National Oceanic and Atmospheric Administration, Global Precipitation Climatological Center, and the Global Runoff Data Centre for their reanalysis and gauge corrected products.

This "acknowledgements" would not be complete without a mention of my family. I would not have reached that point without their support and emotions that gave me the strength to finish this degree. Thanks to all of my family members for being so patient with me until finalized my dissertation.

Table of Contents

Acknowledgements iv

List of Tables xi

Abstract xvii

Chapter 1: Introduction and research outline 1

1.1 Problem statement 3

1.2. Research objectives 4

1.3 Research questions 5

1.2 Dissertation outline 5

1.3 List of publications from the dissertation 8

1.3 References 9

Chapter 2: Challenges and opportunities of hydrologic remote sensing for the Nile River Basin: A review 11

Abstract 11

2.1 Introduction 13

2.2 Challenges to the Nile River Basin 17

Hydrological challenges 17

Extreme events 21

Climate change 22

Population growth 23

Historical challenge 26

Data inaccessibility 27

2.3 Opportunities for hydrological remote sensing 29

Storage change ... 29

Precipitation ... 30

Evapotranspiration ... 32

Surface runoff ... 33

Vegetation Land cover ... 36

2.4 Storage Variability ... 38

2.5 Summary and perspectives ... 44

Acknowledgement ... 45

2.6 References ... 46

Chapter 3: Response of Nile river flow to the climate change ... 51

Abstract ... 51

3.1 Introduction ... 53

Water-energy balance and Budyko Curve ... 57

Objectives ... 59

3.2 Data sets and methodology ... 59

3.3 Nile Basin climates ... 65

3.4 Results and discussion ... 68

Trajectory under Budyko space ... 77

3.5 Summary and conclusion ... 79

Acknowledgement ... 81

3.6 References ... 82

Chapter 4: Investigation of potential sea level rise impact on the Nile ... 86

Delta, Egypt using digital elevation models ... 86

Abstract 86
4.1 Introduction 88
4.2. Study Area 93
4.3. Data and Methodology 93
DEM's Elevation Errors 95
SLR Analysis 97
4.4 Results and Discussion 101
SRTM-based SLR 105
ASTER-GDEM-based SLR 106
4.5 Conclusion 112
Acknowledgements 114
4.6 References 115
Chapter 5: Estimating the Terrestrial Water Storage with Multiscale Remote Sensing and Model Reanalysis in the Nile River Basin 121
Abstract 121
5.1 Introduction 123
5.2 Materials and Datasets 129
Remote sensing data 129
Model reanalysis data 130
Gauged corrected data 132
5.3 Procedure and methodology 140
Data preparation 140
TWS statistical modeling 144

5.4 Result and discussion 145

NRB hydrological variability 145

Statistical model output 149

5.5 Hydroclimate risk assessment 154

5.6 Summary, Conclusion and Future Work 156

Acknowledgement 158

5.6 References 159

Chapter 6: Summary and Conclusion 175

List of Tables

Table 2.1 Summary of the GRDC gauging stations over the Nile Basin (Source: (GRDC, 2015) 34

Table 3.1 Summary of the mathematical forms 64

Table 3.2 Summary of the runoff elasticity in each climate zone across the Basin 77

Table 3.3 Percentage of changes in surface runoff to precipitation and temperature. 79

Table 4.1 Reclassification of IGBP MODIS Land Cover Type-1 classes. 100

Table 4.2 Statistical results of the two DEMs datasets 102

Table 4.3 The total areas (Km2) of projected land cover types vulnerable to SLR at 0.5m and 1m SLR scenarios using original DEM datasets 106

Table 4.4 The total areas (Km^2) of projected land cover types vulnerable to SLR at 0.5m and 1m SLR scenarios using corrected DEM datasets 107

Table 4.5 The percentage of vulnerable Land cover (LC) areas to 1m SLR scenarios using edited DEM datasets 108

Table 5.1 Statistical summary and correlations between TWS_{GRACE} and hydrological variables from multi-sensory and reanalysis data. 142

Table 5.2 Statistical summary of the modeled TWS anomalies using multi-sensory and reanalysis data. 150

List of Figures

Figure 2.1 Nile River Basin, location map and study area. 15

Figure 2.2 Comparison of the temporal variation in the Nile Basin precipitation over different climate zones, GPCC data for the period 1981-2013. 17

Figure 2.3 Gauge corrected ET estimates over different climate zones, data for the period 1982-2013. 19

Figure 2.4 Mean annual potential ET over the Nile River Basin, CRU data from 1982-2013 20

Figure 2.5 Total flooded days over riparian states, data for the period from 1989-2008. Source: (DFO, 2012) 22

Figure 2.6 Total population growth of the Nile Basin's state. Source: (WB, 2016) 24

Figure 2.7 Population density over the Nile Basin, most of the population are concentrated around the main River course and over the Nile Delta, Egypt. 25

Figure 2.8 Nilometer near Elephantine Island southern Egypt, (A) the nilometer top view. Source:(Flickr, 2009). (B) The bottom view of the nilometer, the black line shows the previous water. Source:(Flickr, 2008) 27

Figure 2.9 Total number of hydrometeorological stations in the Nile Basin at Uganda, an example of fluctuated trend (source: (NBI, 2016)). 28

Figure 2.10 Temporal distribution of the GRACE anomaly from the three partners' mission over the Nile Basin for the period 2002-2015. 30

Figure 2.11 Temporal distribution of the precipitation over the Nile River Basin, data from GPCC, TRMM, CRU, and LSMs for the period 2002-2015. 31

Figure 2.12 Temporal distribution of the ET over the Nile River Basin, data from corrected ET products and LSMs for the period 2002-2015. 32

Figure 2.13 Simulated surface runoff over the Nile Basin. 35

Figure 2.14 Spatial distribution of NDVI over Nile River Basin, MODIS data for the period 2002-2015. 37

Figure 2.15 Correlation NDVI and ET over Nile River Basin. 38

Figure 2.16 Storage variation with precipitation, ET, runoff, vegetation, evaporative and dryness index. 40

Figure 2.17 Temporal variation of the storage recovery and the water stress period over the Nile Basin for the period 2002-2015... 41

Figure 2.18 Spatial variation of the water storage and soil moisture over the Nile Basin for the period 2002-2015. 43

Figure 3.1 Nile Basin climate zones indicated by the Normalized Difference Vegetation Index (NDVI)... 56

Figure 3.3 Averages and trends of temperature, precipitation, actual and potential ET, across the Nile basin for the period 1981–2013.. 61

Figure 3.4 Precipitation, temperature, and potential ET estimates over different climate zones in the Nile Basin. 67

Figure 3.5 Monthly precipitation products from CRU, GPCC and TRMM data over the Nile Basin (data from 1998-2013). 68

Figure 3.6 The precipitation trends over the Nile Basin from 1981-2013..................... 69

Figure 3.7 The temperature trends over the Nile Basin from 1981-2013....................... 70

Figure 3.8 The potential (ETo) trends over the Nile Basin from 1981-2013. 71

Figure 3.9 Simulated and observed GRDC surface runoff over the Nile Basin. (A) The annual surface runoff variation, (B) The correlation between the simulated and the observed runoff with $R^2 = 0.89$ and P value = 0.001 72

Figure 3.10 Simulated surface runoff over the Nile Basin. 73

Figure 3.11 Mean annual surface runoff simulated and GRDC data sets (2002-2013).. 74

Figure 3.12 Distribution of different climate zone under the Budyko space................. 76

Figure 4.1 Land cover types from MODIS data of Nile Delta, Egypt. 88

Figure 4.2 Heavy rainfalls accumulation in low elevation areas along Nile Delta shoreline. Photos taken after heavy rainfalls in year 2010 near New Damietta beach... 89

Figure 4.3 GPS locations along the Nile Delta shoreline. 94

Figure 4.4 Schematic chart of the workflow.. 98

Figure 4.5 Correlation between the DEMs and GPS elevations points. A) SRTM and ASTER-GDEM correlation. B) SRTM/ASTER-DEM and GPS elevations Correlation. Total number of sample points (N= 390 points)... 102

Figure 4.6 Contouring of original DEMs using interval 1 meter. A) The SRTM-DEM showed more homogenous elevations that increase from the north to south, while ASTER-GDEM-V2, B) recorded more elevation points and showing less uniform elevation distribution. 104

Figure 4.7 Overestimated SLR impact on the Nile Delta's coastal area using uncorrected SRTM-DEM dataset, A) showing the 0.5m SLR and B) the 1m SLR scenarios respectively. 111

Figure 4.8 Expected future SLR impact on the Nile Delta's coastal area using corrected ASTER-DEM dataset, A) showing the 0.5m SLR and B) the 1m SLR scenarios respectively. 111

Figure 5.1 Nile River Basin elevations, snapshots of the major hydrological systems over the basin, data from Landsat ETM+. 124

Figure 5.2 Mean monthly actual and potential evapotranspiration of the Nile Basin. . 125

Figure 5.3 Estimation of TWS anomalies using the conventional water balance approach, left panel show the time series of the Modeled and TWS from GRACE, the right panel display the coloration results. 128

Figure 5.4 Correlations of gauge-corrected precipitation data with different precipitation products from satellite, reanalysis and LSM 134

Figure 5.5 Time series of annual surface runoff from GRDC observation and surface run off from the four GLDAS models. 135

Figure 5.6 Correlations of gauged corrected ET dataset and ET estimates from GLDAS land surface model data. 137

Figure 5.7 Correlations of GHCN-Tair dataset and other Tair from RSRA data. 139

Figure 5.8 Data sources and schematic workflow to derive the Total Water Storage (TWS). Each subset is correspondent to one of the inputted models. 143

Figure 5.9 Time series of the normalized monthly regional average TWS from different four GRACE products covering the period from 2002-2015. 146

Figure 5.10 Time series of monthly basin-average variations of (a) precipitation, (b) land surface temperature, (c) evapotranspiration, and (d) surface runoff. 148

Figure 5.11 Correlation of the modeled TWS and the TWS from GRACE based anomalies. 152
Figure 5.12 Time series of the modeled monthly basin-average TWS and observation of TWS from GRACE satellite. 153
Figure 5.13 The temporal variation of the TWS (blue line) and the ENSO variation (dotted line) over Nile River Basin. 154
Figure 5.14 The relation between TWS variation and ENSO anomaly, (A) shows their monthly variations, (B) shows the correlation between TWS and ENSO signals. 155

Abstract

This study addresses the impact of climate change on the Nile River Basin (NRB) and its downstream delta, the Nile Delta of Egypt. The NRB region undergoes a huge fluctuation in precipitation and temperatures from year-to-year. Via a combination of multi-scale satellite remote sensing, model reanalysis, and land surface model information, this study evaluates: 1- how this variation in precipitation and temperature affects Nile River flow, 2- to what extent future sea level rise (SLR) could impact the Nile Delta of Egypt, and 3- how historical variations in the El Niño Southern Oscillation (ENSO) signal are responsible for fluctuations in water storage in the basin.

To answer these questions, a comprehensive water budget equation valid under different climate scenarios was formulated. Next, the variation in precipitation and temperatures was used to calculate the elasticity (reliance) of the Nile River flow to climate change. Third, a merger between remotely-sensed digital elevation models and *in situ* elevation measurements was used to estimate the future SLR impact in the Nile Delta.

The study results indicate regular surface flows are maintained when basin-integrated storage changes (expressed as a depth) increase by less than 60 mm. Meanwhile, decreases in storage change of more than 40 mm subject the basin to severe drought conditions. The Nile River flow is highly sensitive to variations in precipitation and temperature. A 10 percent increase in precipitation results in a 20 percent increase in surface runoff. A -0.5°C change in temperatures results in a 5 percent increase in surface runoff. SLR is an imminent threat to the Nile Delta's communities and land; potential impacts are intense but confined to coastal areas. For instance, a 1-m SLR will inundate about 580 km^2 (6 percent) of the total land area, and would necessitate the relocation of

approximately 887,000 people. The reconstruction of historical basin storage changes indicates that there is a connection between the ENSO and the long-term variation in NRB water storage. Specifically, strong El Nino events are associated with droughts in the NRB and strong La Nina events are associated with floods.

Chapter 1: Introduction and research outline

The Nile River Basin (NRB) is one of the most important international basins, which traverses through 11 African nations with more than 300 million people (NBI, 2010). The Nile Basin is a complex hydrological system with varied distribution of climate zones (Hugh Turral et al., 2011; Melesse, 2011; Melesse et al., 2014). The basin possesses uneven distribution of terrains, land covers, cultures and ecosystems (NIS, 2012a; Oestigaard, 2009). However, the basin suffers severe climatic conditions and undergoes larger changes in population, water allocations, land covers than in the past. It remains to be determined how these changes would affect the water resources across the basin. Meanwhile, the basin's flourishing is attributed to the best practices of the available water supply. Most of riparian's water conflict is related to how the Nile waters are being allocated (Barrett, 1994; El-Fadel et al., 2003; Hugh Turral et al., 2011). For instance, Ethiopia as the main upstream nation contributes most of the Nile waters, however, due to the topography, most of their waters being delivered to the downstream area. Although, the upstream countries are more abundant in the water resources, their water shares goes to the downstream sections where basin display more drier conditions (Hassenforder and Noury, 2015).

Meanwhile, climate is the foremost uncertain threat to the NRB. The basin communities are challenged by their infirm relationships with limited to no corporation. Thus, the plans to mitigate the future climate intimidations are still insignificant. The insufficiency of the operational stations hurdles the water resources management over the basin and makes the prediction to a possible climate scenario to be difficult (Conway, 2005). The inconsistent ground observations imped the expansion of a basin-wide adaptive policy that could be effective for climate mitigations. The climate displays two major threats to the Nile Basin; first, the fluctuations in the Nile River flow, and second, the Sea Level Rise (SLR) impact on the Nile Delta shoreline (Hasan et al., 2015a). Without systematic observation, addressing such problems is very hard.

The advances in the satellite technologies, to capture unprecedented hydrologic information, help to understand the hydrological setting over data-poor regions. The gridded geospatial information from satellites, reanalysis data, and land surface models (LSMs) could substitute the lack of the ground observations especially over NRB. The accuracy of the geospatial data increased substantially due to the advances in the microwave-based satellite estimates and the development of gauge-corrected grids.

1.1 Problem statement

Climate projection over the Nile Basin has a huge sway due to; 1- the limitation in *in-situ* data accessibility, 2- insufficient monitoring and gauging station, and 3- the lack of information sharing culture between the riparians. Therefore, the validation of the future projections still questionable, and to portray a possible climate scenario is being impossible. In addition, without accurate hydrological information, planning for mitigation policies is impossible and in most of the cases ineffective. However, in the past, the Nile Basin was thrived by extensive number of nilometers (old hydrometer stations) that periodically monitor the river flow and level the water in the river channels. Since 1950, the total number of the hydrometer stations were declined dramatically with less interest to operate, maintain, or update such stations.

Monitoring the changes in the Nile water flow across the NRB is critical to understanding the disparity of the basin water cycle. Historical variations in precipitation and temperature records are also essential to understand the influence of climate change on the Nile waters. Moreover, the Basin population estimated at 280 million people in 2005 that is expected to reach about 591 million people by 2025 (UNEP, 2000; UNEP, 2013). The rapid population growth will increase the land use pressure and will cause further deterioration to the basin resources. Similarly, irrigation in the Upper Nile countries, severely underutilized relative to its potential, is expected to grow by several orders of magnitude, putting further stress on water resources (NBI, 2010; NBI, 2012).

1.2. Research objectives

This study seeks to evaluate to what extent the hydrological observations from the satellite, model reanalysis and LSMs could substitute the lack of the operational observations over the NRB. In fact, the evidence of discernible storage changes in the NRB caused by global climate change has not been fully studied. Therefore, to assess, understand, and mitigate the future effects of climate variability on terrestrial water systems, reliable record of the storage changes is needed. The satellite-based hydrological data can be representing each term listed in the water balance Equation (1.1).

$$\frac{ds}{dt} = P - ET - Q \pm \varepsilon \tag{1.1}$$

Where $\frac{ds}{dt}$ is the storage changes could provide by the NASA's Gravity Recovery and Climate Experiment (GRACE) satellites. The recent gauge corrected precipitation grids and the evapotranspiration could be valuable sources to estimate precipitation (P), the evapotranspiration (ET). The surface runoff (Q), can be simulated as a residual of precipitation, evapotranspiration and the storage change. The error term ε is so critical to assess the uncertainty levels in the water balance estimates.

This study implementing the basic gridded hydrological information to:

1- Provide a comprehensive water balance equation over the NRB,

2- Address the response of the surface runoff to the climate change,

3- Validate the hydrological utility of the multisensory satellites, reanalysis, and LSMs data sets to better simulate the storage changes over the basin, and

4- Determine the hydroclimatic impacts and assess the water resources risks due to climate El Niño–Southern Oscillation (ENSO) variations.

1.3 Research questions

The key research questions of this study are:

1- How can satellite based storage change, precipitation, evaporation estimate be used to provide a representative water-balance equation over the Nile Basin?

2- How could the variation in precipitation and temperature affect the Nile River flow, and how the Nile Basin is resilient to climate change?

3- What is the potential impact of the SLR on the Nile Delta's land cover and population?

4- How could the variation in ENSO conditions influence the TWS over the basin?

1.2 Dissertation outline

The dissertation is outlined in four core chapters that are written as individual journal articles. Each chapter introduces vital topic to the water resources over the Nile basin. The main topics include the challenges to the water resources management over the basin, the response of the Nile river flow to the climate change, the potential Seal Level Rise (SLR) over the Nile Delta Egypt, the utilization of multi-satellite, reanalysis observations, and LSMs data to estimate the TWS over the basin. Following to that an overall summary and conclusion of our research findings. However, each article/chapter discusses a unique topic some unavoidable repetition may occur in the introduction and the data section. The following section displays a brief summary of each chapter.

Chapter 2: Challenges and opportunities of hydrologic remote sensing for the Nile River Basin: A Review

This chapter discusses the main challenges to the water resources management over the Basin. Climate change, water-allocations, population growth, and data inaccessibility are the major hitches to water management. Meanwhile, satellite-based hydrological observations could help to understand the overall storage changes, the fluctuation in the precipitation, evaporation and surface water flow. Another objective is to construct a representative water-balance equation for the basin. The main contribution of this chapter is using gridded observations to best understand the state of the water resources under the changing climate.

Chapter 3: Response of Nile river flow to the climate change

This chapter addresses how fluctuations in precipitation and temperature could influence the Nile river flow over different climate regions of the Nile Basin. The basin was divided into three main climate zones: the tropical-subtropical, semiarid and arid zone, each characterized by a unique precipitation, evaporation and runoff rates. Based on the functional formulas introduced by Arora (2002) and Pike (1964), the surface runoff elasticity was estimated to understand the basin resilience to the climate change in each climate zone. Another approach adopted was the use of Budyko curve to determine how the basin might transit from energy-limited to a water-limited state.

Chapter 4: Investigation of potential sea level rise impact on the Nile Delta, Egypt using digital elevation models

Addresses how the future SLR could affect the Nile Delta, considered the gift of the Nile to Egypt. The potential SLR estimated based on the two digital elevation models (DEM), the shuttle radar topographic session (STRM) and the Advanced Spaceborne Thermal Emission and Reflection Radiometer (ASTER) along with ground elevations based on the Global Position System (GPS). A linear regression model was developed to assess the DEM accuracy. Land cover information from the Moderate Resolution

Imaging Spectroradiometer (MODIS) and the gridded population datasets were deployed to understand the SLR impact on land cover types and the population.

Chapter 5: Estimating the Terrestrial Water Storage with Multiscale Remote Sensing and Model Reanalysis in the Nile River Basin

Understanding the historical fluctuation of the TWS is prerequisite for hydroclimatic risk assessment. The main approach of this chapter is to use multi regressive parameters from the water/energy balance components in combination with land cover information to investigate the relationship between the TWS anomaly and different hydrologic variables. Then identify the most explanatory variables to the TWS. This chapter aims to reconstruct historical records of 30+ years of TWS along NRB using the MRA approach. Second is to investigate the historical frequencies of water deficit/stress periods, to assess the influence of climate variability on the TWS, and to potentially predict the water availability across NRB hydrologic systems.

1.3 List of publications from the dissertation

Chapter 2:

Hasan, E., Tarhule, A. Kirstetter, P., and Hong, Y., 2016. Challenges and opportunities of hydrologic remote sensing for the Nile River Basin: A Review. Hydro. Sci. Jour. (Under Review).

Chapter 3:

Hasan, E., Tarhule, A. Hong, Y. and Kirstetter, P., 2016. Response of Nile river flow to the climate change. Water Resc. Res. (Under Review).

Chapter 4:

Hasan, E., Khan, S.I. and Hong, Y., 2015. Investigation of potential sea level rise impact on the Nile Delta, Egypt using digital elevation models. Environ Monit Assess, 187(10): 649.

Chapter 5:

Hasan, E., Kirstetter, P., Zhang, K. and Hong, Y. and, 2016. Estimating the Terrestrial Water Storage with Multiscale Remote Sensing and Model Reanalysis in the Nile River Basin. Remote Sensing of Envi. (Under Review).

1.3 References

Barrett, S., 1994. Conflict and Cooperation in Managing International Water Resources, CSERGE Working Paper WM 94-04. Centre for Social and Economic Research on the Global Environment University College London and University of East Anglia.

Conway, D., 2005. From headwater tributaries to international river: Observing and adapting to climate variability and change in the Nile basin. Global Environmental Change, 15(2): 99-114.

El-Fadel, M., El-Sayegh, Y., El-Fadl, K. and Khorbotly, D., 2003. The Nile River Basin: A Case Study in Surface Water Conflict Resolution. Journal of Natural Resourorces Life Science Education 32: 107-117.

Hasan, E., Khan, S.I. and Hong, Y., 2015. Investigation of potential sea level rise impact on the Nile Delta, Egypt using digital elevation models. Environ Monit Assess, 187(10): 649.

Hassenforder, E. and Noury, B., 2015. Managing Transboundary River Basins: Chaper 7. River Basin Management in the Twenty-first Century. Taylor & Francis Group, LLC.

Hugh Turral, Jacob Burke and Faurès, J.-M., 2011. Climate change, water and food security, Itlay.

Melesse, A.M., 2011. Nile River Basin: Hydrology, Climate and Water Use. Springer, Springer Dordrecht Heidelberg London New York.

Melesse, A.M., Abtew, W. and Setegn, S.G., 2014. Nile River Basin: Ecohydrological Challenges, Climate Change and Hydropolitics. Springer, Springer International Publishing Switzerland.

NBI, 2010. Key facts about the Nile basin. Nile Basin Initiative (NBI), Entebbe. http://www.nilebasin.org/newsite/index. Accessed 19th December 2012.

NIS, 2012. Climate Change and its Implications for the Nile Region:Chapter 8.

Oestigaard, T., 2009. Water, Culture and Identity: Comparing Past and Present Traditions in the Nile Basin Region. Nile Basin Research Programme. BRIC Press, Norway.

Chapter 2: Challenges and opportunities of hydrologic remote sensing for the Nile River Basin: A review

Abstract

The Nile River Basin (NRB) is one of the longest transboundary watercourses. The basin challenged by the infirm relationship between the riparian countries, lack of information sharing and insufficient monitoring stations. Under the changing climate, reliable and sufficient information are needed to understand the climate effect on the basin's water flow. Due to the lack of the operational observations, the climate prediction is very uncertain and fluctuate whether will be heavy rainfalls that will induced more flooding events, or drought conditions with diminished surface runoff will be dominant. This chapter evaluates to what extent the available hydrological information from remote sensing and model reanalysis and land surface model (LSM) dataset could substitute the lack of the ground information. Additionally, provide a comprehensive water balance formula for the basin. In the current study, the basic hydrologic information includes storage changes, precipitation, evaporation and surface runoff based on gridded-satellite, reanalysis, LSMs observations vegetation land cover information. The storage changes expressed using NASA's Gravity and Recovery Climate Experiment (GRACE) satellite as overall changes in the total water storage (TWS), the precipitation from Global Precipitation Climatological Center (GPCC), The Tropical Rainfall Measuring Mission (TRMM), Climate Research Unit (CRU), and Global Land Data Assimilation System (GLDAS) products, datasets. The evapotranspiration information were extracted from grid-corrected ET product and the GLDAS data. The surface runoff were estimated as a residual of the precipitation, ET and storage change. The resulting runoff estimates were compared with the runoff information from the Global Runoff Data Centre (GRDC) datasets. The main objective of our research is to evaluate the hydrological changes and the variation in water balance along the NRB. This study: 1- Developed gridded-distributed storage changes, and runoff based estimates, 2- Compared the inter-annual variability of the storage changes with the precipitation, ET, runoff, evaporative index and dryness index, and 3- Defined the water stress and water deficit periods along the Nile Basins. The results indicated that the basin area was influenced by huge storage fluctuations, creating several water stress and water deficit periods.

Keywords: Nile River, remote sensing, reanalysis, water balance, data-poor regions.

2.1 Introduction

The Nile River Basin (NRB) is one of the major continuous transboundary rivers in the world. The word Nile, Nil, or Neilos, means the blue or the dark river, it describes the majestic river that was mentioned frequently in the old scriptures and testimonies. i.e., The Old Testament has mentioned the word "Sihor" to describe the black river in Egypt (Isaiah 23:3; Jeremiah 2:18). Meanwhile, the New Testimony and the Holy Quran commonly described the dark flowing stream in Egypt by the "River" (Genesis 41:1; Exodus 1:22), and (Taha 20:39; El-Qasas 28:7). The Nile River is the source of life and the start of great civilizations that hosts diverse communities and cultures.

Geologically, the Nile originated about 6 million years ago throughout five main stages summarized by (Salama, 1987): Stage one, the *Eonile*, which was a small stream developed due to the dryness of the Mediterranean Sea during the Messinian salinity crisis of the late Miocene. Second, the *Paleonile* stage, which is considered a seasonal river that formed across Egypt. Third, the *Protonile* stage, this also was restricted to Egypt and resulted from occasional precipitations during the arid conditions. Forth, the *Prenile* stage is described as the true beginning of the current Nile River. The *Prenile* formed due to the East-African uplift that created the Ethiopian's highlands and formed the large equatorial lakes of Victoria, Kyoga, George, Albert and Edward. The heavy rainfalls over East Ethiopia created the Blue Nile system, and the flow of the water from the equatorial lakes to Sudd marshes created the White Nile system (Said, 1981; Salama, 1987 ; Salama, 1997). Last, the *Neonile*, where the entire Nile basin developed and the two River systems were well-established to form the longest permanent river system, the Nile.

Starting from Eastern-Central Africa at Lake Victoria and from the Eastern African rift system at Lake Tana in Ethiopia, the Nile River travels a distance of about 6,650 km in length to form one of the longest rivers in the world. The Nile ends its journey in the Mediterranean Sea forming one of the largest inhabited Deltas worldwide, the Nile Delta of Egypt (figure 2.1). The NRB possesses variety of cultures, terrains, and climates. It is the main source of life for more than 300 million people belonging to 11 African nations include; Burundi, Democratic Republic of Congo, Egypt, Eritrea, Ethiopia, Kenya, Rwanda, South Sudan, Sudan, Tanzania, and Uganda. Geographically, the Nile Basin is divided into two main regions: The Eastern Nile region includes three countries: Egypt, Sudan, and Ethiopia, and the Equatorial Lakes region includes Burundi, Democratic Republic of Congo, Kenya, Rwanda, Tanzania and Uganda (NBI, 2010).

The NRB receives the majority of its water from East Ethiopian hills where the heavy rainfalls feed Lake Tana (Kebede et al., 2006; Vijverberg et al., 2009). Other water shares come from the equatorial Lakes, Lake Victoria and Albert. Although the NRB possess number of the biggest freshwater lakes, artificial reservoirs, and open water areas, these lakes represent less than three percent of the basin's total area. The basin's lakes provide a natural protecting buffer against the variations in the seasonal rainfall, also proved a permanent storage to the floodwaters during flood periods. The basin's wetlands and lake areas maintained a regular flow of the Nile water especially during the dry spells.

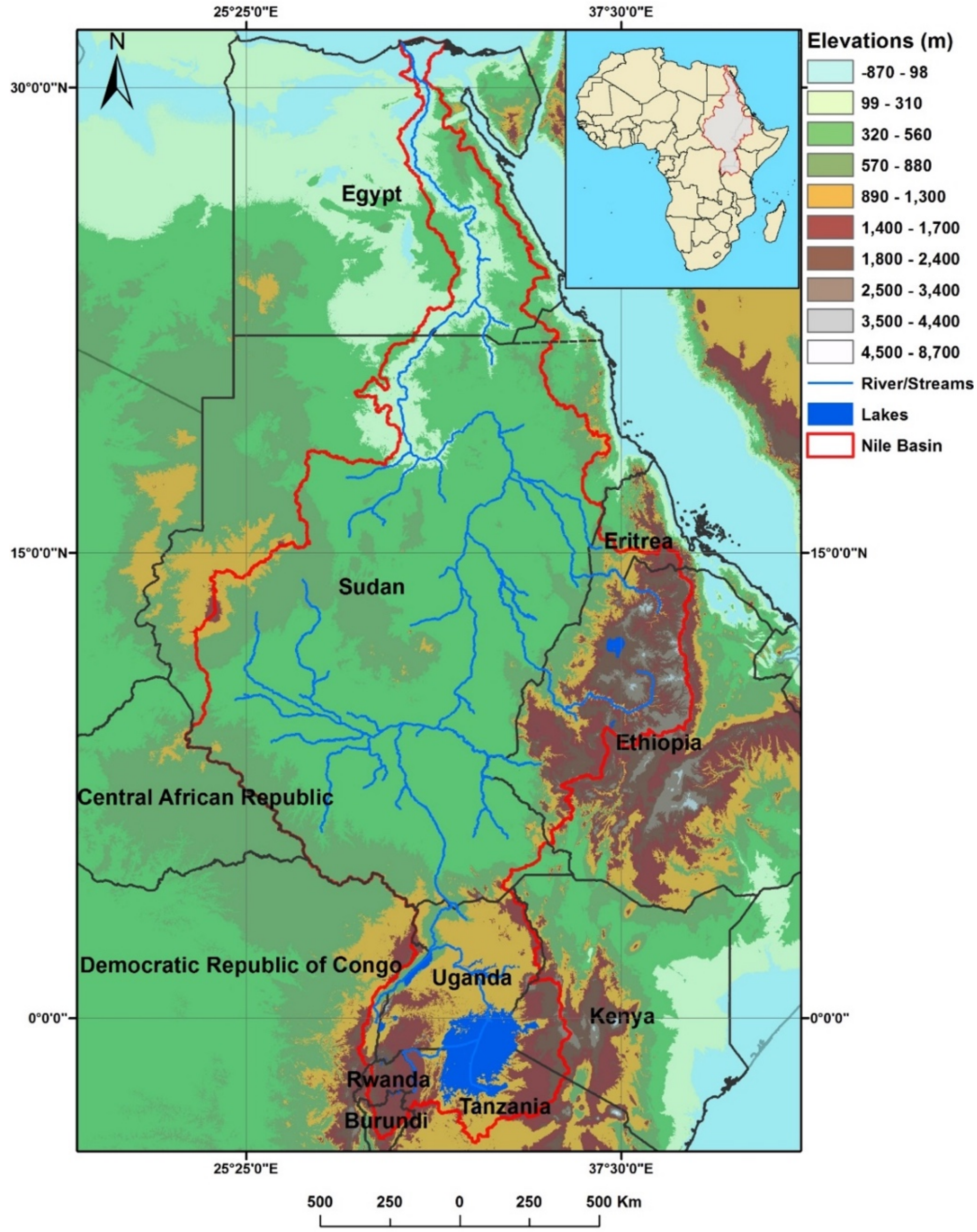

Figure 2.1 Nile River Basin, location map and study area.

Although the White and Blue Nile systems are providing the Nile River with essential water supply, the Blue Nile has a greater importance over the White Nile. Since, about 80 percent of the Nile water flow directly from the Blue River Nile. Additionally, the heavy sediments load carried by the Blue Nile considered the main source of the fertile lands over Sudan and Egypt (Vijverberg et al., 2009). At the conjunction of the Blue and the White Nile near Al-Khartum city North Sudan, a single pursuing stream is formed, the Nile. The Nile traverses about 800 miles through the Egyptian desert to end its journey in the Mediterranean Sea.

Yet, the impact of climate change on the Nile Basin remains less understood due to the lack of the systematic field data that captured enough hydrologic information. Indeed, the Nile Basin has an uneven rainfall patterns, temperature anomalies, and erratic river flow. The Basin challenges are numerous ranging from hydrological to historical ones. The following section presents an overview about the main challenges that hinder the water resources management over the Nile Basin. Understanding such issues can help the riparian nations to better plan for future agreement and develop adaptive measures for climate mitigations. In fact, as the basin nations sharing the water, they are challenged by the same future. Absolutely, there is no buffer or limit that the climate effect can stop at and to develop potential adaptive policies by the upstream and the downstream countries is certainly crucial for better resources managements under the changing climate.

2.2 Challenges to the Nile River Basin

Hydrological challenges

The Nile Basin is a complex hydrologic system with varied climate zones, terrains and discrete patterns of precipitation, water flow, and evaporation. The equatorial lake areas and Lake Tana receive more than 1000 mm of precipitation a year. Northward, the basin experiences an extensive decline in the precipitation rates. Where, at the conjunction between the Blue Nile and the White Nile River systems, the annual precipitation rates dwindle to be around 200mm/y. Furthermore north, Sudan and of Egypt depict a transit toward more drier and arid climate conditions, the precipitation rates decreases to almost zero mm/y. The fluctuation in precipitation influences the water shares from each riparian and the rate of water flow to the downstream areas (figure 2.2).

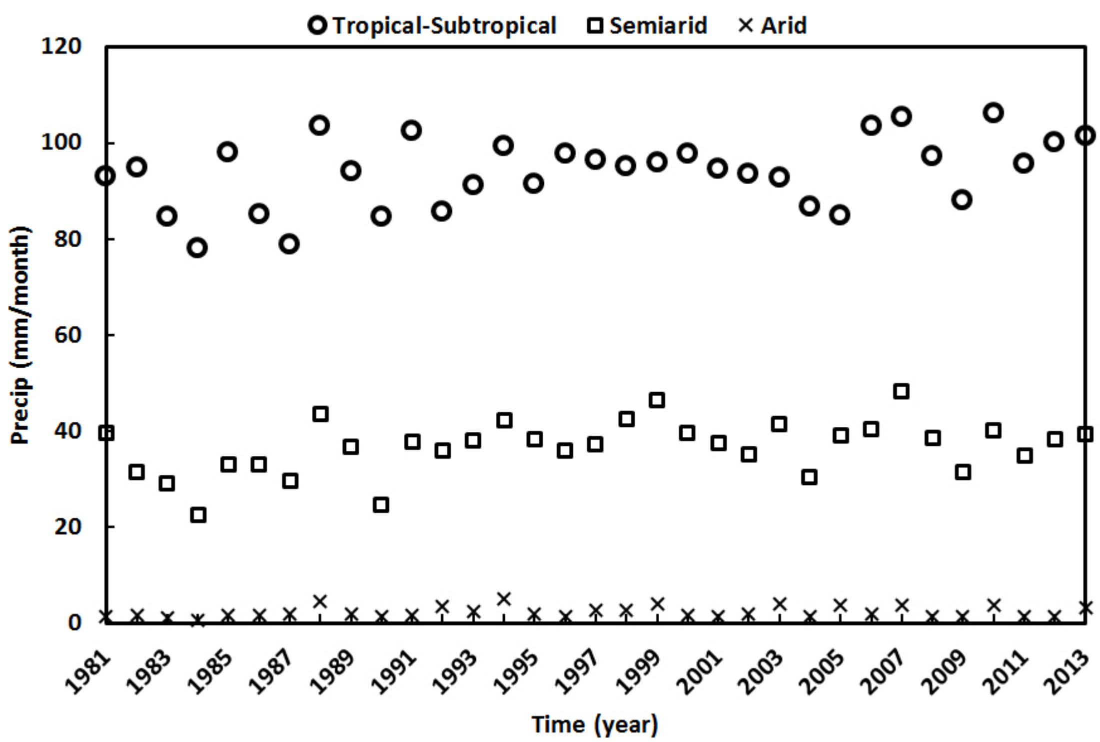

Figure 2.2 Comparison of the temporal variation in the Nile Basin precipitation over different climate zones, GPCC data for the period 1981-2013.

The Nile River receives major water flow from the Blue Nile Basin (BNB), about 76 to 80 percent of the water flows from Lake Tana. During the summer monsoon (June to September), Ethiopian highlands receives heavy rainfalls and the water rises in the channels to the maximum levels between August and September. The Nile flows northward to Sudan, in May, the water reaches to the maximum levels which grasps in June at Aswan, Egypt (Collins, 2002). The flow rates of the Nile water considers very slow when it compared to other river systems worldwide. The water flow requires about three months to traverse over the low lands of the Sudd marshes south-west Sudan. The water flow average is about 0.98 $L/s/Km^2$, which depicts a very slow rates of surface discharge and high rates of water loss due to evaporations (Moges and Gebremichael, 2014). The Nile flow is highly dependent on the rainy seasons; the water flow is highly sensitive to any changes in temperatures that depicts high potentials of the evapotranspiration rates.

Evapotranspiration is responsible for significant water loss over the Nile Basin. The total annual evapotranspiration diminishes about 310 to 260 BCM of water over the equatorial lakes, Lake Tana and Sudd marshes annually (NIS, 2012b). The man-made reservoirs, e.g. the Lake Nasser southern of Aswan High Dam (AHD), conveyance losses of about 19 BCM of water annually. The reported evapotranspiration rates at the conjunction of the two river systems is about 7 BCM per year. Owing to the extensive temperatures and varied precipitation influx, the Nile undergoes high evapotranspiration and extensive loss of the surface runoff (figure 2.3) (NIS, 2012b).

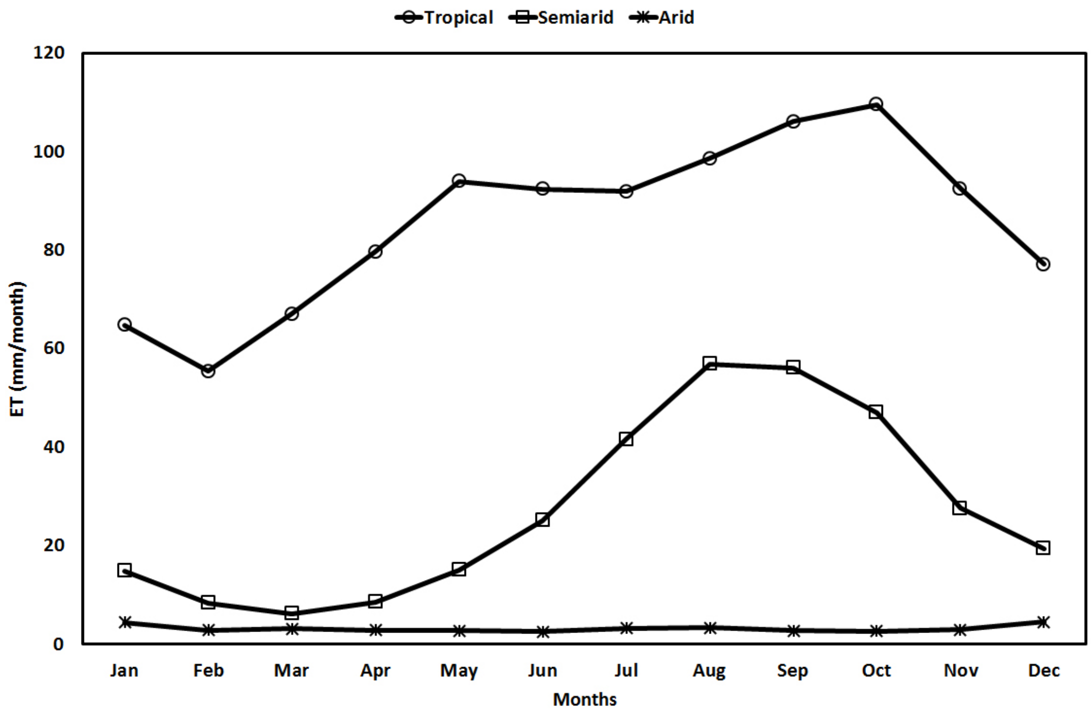

Figure 2.3 Gauge corrected ET estimates over different climate zones, data for the period 1982-2013.

Meanwhile, the potential evaporation is controlled by the topography, where at mountains areas and equatorial lakes the potential evaporation is relative low when compared to those over semiarid and arid zone. The potential evapotranspiration shows a pattern of gradual increase northwards as the humidity level decreases and temperature relatively higher (figure 2.4) (Alemu et al., 2014).

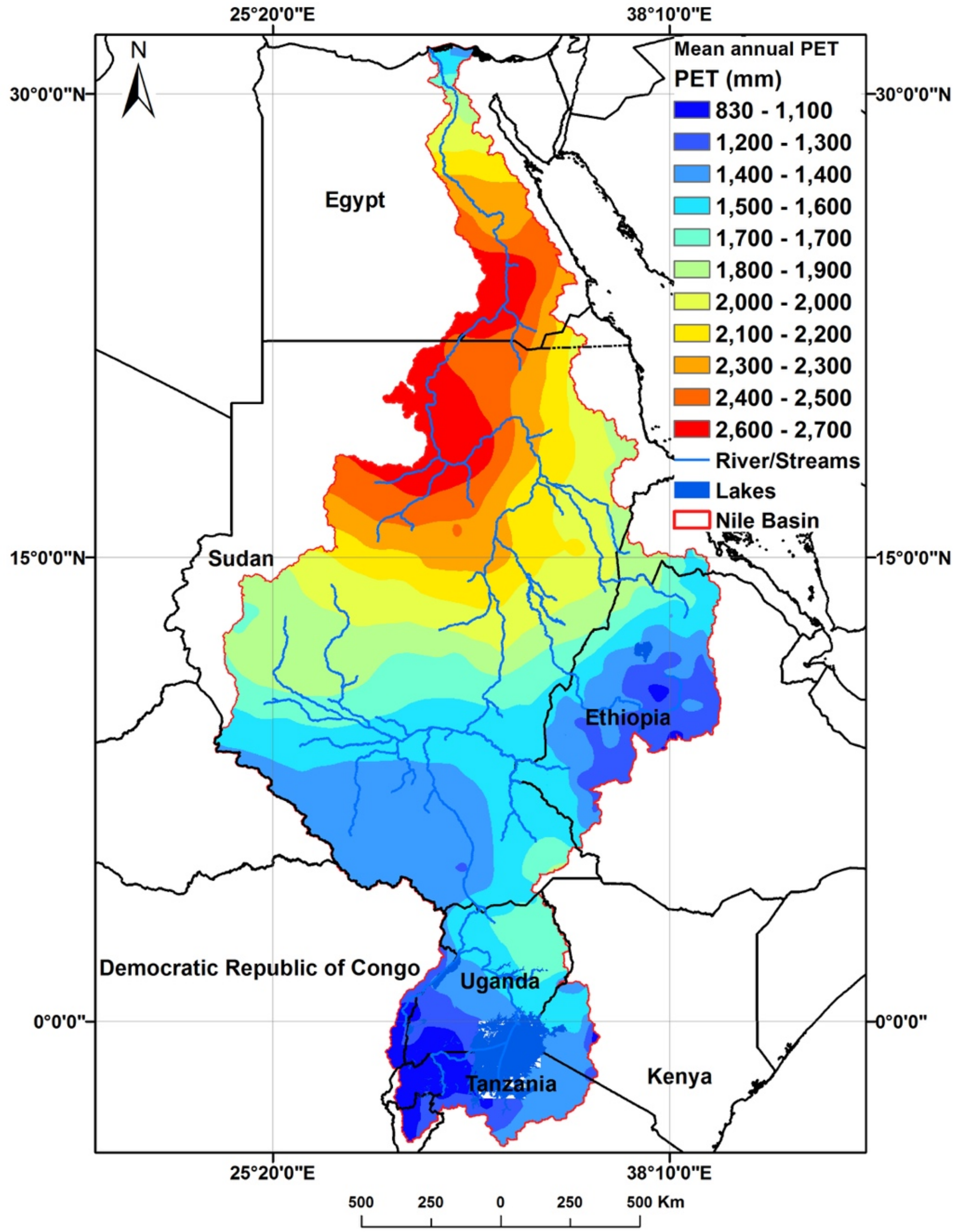

Figure 2.4 Mean annual potential ET over the Nile River Basin, CRU data from 1982-2013.

Extreme events

The Nile Basin is subject to frequent droughts and flooding events. Generally, the semiarid and arid climate zones struck by severe droughts due to the fluctuated precipitation rates (Erian et al., 2012). Currently, the downstream nations are under the state of water scarcity, where the annual amount of available water per person is less 1,000 m^3/person/year as reported by the (UNEP, 2013). However, the upstream riparian flourished with ample of precipitations; during El Nino events, the rainfall impeded to reach Ethiopian hills to cause severe droughts. In response, the water level in Lake Nasser northward can be lowered to unprecedented levels (Collins, 2002; Erlich, 2000). Drought is connected to precipitation absence and excess of temperature plumes. Flooding is another serious dilemma that stalks the upstream riparians due to the rigid topography and high precipitation rates. During La Nina events, dramatic rainfall is prevailed resulted in severe flooding (figure 2.5) (NIS, 2012a; UNEP, 2013). The unequal allocations of precipitation along the basin can either trigger drought or flood extremes (Beyene et al., 2009). Consequently, provoking threats transferred to the basin's resources, ecosystems, agricultural productivity and water management (El-Quosy, 2009; UNISDR, 2011). Meanwhile, the gap between the countries' demands for water and the available water resources substantially influence stability and national security.

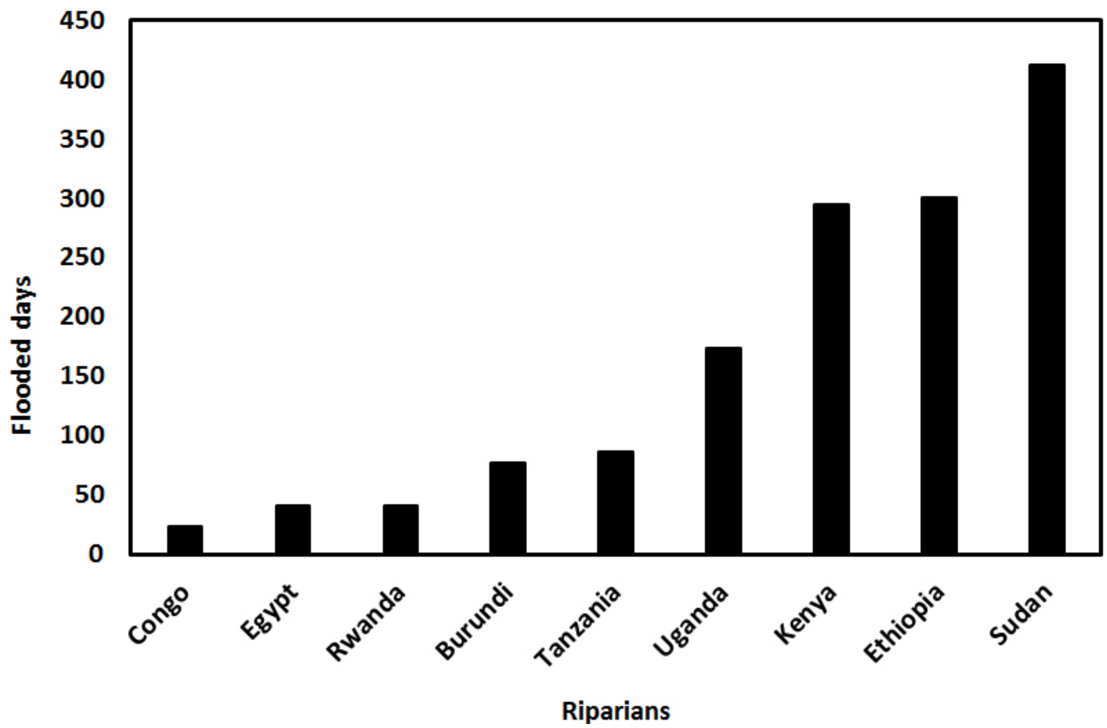

Figure 2.5 Total flooded days over riparian states, data for the period from 1989-2008. Source: (DFO, 2012)

Climate change

The Nile Basin endures significant temperature increase as result of the climatic conditions. As the Intergovernmental Panel on Climate Change (IPCC) reported that the northern and eastern African nations are influenced by an increase of the average temperature of about 1°C above the normal of 1961–1990 in year 2013 (Niang et al., 2014). Meanwhile, temperature controls the regional climate pattern and generally responsible for major drastic events (Lynas, 2008). The Basin witnesses high temperature rates along the arid and semiarid regions rather than the tropical and subtropical zones (Camberlin, 2009). The increase of land surface temperature rises the potential evaporation and reduces the surface runoff. As the potential evaporation increased the basin moves towards more moisture-constrained conditions (NIS, 2012a). In year 2011, the Blue Nile Basin (BNB) swayed by precipitation deficit and the region experienced severe drought conditions due to the surges in temperature and the failure in rainy seasons (Lott et al., 2013).

Population growth

The Nile Bain inhabiting more than 300 million people who are projected to increase by the year 2030 to 600 million (figure 2.6) (Oestigaard, 2010). Currently 54% of the total population lives within the main Nile riverbanks and around the lake areas. The population density displays higher percentage over East African Plateau, Ethiopian highlands, Khartoum city, Nile valley, and Nile Delta. Rapid population exerted more pressures on the water resources, the land, and the agriculture productivity of the basin. Mostly, people are stretching around and over the agricultural areas with a great tendency toward more urbanizations (figure 2.7). Moreover, people intervention to ecosystem and the local environment through deforestation, sweeping the agricultural land, and taming waters causing ecosystem stability and increase the land degradations.

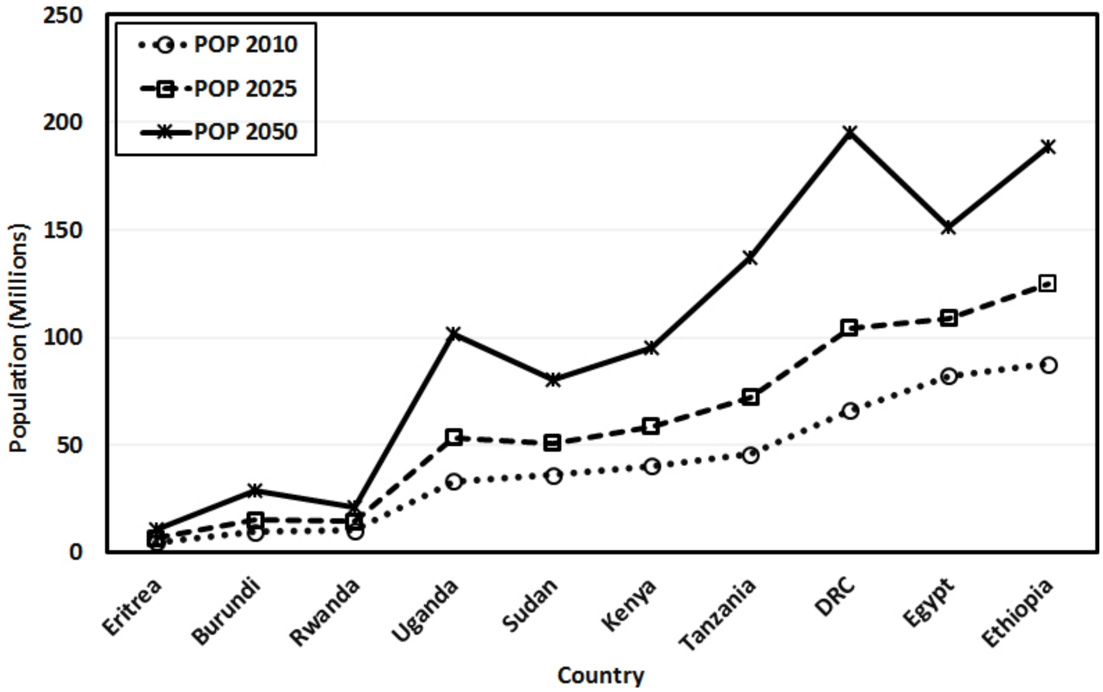

Figure 2.6 Total population growth of the Nile Basin's state. Source: (WB, 2016)

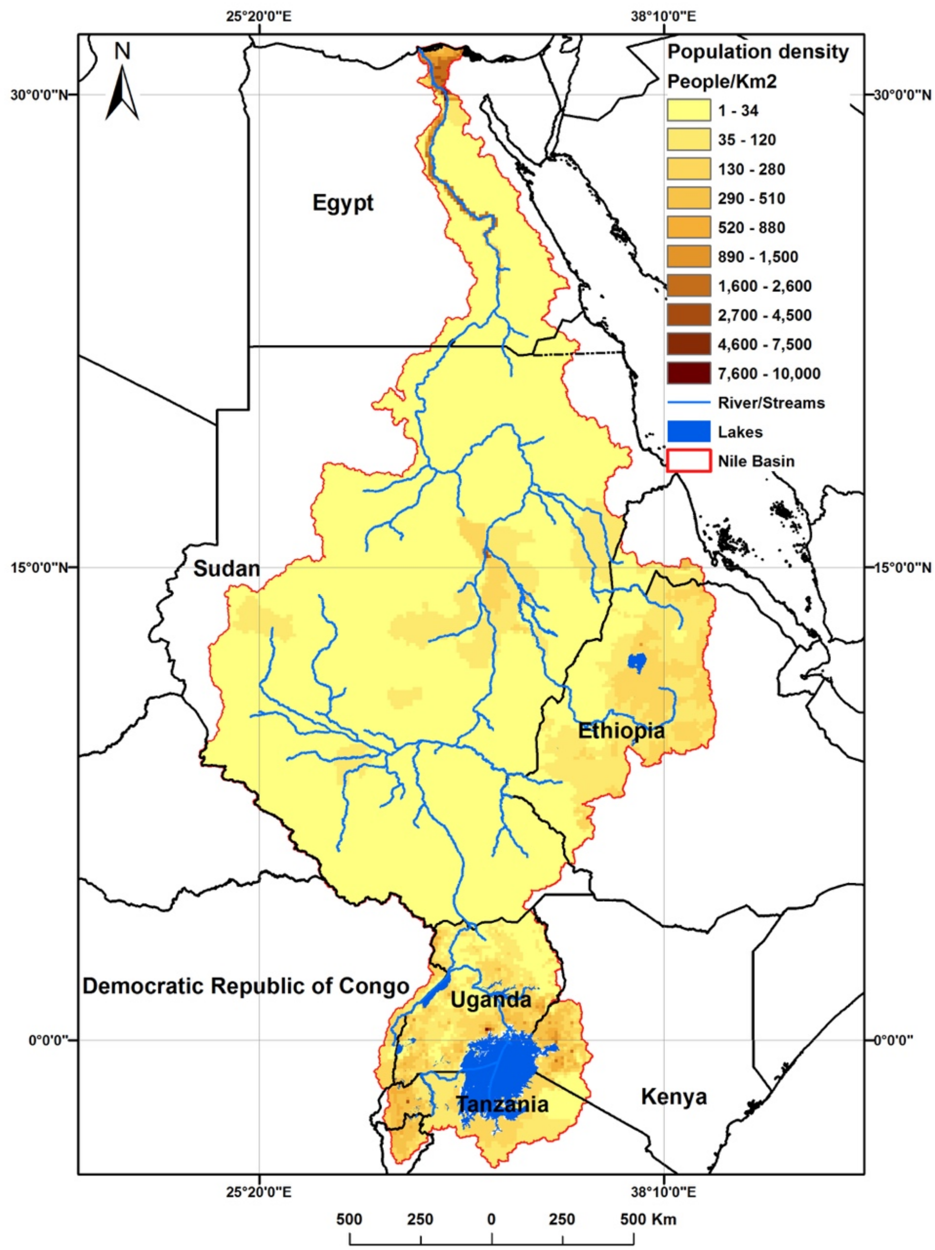

Figure 2.7 Population density over the Nile Basin, most of the population are concentrated around the main River course and over the Nile Delta, Egypt.

Historical challenge

The water flow is the Nile's greatest wealth. The debate who owns the Nile and control the river flow is a historical challenge between the upstream and downstream nations especially Ethiopia and Egypt. Meanwhile, the sole downstream users considered the Nile as their source of life. Likely wanted to see their own water shares unchanged. Historically, Pharaonic kingdom had reached and controlled to the Nile main sources. Preventing any trial of sealing the water from flowing to Egypt. This custom persisted during the Roman Empire and the Arab conquest. In fact, the continuous of the ruling regime in Egypt was contingent to the Nile flow. Moreover, the British colonialization prevented the upstream countries to build or construct any means for water sealing within their borders. Where, in 1929, Egypt and Britain signed a treaty on behalf of the riparians stated that "no irrigation or power works or measures are to be constructed or taken on the Nile River and its branches, or on the lakes from which it flows in such a manner as to entail any prejudice to the interests of Egypt" (Kieyah, 2007; Oestigaard, 2010). Since 1950, Egypt role retreated and become less effective in the region; most of the upstream countries revolted such treaties without Egypt consent and started to construct water-taming projects. Indeed, the upstream countries strive for their wellbeing through managing the water resources and increasing the potential use of water. However, Egypt historical rights in Nile's water could not be ignored or neglected, a sort of agreement should be nudged by all riparians to develop mutual corporation theme on the Nile water. In 1999, the Nile Basin Initiative (NBI) was declared to connect the eleven riparian nations for the first time and to address the basin water issues (NBI, 2010; NBI, 2012).

Data inaccessibility

Historically, the Nile Basin managed to be as well-studied river with extensive network of nilometers and gauging across the Nile course (figure 2.8).

Figure 2.8 Nilometer near Elephantine Island southern Egypt, (A) the nilometer top view. Source:(Flickr, 2009). (B) The bottom view of the nilometer, the black line shows the previous water. Source:(Flickr, 2008).

Meanwhile, since 1968, the total numbers of hydrometers and meteorological stations were declined dramatically (figure 2.9). To date, the gap of ground information is significant making the prediction of possible climate change scenarios over the basin too difficult. The lack of data sharing and the institutional bureaucracies among riparian nations hurdle the water management policies. Without unlimited data accessibility and availability, the Nile Basin is sort of data-poor region. Establishes a comprehensive real-time network for data acquisition over the basin is essential. The *in-situ* data is not only a key to water resources management but also a priority to develop a mutual adaptive capacity between the riparian states. The riparian countries are challenged by their infirm relationships, lack of information sharing culture and insufficient monitoring stations. A reliable data overtime is essential to understand the temporal and spatial consequences of climate variation. Therefore, in lieu of hydrological observation, the geospatial information from satellite, reanalysis and land surface models provide unprecedented hydrological observations. Likely, geospatial data enables to address an inclusive water balance equation that describes the entire water components and defines the state of water resources in the basin. The following section displays the opportunities for hydrological remote sensing over the Basin for best water management strategies.

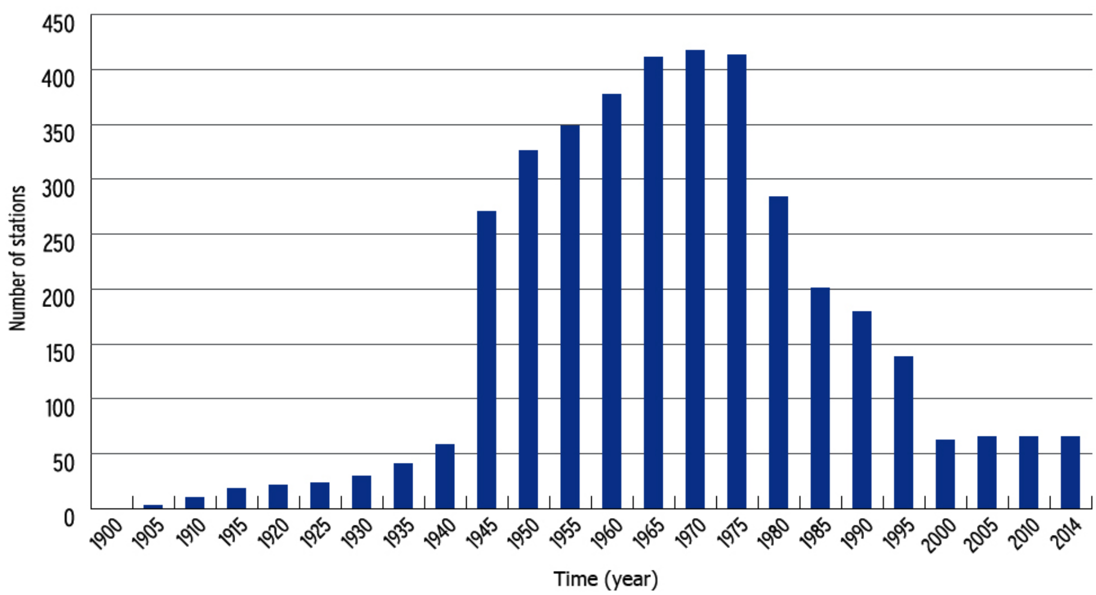

Figure 2.9 Total number of hydrometeorological stations in the Nile Basin at Uganda, an example of fluctuated trend (source: (NBI, 2016)).

2.3 Opportunities for hydrological remote sensing

The onboard satellite sensors viewing and monitoring the Earth's surface at regular intervals using physical earth's characteristics such as electromagnetic radiation and gravity. The continuous physical measurements from satellite systems helped to address wide range of problems especially when the *in-situ* and gauging stations are absent. This section reviewing the opportunities to understand the Nile Basin's water balance using multisensory remote sensing, reanalysis data and blind-gauge corrected grids. Despite the recent advances in the geospatial data gathering and manipulating, our understanding of water resources for the emerging regions could be limited. The following section addressing what is the best geospatial information that could be best representing each component of the water balance listed in Equation 2.1.

$$\frac{\Delta S}{\Delta t} = P - ET - Q \pm \varepsilon, \tag{2.1}$$

Where, $\frac{\Delta S}{\Delta t}$ Storage change within time, P Precipitation, ET Evapotranspiration, Q runoff, and ε is the error term.

Storage change

The storage change is an inclusive measure about the state of water and whether it normal, surplus or in deficit state. Since 2002, the mission Gravity Recovery and Climate Experiment (GRACE) satellite provides unprecedented measures about the changes in the Total Water Storage (TWS). GRACE is a unique precise microwave ranging system measures the changes in the TWS as a function of the earth's mass gravity. GRACE grids represent 1° of water column from the surface, soil moisture and groundwater. The GRACE data are collected, processed, and made accessible through three main mission partners; the Center for Space Research (CSR) at University of Texas, the Geo

Forschungs Zentrum (GFZ) Potsdam, and the Jet Propulsion Laboratory (JPL). Figure 2.10 display the monthly average of the GRACE signals over the Nile Bain from the three data centers, along with the new GRACE Mass Concentration Block (Mascon) signal.. GRACE observations can track the fresh water availability, the variation in water cycle, the groundwater variability, and can be a unique tool to construct the evapotranspiration as a residual of the storage changes (Ahmed et al., 2014; Ahmed et al., 2011; Cao et al., 2015; Houborg et al., 2012; Long et al., 2013; Long et al., 2014). In this research, the monthly GRACE product from (2002-2016) (R05L2) data was implemented.

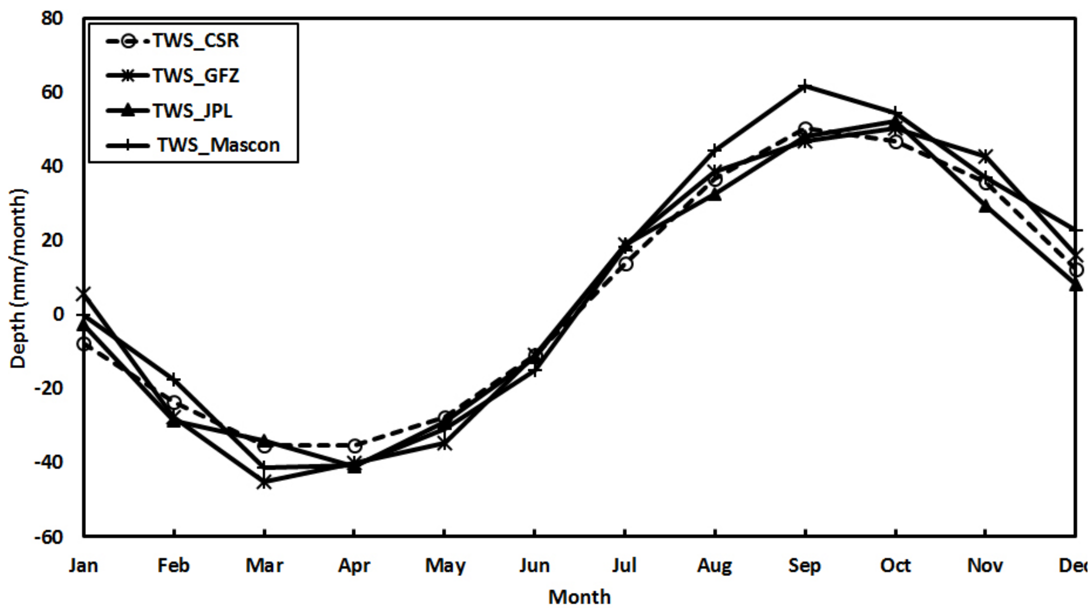

Figure 2.10 Temporal distribution of the GRACE anomaly from the three partners' mission over the Nile Basin for the period 2002-2015.

Precipitation

Precipitation is the most important component of the water cycle. Several precipitation products are available at different temporal and spatial scale from satellites, model reanalysis, and land surface models. Meanwhile, the precipitation products at high temporal resolution (hourly and daily products) are exhibiting high form of uncertainties.

Contrary, the monthly temporal precipitation data display high agreement when it compared with gauge observations. In this research, number of monthly precipitation products are implemented to assemble the precipitation record over the Nile basin. The precipitation data include: the monthly research product from the Tropical Rainfall Measuring Mission (TRMM), the hydrological monitoring products from the Global Precipitation Climate Center (GPCC) research product (Schneider et al., 2011), the Climate Research Unite (CRU) precipitation data (CRU, 2015)., and Global Land Data Assimilation System (GLDAS) (Rui, 2011) (figure 2.11). The data were covered the time-period from 2002 to 2016 with varied spatial grids of 0.25°, 0.5° and 1° latitude-longitude grids.

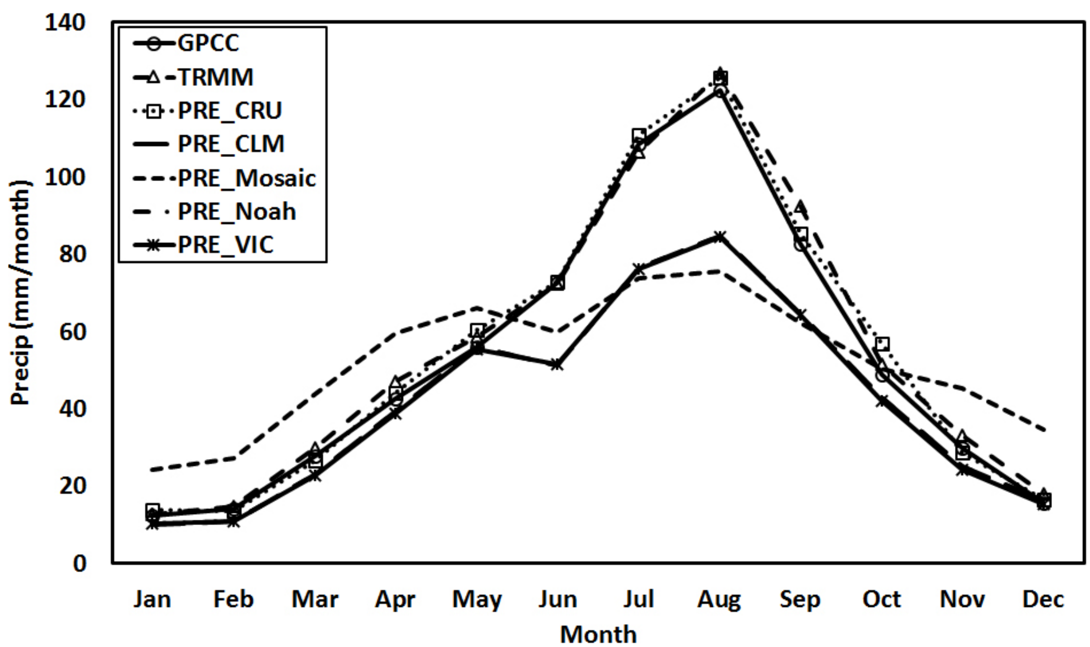

Figure 2.11 Temporal distribution of the precipitation over the Nile River Basin, data from GPCC, TRMM, CRU, and LSMs for the period 2002-2015.

Evapotranspiration

Actual evapotranspiration (ET) depicts the water flux from the plant surface and water bodies. The ET plays a key role in runoff and water availability and can be used for irrigation management, drought detection, water productivity and groundwater management. The ET computation can be based on different strategies include: water balance approach, energy budget, and penman-month approach. The ET data are available through satellite-based estimates such as MOD16 global evapotranspiration product, LSM such as GLDAS ET, and gauge corrected ET products. In the current research, the monthly ET data from GLDAS and the corrected ET grids deployed to understand the spatial and temporal variation of the ET over the basin (figure 2.12).

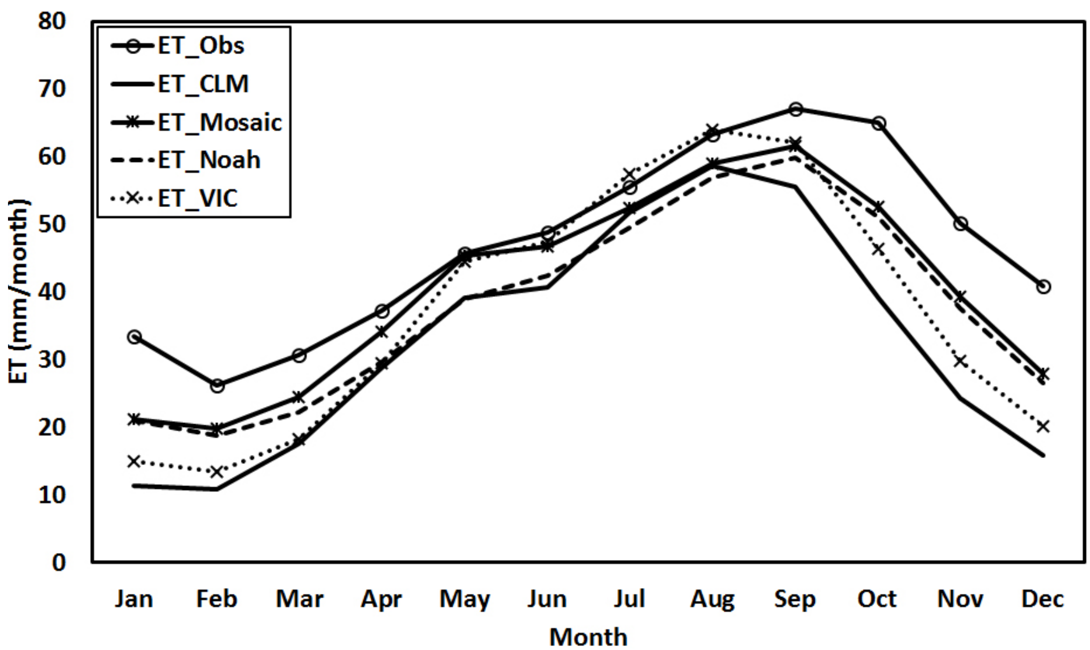

Figure 2.12 Temporal distribution of the ET over the Nile River Basin, data from corrected ET products and LSMs for the period 2002-2015.

Surface runoff

The Nile water surface flow is generated from the heavy rainfall over the equatorial lakes and East Ethiopia. Nile flow is most critical water component to all riparian nations. The surface runoff over the Equatorial lake display a unimodal flow over the year, meanwhile, the Blue Nile Basin display bimodal flow. The Global Runoff Data Centre (GRDC) provide the most accepted surface runoff grids worldwide. The GRDC data is an international archive of data up to 200 years old of unique collection of river discharge data collected at daily or monthly intervals from more than 9,200 stations in 160 countries. The GRDC operates under the supervision of the World Meteorological Organisation (WMO) and maintained by the German Federal Institute of Hydrology (Bundesanstalt für Gewässerkunde or BfG). The GRDC provide about thirteen surface runoff stations over the Nile Basin (table 2.1).

Table 2.1 Summary of the GRDC gauging stations over the Nile Basin (Source: (GRDC, 2015)

Name	Data scale	River Name	Country	Start Month	Start Year	End Month	End Year	MeanQ[m3/s]
el Ekhsase	Monthly	Nile	EG	1	1973	12	1984	1251.33
Aswan Dam	Monthly	Nile	EG	7	1869	12	1984	2759.84
Paara	Monthly	Victoria	UG	1	1948	12	1970	946.01
Owen Reservoir	Monthly	Victoria	UG	1	1973	12	1982	1175.92
Dongola	Monthly	Nile	SU	1	1912	12	1984	2621.89
Khartoum	Monthly	Blue Nile	SU	1	1900	12	1982	1512.81
Roseires Dam	Monthly	Blue Nile	SU	1	1912	12	1982	1548.42
Kilo 3	Monthly	Atbara	SU	1	1912	12	1982	358.55
Mogren	Monthly	White Nile	SU	1	1973	12	1982	897.27
Malakal	Monthly	White Nile	SU	1	1912	12	1982	938.57
Mongalla	Monthly	Bahr el Jebel	SU	1	1912	12	1982	1050.25
Kanzenze	Monthly	Nyabarongo	RW	1	1965	12	1984	109.01
Rusumo	Monthly	Kagera	RW	2	1965	12	1984	224.03

Additionally, a gridded runoff product is available at yearly scale from the same center for the period 2002-2013. Due to the limitation of the available gauging stations, the surface runoff over the basin simulated at relatively finer temporal scale using gridded observations from GRACE, GPCC and the corrected ET estimates with high correlation with eh GRDC data (figure 2.13).

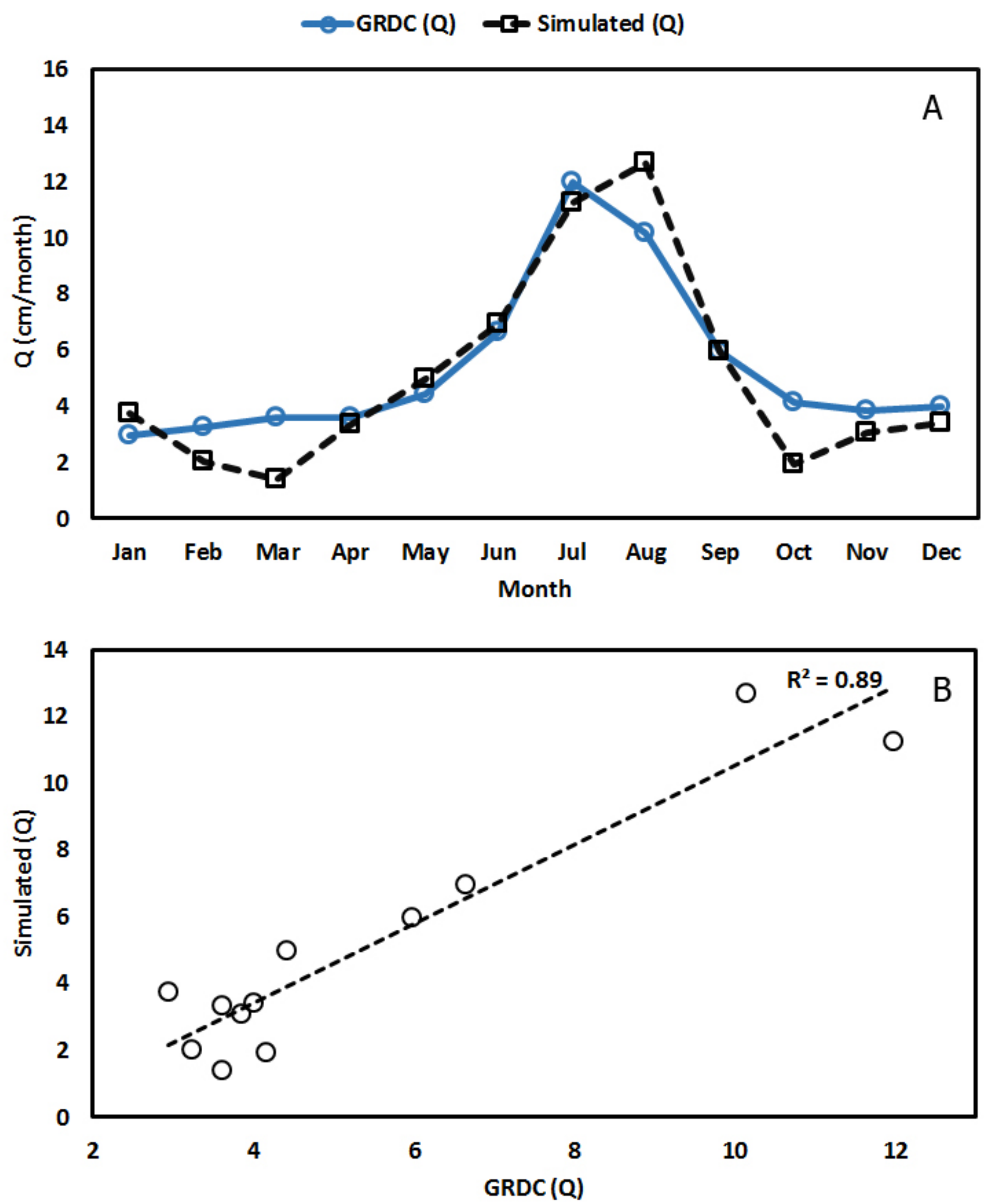

Figure 2.13 Simulated surface runoff over the Nile Basin.

Vegetation Land cover

The terrestrial vegetation is a sensitive indicator to climatic and anthropogenic influences. The Moderate Resolution Imaging Spectroradiometer (MODIS) observational data offer the opportunity to monitor and investigate large-scale changes in vegetation in response to human actions as well as climate and environmental changes. The spectral reflectance properties of plants reveal the importance of the near-infrared (NIR) region for vegetation monitoring using remote sensing observation (Ollinger, 2010). The green pigments in the leaves absorb a portion of the red and blue spectrum while reflecting the green and NIR portion of electromagnetic radiation. Based on these characteristics, impressive number remote sensing parameters were developed such as Vegetation Indices, leaf area index, the gross primary production, light use efficiency, and plant water status to provide a robust monitor tool for annual phenology changes in the plant canopy. The surface reflectance from MODIS data are implemented to determine the Normalized Difference Vegetation Index (NDVI) as follow:

$$NDVI = \frac{(NIR-Red)}{(NIR+Red)} \tag{2.2}$$

The NDVI provides consistent land cover phenology change, spatial and temporal information about vegetation. For instances, figure 2.14, represents the green biomass distribution along the Nile Basin using the mean annual NDVI data from 2002-2015. This figure shows that the green vegetation is extensively distributed along the southern and eastern parts of the basin, mainly around the water bodies and in the areas where there is a sufficient amount of rainfall. The northern part of the basin has dispersed vegetation cover due to the insufficient rainfalls. The NDVI data is highly correlated with the ET as shown in figure 2.15.

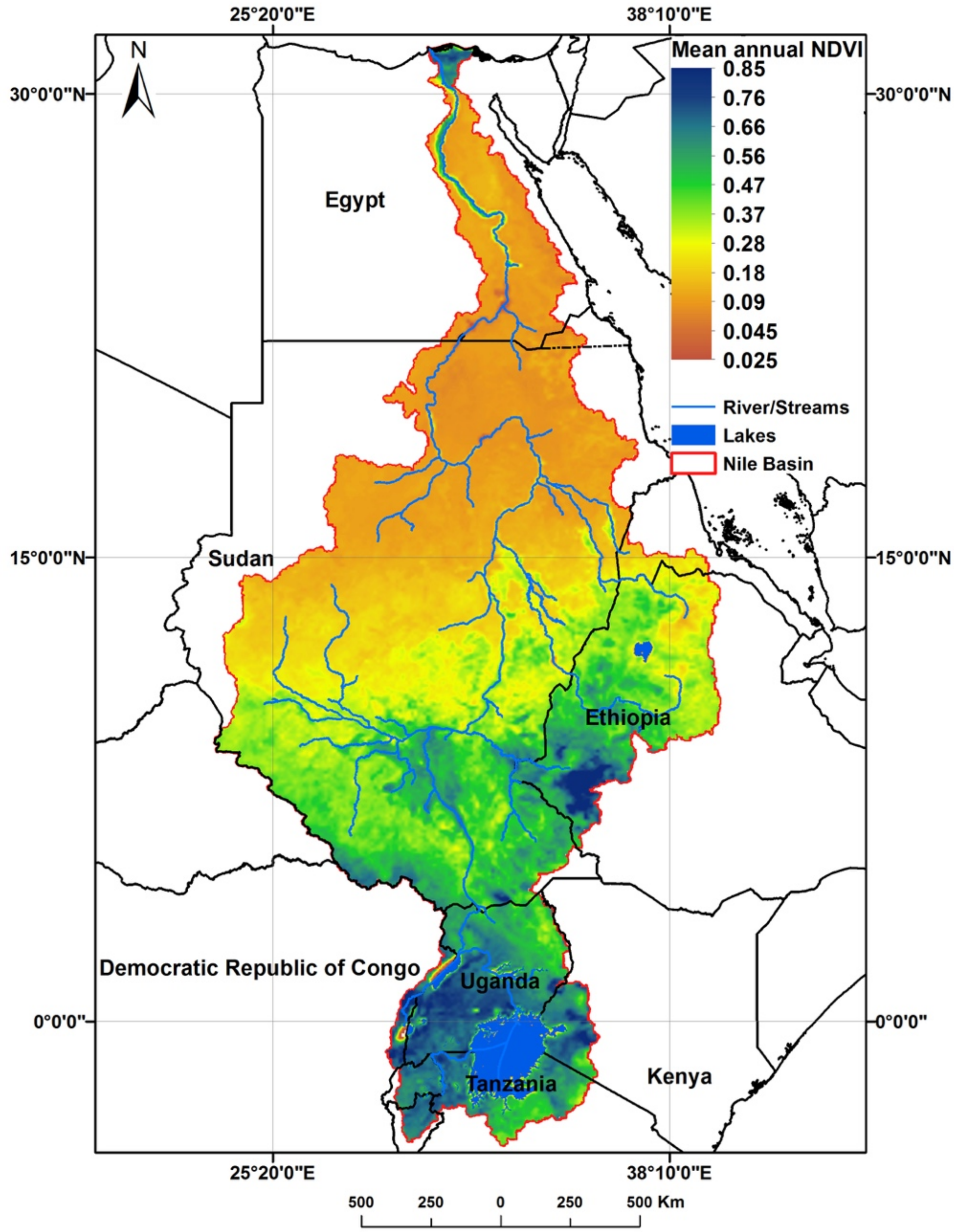

Figure 2.14 Spatial distribution of NDVI over Nile River Basin, MODIS data for the period 2002-2015.

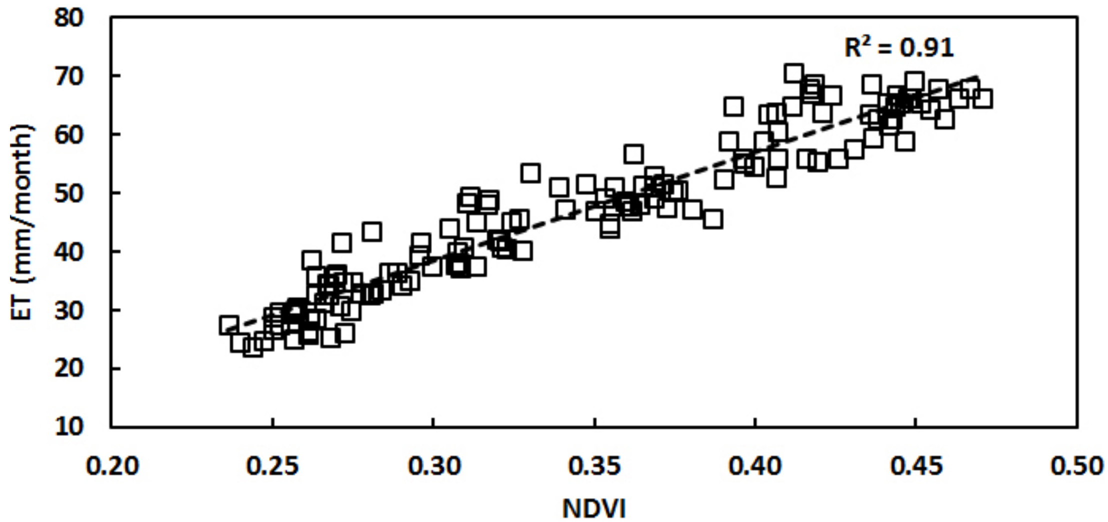

Figure 2.15 Correlation NDVI and ET over Nile River Basin.

2.4 Storage Variability

The monthly variation in the Nile water storage indicated an alternation between two main cycles during the year, the wet and dry cycle (figure 2.14). The top panel shows from left to right the relation between the storage change and precipitation, ET, runoff. The monthly storage from GRACE anomalies during the period from 2002 to 2015 has a peaks starts in August and reach to the maximum in October, while the minimum recorded in January. Meanwhile, the storage recovered potentially with precipitation, there is almost two months lag between the precipitation peak and the storage recovery. The precipitation started during May and declined after October, where the maximum precipitation peak is usually during August. The relationship between storage recovery and evapotranspiration showed that mostly both have similar pattern, where the ET peak and the storage recovery mostly at the same time. The ET is highly connected with precipitation, the maximum ET is about 70 mm during September, while the minimum is reported in February. The variation in the runoff as indicated by the relation between precipitations minus the evaporation indicated a two months lag of the storage recovery with the runoff. The surface runoff reaches to the maximum during the month August and declined in January.

The lower panel of the figure 2.16 compares the monthly variation in the storage change with the vegetation index, evaporative and the dryness indices (evaporative and dryness indices are representing the relation between the evaporation and potential evaporation that are normalized by precipitation respectively). The comparison between the storage recovery and vegetating revealed a monthly lag between each other. The vegetation replenish is highly connected to precipitation, however a relatively small lag in the peak of the vegetation, which usually incident after the precipitation occurred. The relation between the storage recovery and evaporative and dryness indices showed negative correlation, since both indices are describing limited-water yield conditions. The actual ET increased while there is enough rainfall, while the dry periods in the most of the time have the maximum peaks of the PET.

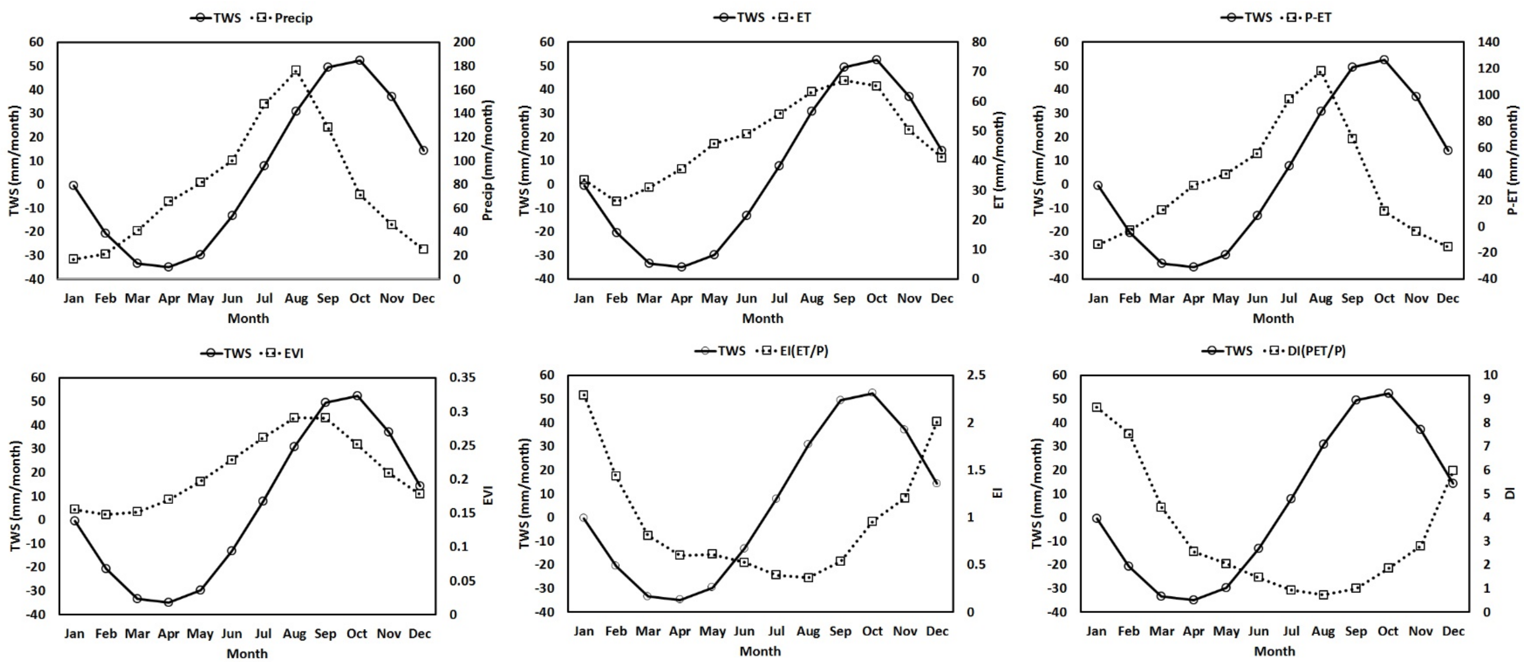

Figure 2.16 Storage variation with precipitation, ET, runoff, vegetation, evaporative and dryness index.

To determine the relationship between the storage recovery and the water stress period, the water stress index calculated as:

$$WS = \frac{PET - ET}{PET} \tag{2.3}$$

Where, WS is the water stress, PET is the potential ET, ET is the actual evaporation. Figure 2.17 indicates a high consistence between the peak of the storage recovery and the water yield period that has less stress, values greater than zero at the WS scale.

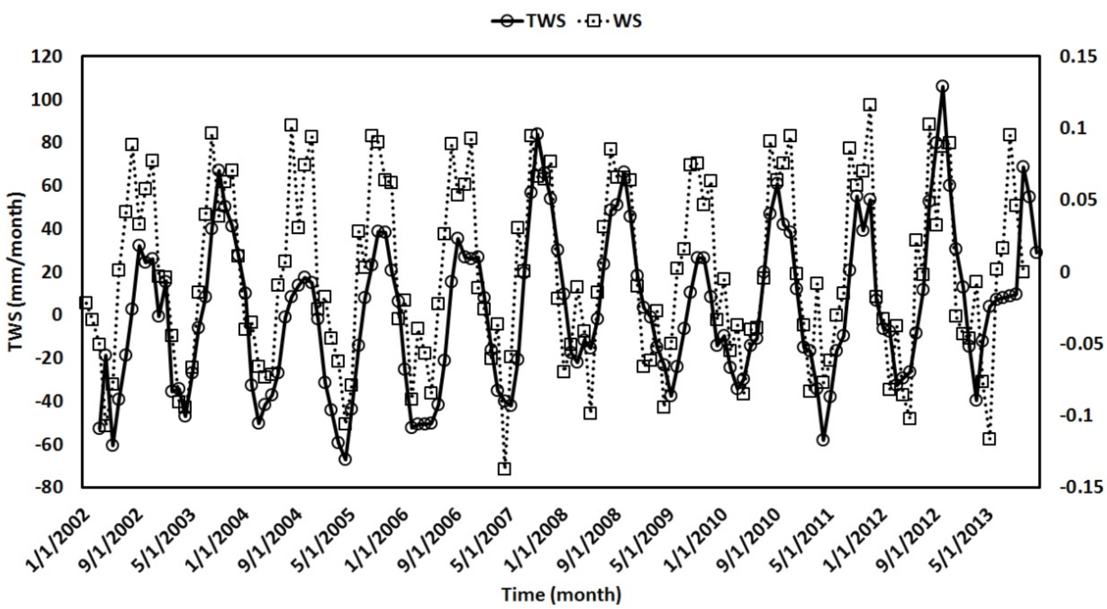

Figure 2.17 Temporal variation of the storage recovery and the water stress period over the Nile Basin for the period 2002-2015.

Based on the relation between the storage changes and different hydrological parameters, the overall storage changes ($\frac{\Delta S}{\Delta t}$) during drought events estimated to be <= – 40 mm, while during the flooding event the ($\frac{\Delta S}{\Delta t}$) was almost >= 60 mm. According to the correlation coefficient between the gridded hydrological parameters and the available observations, the uncertainty in water balance can be expressed by as following:

$$\frac{\Delta S}{\Delta t} = P \pm 20mm - ET \pm 33mm - Q \pm 12mm \tag{2.4}$$

In fact, the storage changes from the GRACE anomaly is valuable indicator that measures all changes in the water column in different forms include: surface water, ground water, and soil moisture according (Equation 2.5):

$$\Delta TWS = \Delta SW + \Delta GW + \Delta SM \tag{2.5}$$

Where, ΔTWS is the total water storage anomalies from GRACE, ΔSW is the surface water anomalies, ΔGW is the groundwater storage anomalies, and ΔSM is the soil moisture anomalies. Figure 2.18 illustrated the spatial distribution of water storage and soil moisture estimates from the CPC data set. The source areas show high rates of soil moisture and positive TWS anomalies. While, the downstream areas display low soil moisture record and negative storage.

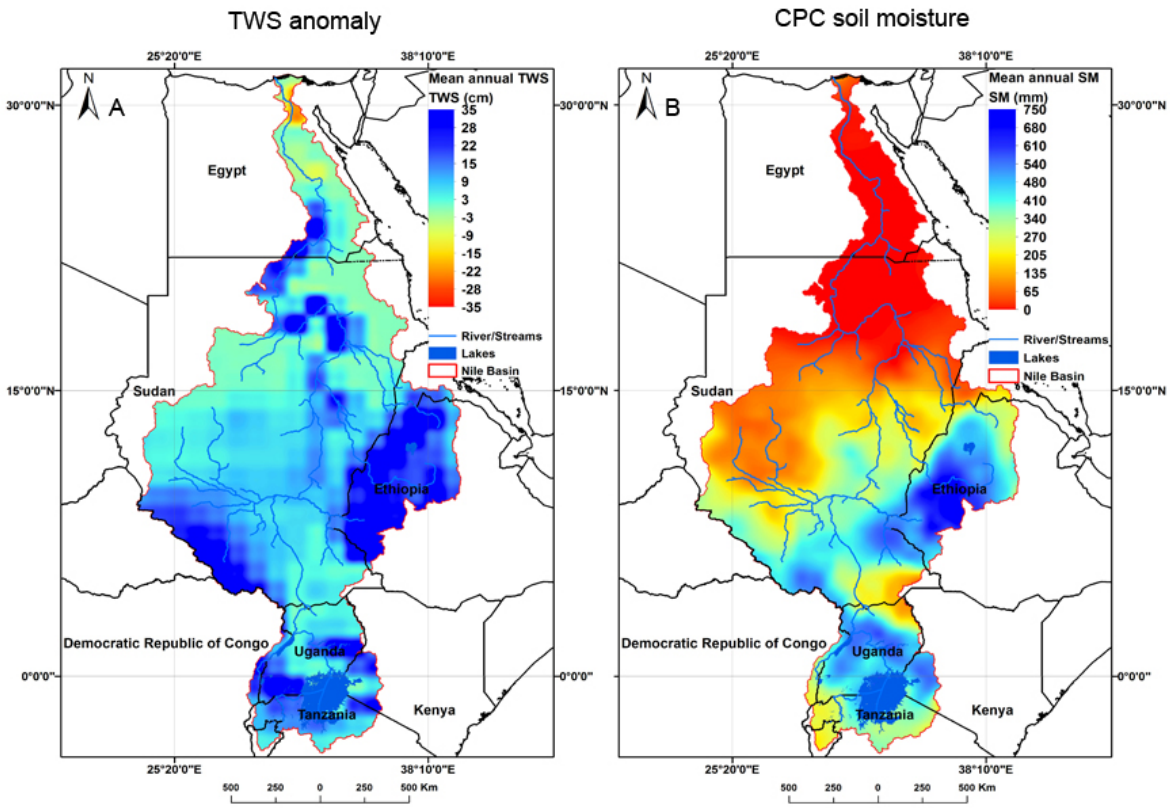

Figure 2.18 Spatial variation of the water storage and soil moisture over the Nile Basin for the period 2002-2015.

2.5 Summary and perspectives

The Nile Basin is one of largest river basin worldwide. Regarding to ground observation availability, the basin considered as a data-poor region. The Nile water resources is hindered by many factors such as, climate, the lack of information sharing, the isolation and the political conflict. The climate variability includes the variation in precipitation, temperature patterns that influence the evapotranspiration and surface runoff rates. The management of water resources is connected to the access to a reliable climate information. Remote sensing, model reanalysis and land surface models could potentially provide valuable source for hydrological monitoring data. In this research, the storage changes from GRACE satellite, GPCC precipitation data and the gridded-corrected ET were utilized to understand the water variability in the NRB. The comprehensive water balance of the basin can be written with the following uncertainty level for each term:

$$\frac{\Delta S}{\Delta t} = P \pm 20mm - ET \pm 33mm - Q \pm 12mm$$

The TWS and the gridded-based hydrological variables showed high correlations in the seasonal cycles over the basin. The maximum TWS is coinciding with the annual peak in cumulative precipitation, while the minimum TWS is connected with less precipitation amount. The ET as is highly connected with the precipitation increase and display consistent pattern with the TWS anomaly. During the growing seasons, the green biomass is relatively abundant, with higher vegetation index values. The result showed higher agreement between the vegetation abundant and rainfall timing.

Acknowledgement

The first author thanks the Institute for Study of Human Flourishing, University of Oklahoma for providing the research fund for this study in form of a PhD dissertation fellowship to the first author. Thanks goes to the Advanced Radar Research Center (ARRC), and the Hydrometrology and Remote Sensing Laboratory (HyDROS) lab at University of Oklahoma, USA for providing the research facilities, workspace and the equipment to accomplish this research.

Thanks goes to the data centers that made GRACE, remote sensing and reanalysis data sets be available and downloadable: The Goddard Earth Science Data and Information Service Centers (GES DISCs), the Climatic Research Unit at the University of East Anglia, the National Oceanic and Atmospheric Administration, Global Precipitation Climatological Center, and the Global Runoff Data Centre.

2.6 References

Ahmed, M., Sultan, M., Wahr, J. and Yan, E., 2014. The use of GRACE data to monitor natural and anthropogenic induced variations in water availability across Africa. Earth-Science Reviews, 136: 289-300.

Ahmed, M., Sultan, M., Wahr, J., Yan, E., Milewski, A., Sauck, W., Becker, R. and Welton, B., 2011. Integration of GRACE (Gravity Recovery and Climate Experiment) data with traditional data sets for a better understanding of the time-dependent water partitioning in African watersheds. Geology, 39(5): 479-482.

Alemu, H., Senay, G.B., Kaptue, A.T. and Kovalskyy, V., 2014. Evapotranspiration Variability and Its Association with Vegetation Dynamics in the Nile Basin, 2002–2011. Remote Sensing, 6: 5885-5908.

Beyene, T., Lettenmaier, D.P. and Kabat, P., 2009. Hydrologic impacts of climate change on the Nile River Basin: implications of the 2007 IPCC scenarios. Climatic Change, 100(3-4): 433-461.

Camberlin, P., 2009. Nile Basin Climates. In: H.J. Dumont (Editor), The Nile : Origin, Environments, Limnology and Human Use. Springer, Monographiae Biologicae, pp. 307-333.

Cao, Y., Nan, Z. and Cheng, G., 2015. GRACE Gravity Satellite Observations of Terrestrial Water Storage Changes for Drought Characterization in the Arid Land of Northwestern China. Remote Sensing, 7(1): 1021-1047.

Collins, R., 2002. The Nile. Yale University Press/ New Haven and London.

CRU, 2015. Climate Research Unite Data.

DFO, 2012. Dartmouth Flood Observatory

El-Quosy, D.E., 2009. Fresh Water In: M.K. Tolba and N.W. Saab (Editors), In Impact of Climate Change on Arab Countries Arab Forum for Environment and Development, Beirut.

Erian, W., Katlan, B., Ouldbedy, B., Awad, H., Zaghtity, E. and Ibrahim, S., 2012. Agriculture Drought in Africa Mediterranean and Middle East, Geneva, Switzerland.

Erlich, H., 2000. The Nile: Histories, Cultures, Myths. Lynne Rienner, Boulder, Colorado.

Flickr, 2008. Nilometer.

Flickr, 2009. Nilometer on Elephantine.

Goulden, M.C. and Conway, D., 2013. Responding to flood in the Nile Basin: A case study of the 1997-1998 flood in the Upper White Nile. In: S. Boulter, J. Palutifok, D.J. Karoly and D. Guitart (Editors), Natural Disatster and Adaptation to Climate Change. Cambridge University Press

GRDC, 2015. Long-Term Mean Monthly Discharges and Annual Characteristics of GRDC Stations. GRDC center.

Houborg, R., Rodell, M., Li, B., Reichle, R. and Zaitchik, B.F., 2012. Drought indicators based on model-assimilated Gravity Recovery and Climate Experiment (GRACE) terrestrial water storage observations. Water Resources Research, 48(7): n/a-n/a.

Kebede, S., Travi, Y., Alemayehu, T. and Marc, V., 2006. Water balance of Lake Tana and its sensitivity to fluctuations in rainfall, Blue Nile basin, Ethiopia. Journal of Hydrology, 316(1-4): 233-247.

Kieyah, J., 2007. The 1929 Nile Waters Agreement: Legal and economic analysis. Available at: http://works.bepress.com/joseph_kieyah/1.

Long, D., Scanlon, B.R., Longuevergne, L., Sun, A.Y., Fernando, D.N. and Save, H., 2013. GRACE satellite monitoring of large depletion in water storage in response to the 2011 drought in Texas. Geophysical Research Letters, 40(13): 3395-3401.

Long, D., Shen, Y., Sun, A., Hong, Y., Longuevergne, L., Yang, Y., Li, B. and Chen, L., 2014. Drought and flood monitoring for a large karst plateau in Southwest China using extended GRACE data. Remote Sensing of Environment, 155: 145-160.

Lott, F.C., P. A. Stott, D. M. Mitchell, N. Christidis, N. P. Gillett, L. Haimberger, J. Perlwitz and Thorne, P.W., 2013. Models versus radiosondes in the free atmosphere: A new detection and attribution analysis of temperature. Journal of Geophysical Research, 118: 2609-2619.

Lynas, M., 2008. Six Degrees: Our Future on a Hotter Planet. National Geographic.

Moges, S.A. and Gebremichael, M., 2014. Climate Change Impacts and Development-Based Adaptation Pathway to the Nile River Basin. In: A.M.M.e. al. (Editor), Nile River Basin. Springer International Publishing Switzerland.

NBI, 2010. Key facts about the Nile basin. Nile Basin Initiative (NBI), Entebbe. http://www.nilebasin.org/newsite/index. Accessed 19th December 2012.

NBI, 2012. State of River Nile Basin 2012. Nile Basin Initiative (NBI), Entebbe.

NBI, 2016. The Nile Basin Water Resources Atlas. NBI: Nile Basin Initiative

Niang, I., Ruppel, O.C., Abdrabo, M.A., Essel, A., Lennard, C., J. Padgham and Urquhart, P., 2014. Africa. In: Climate Change 2014: Impacts, Adaptation, and Vulnerability. Part B: Regional Aspects. Contribution of Working Group II to the

Fifth Assessment Report of the Intergovernmental Panel on Climate Change. In: V.R. Barros, C.B. Field, D.J. Dokken, M.D. Mastrandrea, K.J. Mach, T.E. Bilir, M. Chatterjee, K.L. Ebi, Y.O. Estrada, R.C. Genova, B. Girma, E.S. Kissel, A.N. Levy, S. MacCracken, P.R. Mastrandrea and L.L. White (Editors). Cambridge University Press, Cambridge, United Kingdom and New York, NY, USA, pp. 1199-1265.

NIS, 2012a. Climate Change and its Implications for the Nile Region:Chapter 8.

NIS, 2012b. Nile Basin Evapotranspiration.

Oestigaard, T., 2010. Nile Issues, Small Streams from the Nile Basin Research Programme. Fountain Publishers, Kampala-Uganda.

Ollinger, S.V., 2010. Tansley review. Sources of variability in canopy reflectance and the convergent properties of plants. New Phytologist

Rui, H., 2011. Global Land Data Assimilation System Version 1 (GLDAS-1) Products: README Document.

Said, R., 1981. The geological evolution of the River Nile. Springerverleg.

Salama, R.B., 1987 The evolution of the River Nile. The buried saline rift lakes in Sudan. Journal African Earth Sciences 6(6): 899-913.

Salama, R.B., 1997. Rift basins of Sudan. African basins, Sedimentary basins of the World. 3. Elsevier, Amsterdam.

Schneider, U., Becker, A., Meyer-Christoffer, A., Ziese, M. and Rudolf, B., 2011. Global Precipitation Analysis Products of the GPCC, Deutscher Wetterdienst, Offenbach a. M., Germany.

WB, 2016. The World Bank: Global population data.

UNEP, 2013. Adaptation to Climate-change Induced Water Stress in the Nile Basin A Vulnerability Assessment Report.

UNISDR, 2011. Global Assessment Report on Disaster Risk Reduction, Geneva, Switzerland: United Nations International Strategy for Disaster Reduction.

Vijverberg, J., Sibbing, F.A. and Dejen, E., 2009. Lake Tana: Source of the Blue Nile. Nile: Origin, Environments, Limnology and Human Use. Springer Science + Business Media B.V. 2009.

Chapter 3: Response of Nile river flow to the climate change

Abstract

This chapter addresses how the temporal variability in precipitation (P) and temperature (T) could affect the surface runoff (Q) in the Nile Basin. The monthly gauge-corrected precipitation, temperature and potential ET (ET_o) grids products from the Climate Research Unite (CRU) at University of East Anglia (UEA) are utilized to assess the surface runoff elasticity to precipitation (ε_p), potential ET ($\varepsilon_{ET\circ}$), and temperature (ε_T) from 1981-2013. The Nile Basin classified into three main climate zones, the tropical subtropical climates, the semiarid and the arid zone. Using Budyko Curve illustration, the (ε_p) calculated for each climate zone and for the basin average. Additionally, the ($\varepsilon_{ET\circ}$), and (ε_T) are calculated based on functional forms introduced by Arora 2002, and Pike 1964. The results of runoff elasticity to precipitation (ε_p) for the tropical-subtropical zone showed at 10 percent increase in precipitation the runoff expected to increase by 20 percent. As gradually moved to the arid zone the runoff recovered by 3 percent at 10 percent increase in precipitation. As the temperature decreases by (-0.5°C) for the tropical-subtropical zone, the surface runoff will increase by 5 percent. Accordingly, the runoff elasticity to potential ET ranging from (-0.52 to -1.70) for the tropical-subtropical to the arid zone. Generally, the runoff elasticity to precipitation that greater than 1

describes an elastic system (resilient to climate change). Therefore, the subtropical-tropical region in the Nile Basin can be considered as resilient under the current climate conditions compared with the other climate zone in the basin.

Keywords: Nile River Basin, Runoff, elasticity, climate change

3.1 Introduction

The shared water resources in the Nile River Basin (NRB) is substantially vulnerable to water-stress under climate change. The temporal variability in precipitation (P) and temperature (T) likely influence the rate of surface water flow (Q). According to the Representative Concentration Pathways (RCPs) scenarios, IPCC 2014, the projected increase in the mean surface temperature over the Nile Basin by the end of the 21st century (2081–2100) likely to be 2°C as the RCP2.6 scenario designated. Other varied projections were suggested by the RCP4.5, RCP6.0, and the RCP8.5 (i.e. temperature will increase according to each scenario by 2.6°C, 3.5°C, or by 4.0°C respectively). Additionally, each scenario has a unique perspective for the projected precipitation. For instance, the RCP2.6 indicated that the Nile Basin will experience an increase in the precipitation rates by 14 percent, while, the RCP8.5, the worst case scenario, projected the precipitation to likely decreases by 15 percent (IPCC, 2014).

The wide range of uncertainty of these projections gave no clear indications of how certainly the river flow would be affected by climate change (i.e. no assurance whether the flow will increase or diminish since there is no certain climate scenarios) (Conway, 2005). Nevertheless, any fluctuation in precipitation rates (increase or decrease) and the future surges of temperature trends will certainly influence the surface water flow of the Nile Basin. In addition, the seal level rise, which is another serious concern, could adversely affect the Nile Delta region in Egypt, the main coastal area in basin downstream country (Hasan et al., 2015a). However, the riparian nations are incompetent to mitigate with such intimidations. Owing to the insufficient joint adaption measures and the lack of information sharing culture, the basin communities are threatening by and unable to cope with the negative climate variability. Meanwhile, projection change will exacerbate the human induce on land cover and will rise the pressure on the basin's natural resources.

The Nile River basin exhibits varied climates, spatiotemporal variability in precipitation and temperatures. The basin can be generally classified into three main climate zones: the tropical-subtropical zone, the semiarid, and the arid zone. Each zone is characterized by distinct rates of precipitation and remarkable range of vegetation cover as indicated by the Normalized Difference Vegetation Index (NDVI) from Moderate Resolution Imaging Spectroradiometer (MODIS) (figure 3.1). The tropical-subtropical climates characterized by overwhelming precipitation that contribute substantially to the river flow. The semiarid zone however receives significant amount of seasonal precipitation, this zone characterized by large inter-annual variability and less contribution to the river flow due to the loss of water to the atmosphere by the high evaporation rates. The arid zone is mostly described as desert area with little to no rainfalls and no to less contribution of water to the basin flow. Examining how the seasonal variability in precipitation and temperature governing the water balance in the basin and significantly affecting the water flow is highly linked with sufficient inputs od spatial information. To date, the gap in ground observations over the basin is notorious, and the corporation between riparian nations is hurdled by institutional bureaucracies and ineffective policies. While the basin population is projected to increase significantly that emerging increase in water demands. Unless establishes a framework of corporation, the basin communities are threatened and are unable to mitigate with the possible changes of the Nile flow.

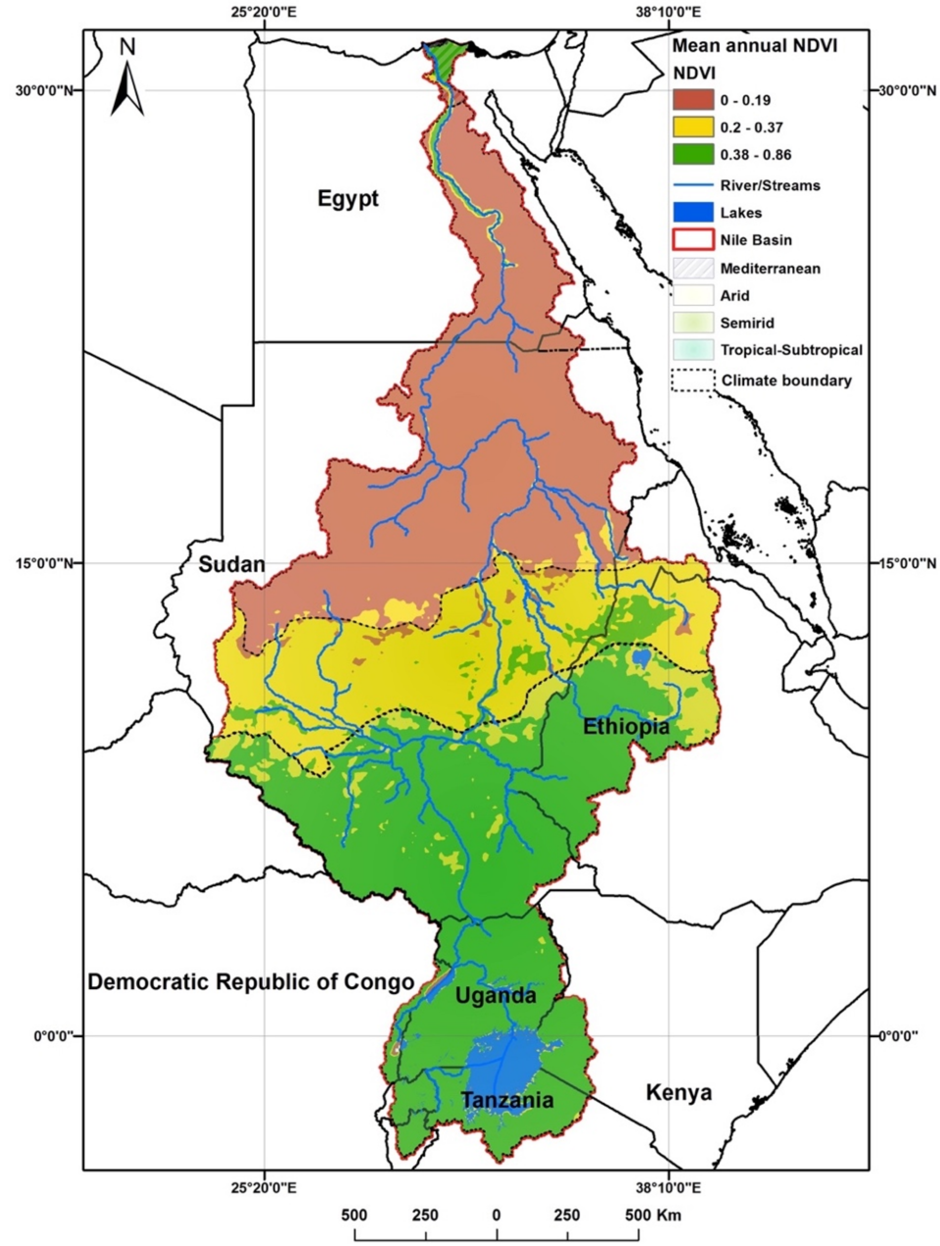

Figure 3.1 Nile Basin climate zones indicated by the Normalized Difference Vegetation Index (NDVI).

Water-energy balance and Budyko Curve

Partitioning of precipitation to evapotranspiration and runoff is controlled by the available energy. According to Arora (2002), the energy, which better expressed by the potential evapotranspiration, and the precipitation, both are controlling the rates annual flow (Arora, 2002). The ratio between potential evapotranspiration and precipitation (aridity/dryness index), and the ratio between the actual evapotranspiration and precipitation (evaporative index), could be utilized to determine the water yield and surface runoff rates according to Budyko Curve (Budyko, 1974). The Budyko Curve depicts the relation between actual evapotranspiration (ET) and potential (ET_o) both are normalized by precipitation to determine the potential water yield, and runoff for any catchment (Creed et al., 2014).

The Budyko curve illustrates three main characteristics: 1- the water limits, 2- the energy-limits, and 3- the transition from the energy constrain to water constrain conditions (figure 3.2). For instance, when the actual ET equals precipitation, this represents the water limits, where a site cannot be plotted above this limit unless there is an additional input beyond the precipitation. When the potential ET_o equals precipitation that means that the basin/watershed ready to move from energy-limit conditions to the state where the water/moisture become so limited, the basin at this point falls in the energy-limit conditions. When the actual ET equals the potential ET, this mainly represented by the energy-limits, the plot cannot exceed the energy-limits unless the precipitation is being lost to groundwater in the system.

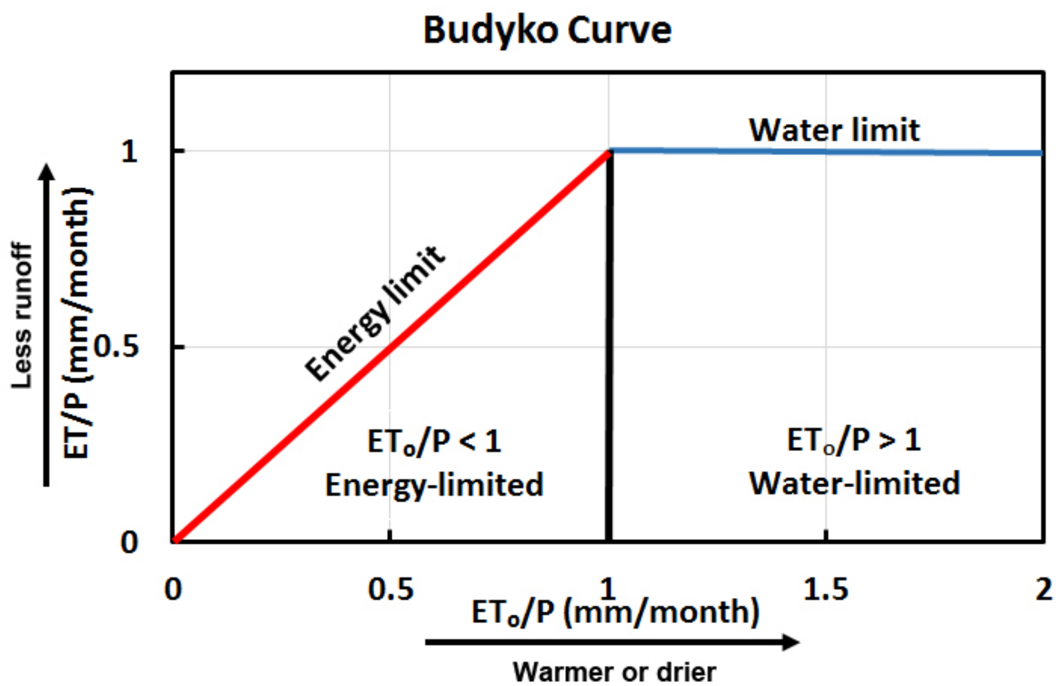

Figure 3.2 Illustration of Budyko curve.

Budyko curve has been utilized in various studies to provide a reference of the water balance condition for any watershed/catchment (Arora, 2002; Creed et al., 2014; Di Baldassarre et al., 2011; van der Velde et al., 2014). Thru Budyko curve, the catchment responsivity (resistance) can be measured from the deviation in the evaporative index. And the catchment water yield elasticity (resilience) to changing climatic conditions can be measured as a ratio of deviations in dryness index to evaporative index. The long deviation in the evaporative index described lower elasticity that results in less resilient and longer recovery times in water yields.

Objectives

This chapter discusses the sensitivity of the Nile River flow to the changes in precipitation and temperature. The functional forms introduced by (Arora, 2002; Grijsen et al., 2013; Pike, 1964), and the Budyko framework (Budyko, 1974) were utilized to assess how the fluctuation in precipitation and temperature could influence the surface runoff over different climate zones across the Nile Basin. Meanwhile, the Nile Basin is characterized by very uneven distribution of water resources over distinct hydrologic-climate zones.

The main objective of this chapter is to: assess how each climate zone will response to climate variability as manifested by precipitation and temperature changes. This chapter highlighted the water availability especially for the downstream riparians thru an effective robust approach that will allow water managers in the region to understand the state of water resources over the basin. This chapter is arranged in four main sections: section 3.2 about the data set and methodology, section 3.3 about the results and discussion, finally section 3.4 is a conclusion and remarks.

3.2 Data sets and methodology

Giving that the amount of operational gauging and monitoring stations (*in-situ*) information is limited, several hydrological monitoring grids and satellite observations were utilized. For long-term climate analysis, the gauge corrected precipitation grids, the temperature and the Potential ET_o estimates from the Climate Research Unite (CRU) at University of East Anglia (UEA) at 0.5° resolution grids between year 1981-2013 (CRU, 2015) were utilized. A 0.5° satellite actual ET data cover the period from 1981-2013 were implemented. The ET gridded product for the period from (1981-2013) derived according to a method introduced by (Zhang et al., 2010). Other gridded data sets at different temporal and spatial resolution were also implemented such as: The monthly Gravity Recovery Climate Experiment (GRACE) satellite data from (2002-2015) and at 1° grids from the Center of Space Research (CSR) at University of Texas Austin, (RL05 Products, Release-05 Level-2), the data processed according to (Swenson and Wahr, 2006). The annually gauge-corrected surface runoff estimates from 2002-2012 acquired from the Global Runoff Data Center (GRDC) at 0.5° resolution (Fekete et al., 2002). By combining the records from temperature, precipitation, potential ET and actual ET over the basin, mean annual average maps were constructed for each variables with their overall anomaly trends as shown in figure 3.3.

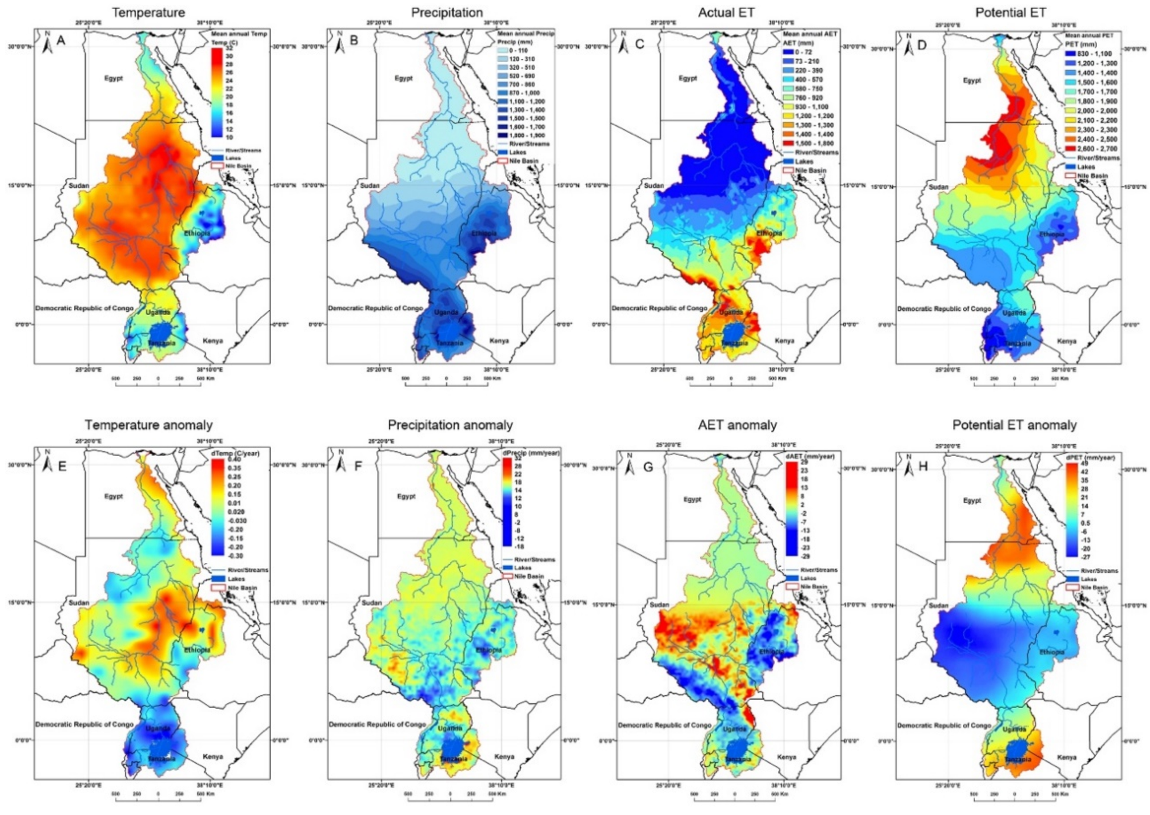

Figure 3.3 Averages and trends of temperature, precipitation, actual and potential ET, across the Nile basin for the period 1981–2013.

The changes in the runoff rates to the climate conditions can be defined using the runoff elasticity (ε). The elasticity evaluates the ability of the system to resilient and restore its initial conditions upon certain changes. In this paper, we measured the surface runoff elasticity thru illustration of Budyko Curve (Budyko, 1974), and number of functional forms modified after (Arora, 2002; Budyko, 1974; Creed et al., 2014; Hargreaves and Samani, 1985; Pike, 1964; van der Velde et al., 2014). Using the ratio between actual (ET) and precipitation, evaporative index (EI). (Equation 3.1), and ratio between the potential (ET_o) and precipitation, dryness index (DI). (Equation 3.2), the Budyko Curve can be illustrated demonstrated. The rate changes in the (DI) to the rate of changes in the (EI) can indicate the (ε) of the system as shown in Equation 3.3.

$$EI = \frac{ET}{P}, \tag{3.1}$$

$$AI = \frac{ET_o}{P}, \tag{3.2}$$

$$\varepsilon = \frac{\Delta\, AI}{\Delta\, EI}, \tag{3.3}$$

According to Arora (2002), the changes in surface runoff can be expressed as a function of the changes in the precipitation (ΔP) minus the changes in potential ET (ΔET_o) as follow:

$$\frac{\Delta Q}{Q} = \frac{\Delta P}{P}\,(1+\beta) - \frac{\Delta ET_o}{ET_o}\,\beta, \tag{3.4}$$

Where the coefficient β is the sensitivity index, this index implies larger changes in the runoff based on the changes in the precipitation and potential ET. The value of the coefficient β is proportionally positive to the aridity index (Arora, 2002). At best practice, we calculated the coefficient β for each climate zone according to (van der Velde et al., 2014) as:

$$\beta = \sqrt{((\frac{\Delta ET.\ \bar{P} - \overline{\Delta ET}\ .\ \Delta P}{\overline{P^2}})^2 + (\frac{\Delta ET_O.\ \bar{P} - \overline{\Delta ET_O}\ .\ \Delta P}{\overline{P^2}})^2)}, \tag{3.5}$$

The surface runoff in the tropical and subtropical zone will be solely controlled by the changes in the precipitation therefore Equation (3.1) can be rewritten as:

$$\frac{\Delta Q}{Q} = \frac{\Delta P}{P}\ (1 + \beta), \tag{3.6}$$

Therefore the surface runoff elasticity to precipitation (ε_p) can be calculated as:

$$\varepsilon_p = \frac{\left[\frac{\Delta Q}{Q}\right]}{\left[\frac{\Delta P}{P}\right]} = 1 + \beta, \tag{3.7}$$

Equation (3.4) is most applicable to calculate the surface runoff elasticity to precipitation in tropical-subtropical climate zones where there is a sufficient input of precipitation.

Next, the surface runoff elasticity to potential ET, ($\varepsilon_{ET\circ}$), can be calculated as

$$\varepsilon_{ET\circ} = \frac{\left[\frac{\Delta Q}{Q}\right]}{\left[\frac{\Delta ET_O}{ET_O}\right]} = -\beta, \tag{3.8}$$

Finally, the surface run off elasticity to temperature can be calculated as:

$$\varepsilon_{ET_\circ} = \frac{\left[\frac{\Delta Q}{Q}\right]}{\left[\frac{\Delta T}{T}\right]} = -0.60 \times \beta, \tag{3.9}$$

Equation 3.6 is derived based on (Hargreaves and Samni, 1982). Table 3.1 Summaries the main functional forms.

Table 3.1 Summary of the mathematical forms

Functional forms	Equation name	Reference
$\boldsymbol{AI = ET_o/P}$,	Aridity Index (AI),	
$\boldsymbol{EI = ET/P}$	evaporative indices, (EI)	(Budyko, 1974)
$\boldsymbol{\varepsilon = [\Delta AI]/[\Delta EI]}$	Elasticity	(Creed et al., 2014)
$\boldsymbol{\beta = [\varphi F'(\varphi)]/[1 - \varphi F'(\varphi)]}$	Sensitivity coefficient	(Arora, 2002)
$\boldsymbol{Q/P = 1 - ET/P}$	Runoff coefficient	(Grijsen et al., 2013)

Based on the water balance direct approach stated in Equation 3.10, the surface runoff over the Nile basin has been simulated for the period from 2002 to 2015.

$$\frac{\Delta S}{\Delta t} = P - ET - Q, \tag{3.10}$$

The changes in storage $\frac{\Delta S}{\Delta t}$ estimated using GRACE total water storage anomalies (TWSA) data according to (Syed et al., 2008).

3.3 Nile Basin climates

The climate zones across the Nile Basin displayed distinct characteristics of precipitation, temperature and evapotranspiration, and potentially distinct pattern of runoff figure 3.4 The tropical-subtropical zone where the upstream countries lie, receive high amounts of rainfall annually that exceeds the 1000 mm/y (Hassenforder and Noury, 2015; Karyabwite, 2000). The downstream countries, Sudan and Egypt, lie on arid to semiarid zone with rainfall rates that less than 150 mm/y. The temperature regionally controls the climate pattern and the circulation of drastic changes across the basin (Lynas, 2008). The Nile Basin witnesses higher temperature rates along the arid and semiarid region compared with the tropical and subtropical zones (figure 3.4B) (Camberlin, 2009). Increase of surface temperature releases more water to the atmosphere thru evapotranspiration. Resulting in in less water flow and moving the basin from energy-constrained to moisture-constrained region (NIS, 2012a).

Hence, the evapotranspiration is crucial water cycle component, it accounts for the water circulation from plants and soil surfaces to the atmosphere. Meanwhile, potential (ET_o) measures amount of water evaporated under sufficient water supplies, the actual (ET) measures the evaporated water under limited supply (Allen et al., 1998). Across the Nile region, the spatial and temporal trends of (ET_o) and (ET) vary considerably (figure 3.3). For the semiarid and arid zones, the potential (ET_o) rates compared to tropical zone (figure 3.4C). The evapotranspiration is responsible for significant water loss in the basin and affect the rates of water flow (Collins, 2002).

The surface runoff is a function of rainfall, potential evapotranspiration, land-cover, and the basin topography. Accordingly, the water flow profile varied for different places along the course of the Nile Basin. The runoff is highly influenced by the climate variability especially the ENSO event (Eltahir, 1996). Meanwhile, the future developments of rainfall patterns over the Nile Basin remain uncertain, the consequences of climatic change on the surface runoff and the water availability is significant (Camberlin, 2009; NIS, 2012a). Depends on the climate regions, the riparian states contribute unequally to the Nile water flow. For instance, the Blue Nile Basin in Ethiopia provides about 76 percent of the Nile's water with bimodal flow during the year. The White Nile Basin contributes about 24 percent of the Nile water flow with consisting flow rate during the year (Collins, 2002).

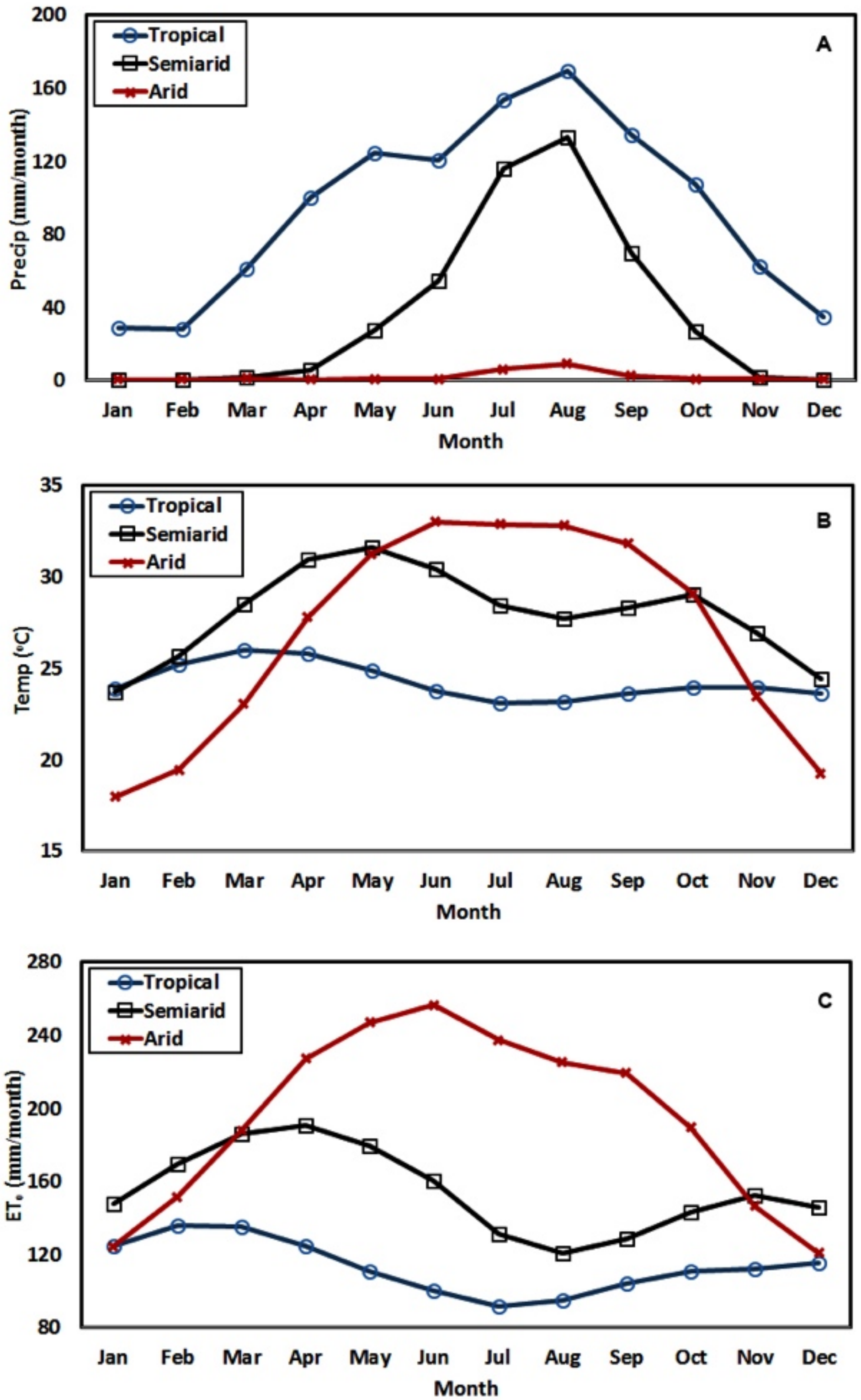

Figure 3.4 Precipitation, temperature, and potential ET estimates over different climate zones in the Nile Basin.

3.4 Results and discussion

The monthly precipitation estimates from the CRU data showed high agreement when compared with other gauge-corrected grids from the Global Precipitation (GPCC) (Schneider et al., 2011). Additionally, the CRU precipitation data displayed similar consistent pattern when compared with the research product from Tropical Rainfall Measuring Mission (TRMM- 3B42-V7) figure 3.5.

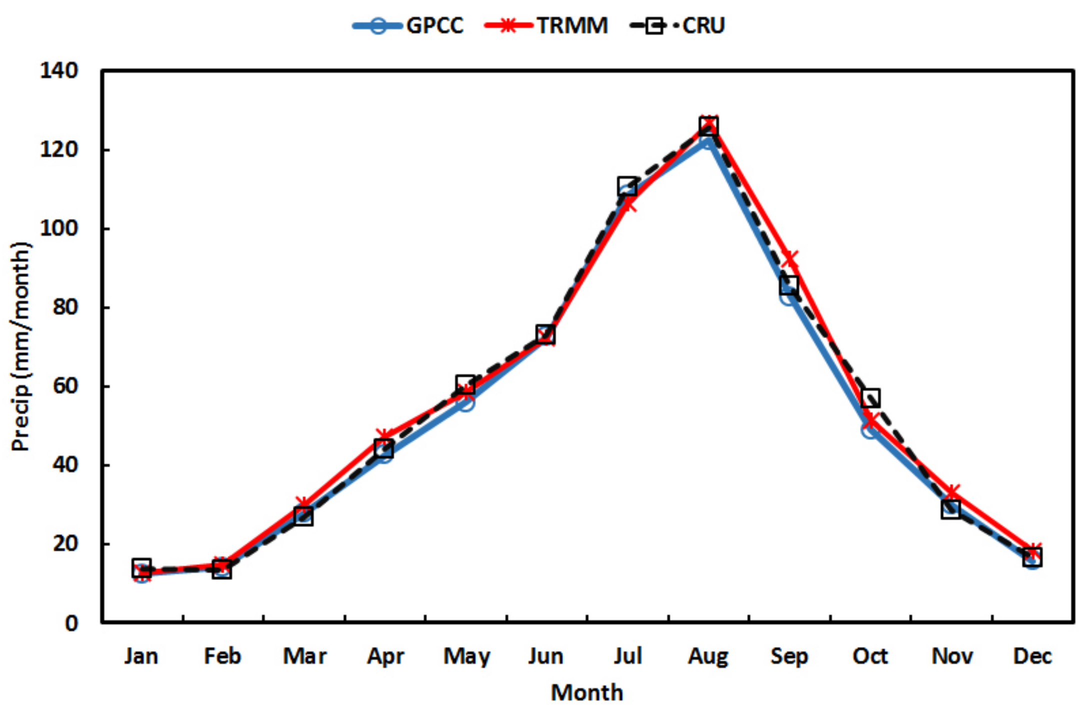

Figure 3.5 Monthly precipitation products from CRU, GPCC and TRMM data over the Nile Basin (data from 1998-2013).

Over the period from 1981-2013, the precipitation shows slightly positive trends with some spikes and other flat periods (figure 3.6).

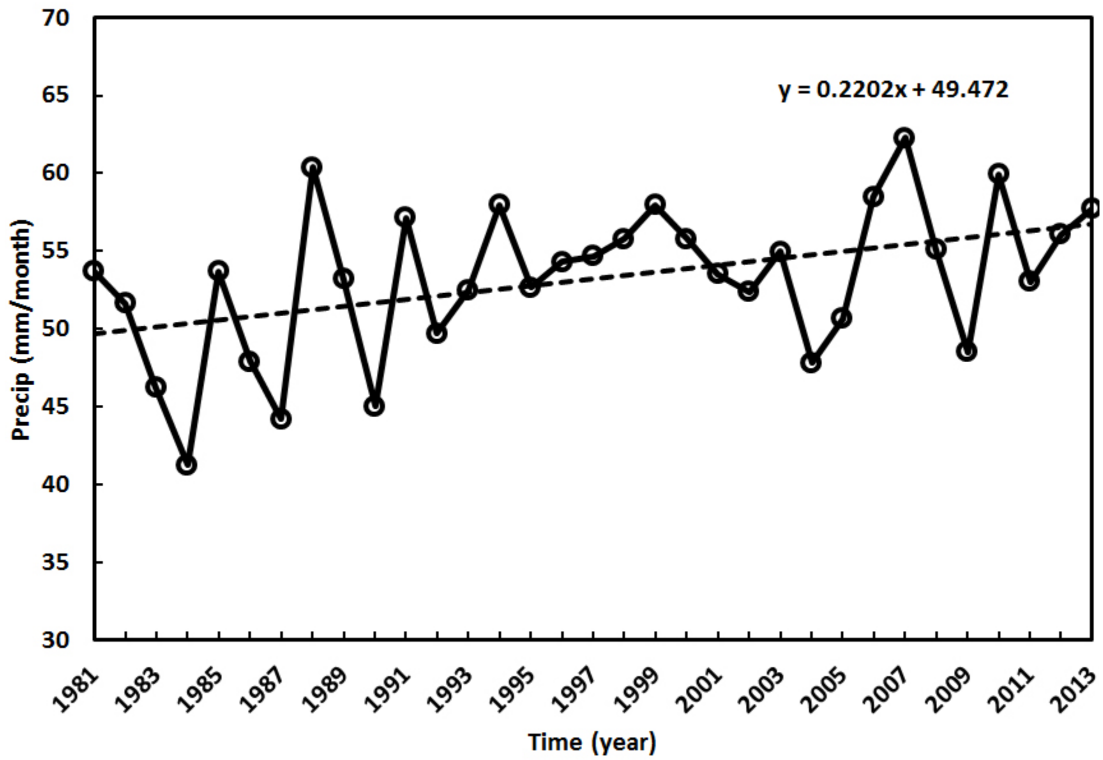

Figure 3.6 The precipitation trends over the Nile Basin from 1981-2013.

Comparing the precipitation trends to the monthly temperature trends over the same period, the data showing relatively more steep positive trends with of about 2°C increase (figure 3.7).

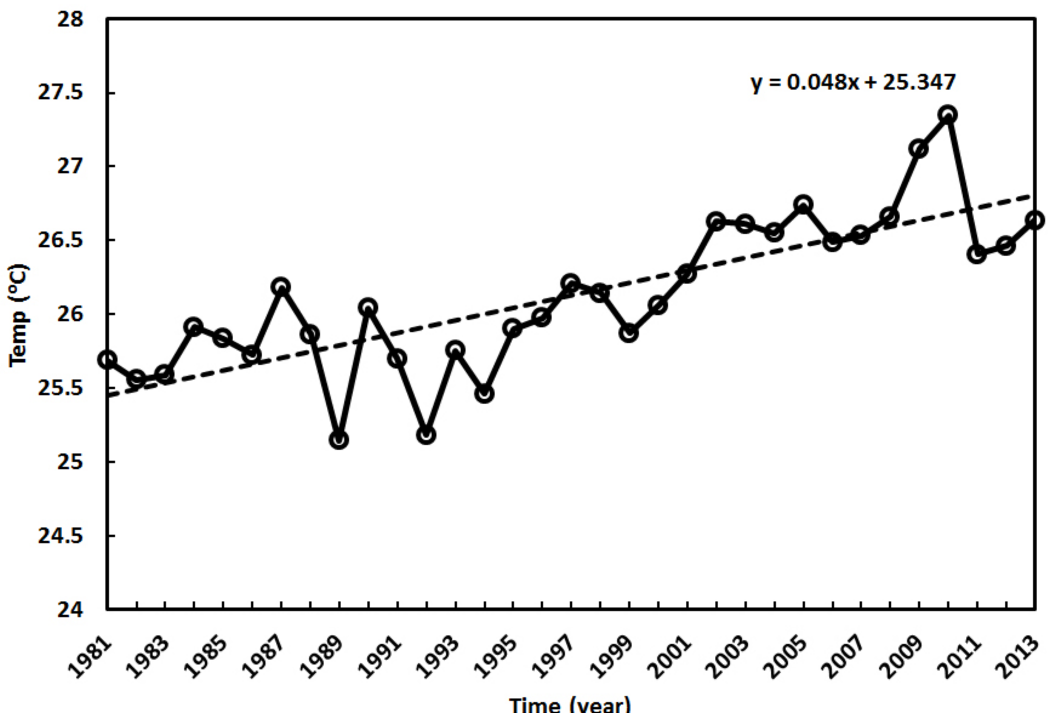

Figure 3.7 The temperature trends over the Nile Basin from 1981-2013.

The potential (ET_o) trends is highly proportionally with the temperature trends over time, the data shows similar steep trend of the potential (ET_o), figure 3.8.

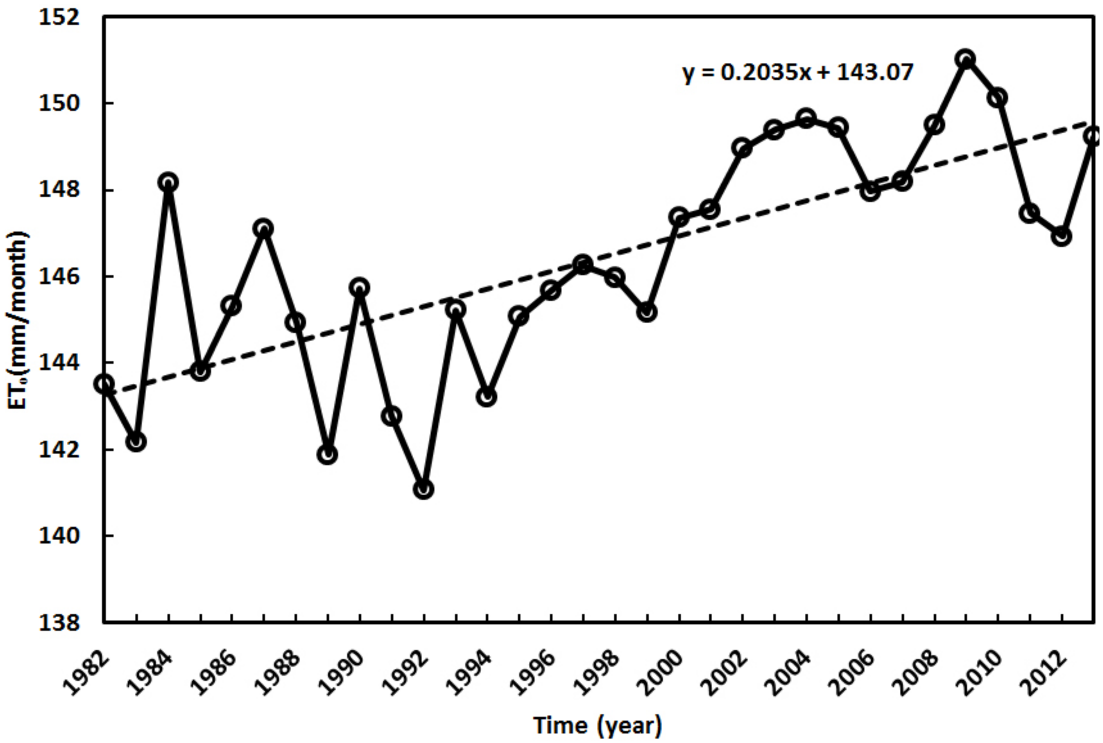

Figure 3.8 The potential (ET_o) trends over the Nile Basin from 1981-2013.

Using the simulated surface runoff records that only covers the period from (2002-2103) based on the introduced in equation 10. However, the simulated runoff record not covers the full time period from (1981-2013), the data still displays a consistent result with the previous trends of precipitation and temperature. Meanwhile, the temperature record showed a steady increase in corresponding time period to the simulated runoff the data, the over-all surface runoff trends is slightly plunging down (figure 3.9A). The correlation between the simulated runoff and the GRDC runoff estimates showed a correlation coefficient of 0.89 and P-value of 0.001 (figure 3.9B).

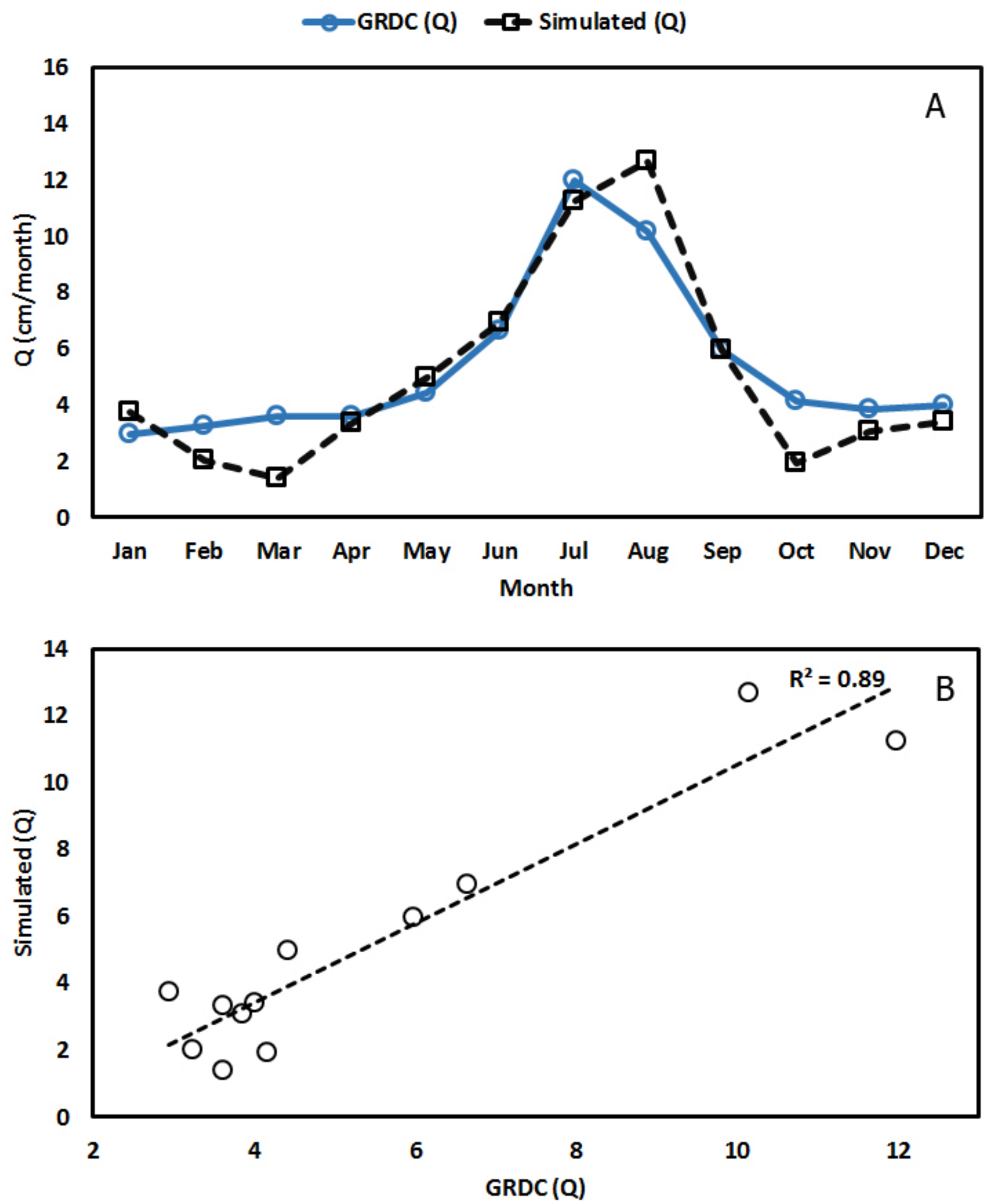

Figure 3.9 Simulated and observed GRDC surface runoff over the Nile Basin. (A) The annual surface runoff variation, (B) The correlation between the simulated and the observed runoff with $R^2 = 0.89$ and P value = 0.001

According to (Gleick, 1991), any increases in temperature will slightly decreases the precipitation rate and will substantial decreases the Nile water flow. Remarkably notice that the precipitation, temperature and runoff trends have dramatic trend year 2009. Where, temperature records showed high trend that associated with major decline in less precipitation and runoff flow (figure 3.10). The main attributed factor to this result is the major La Nino event that hit blue Nile Basin and caused a severe drought (Zaroug et al., 2014).

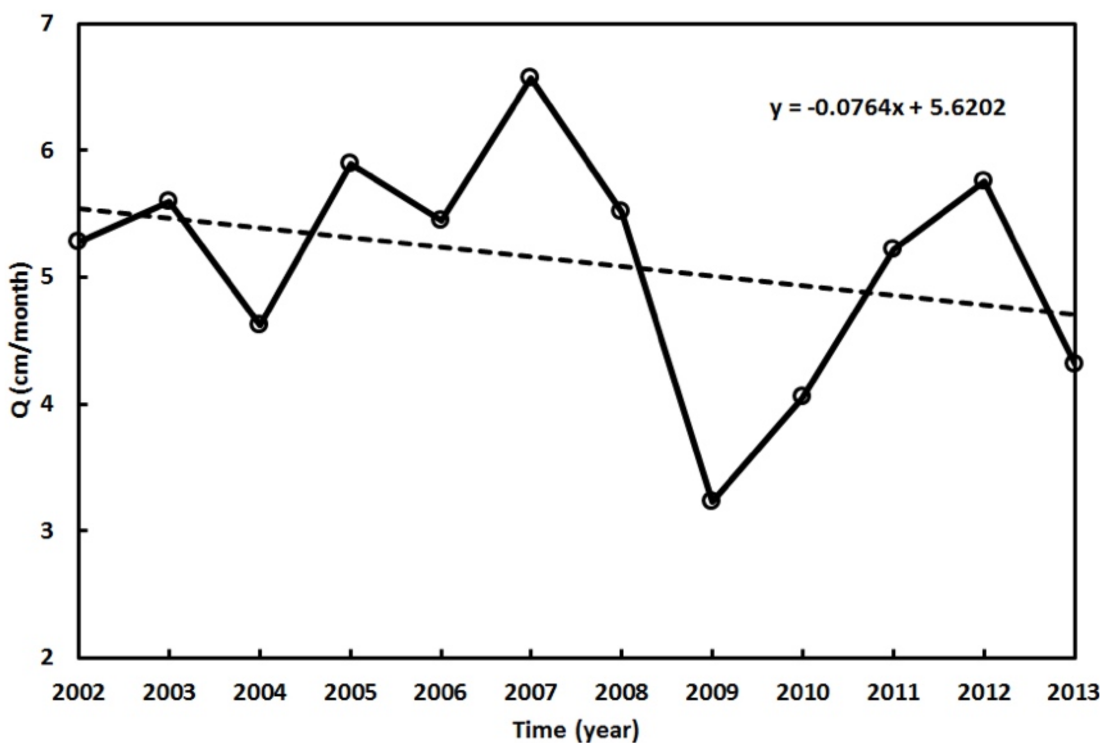

Figure 3.10 Simulated surface runoff over the Nile Basin.

The gridded product of the mean annual simulated surface runoff showed in figure 3.11 along with mean annual runoff from the GRDC data set.

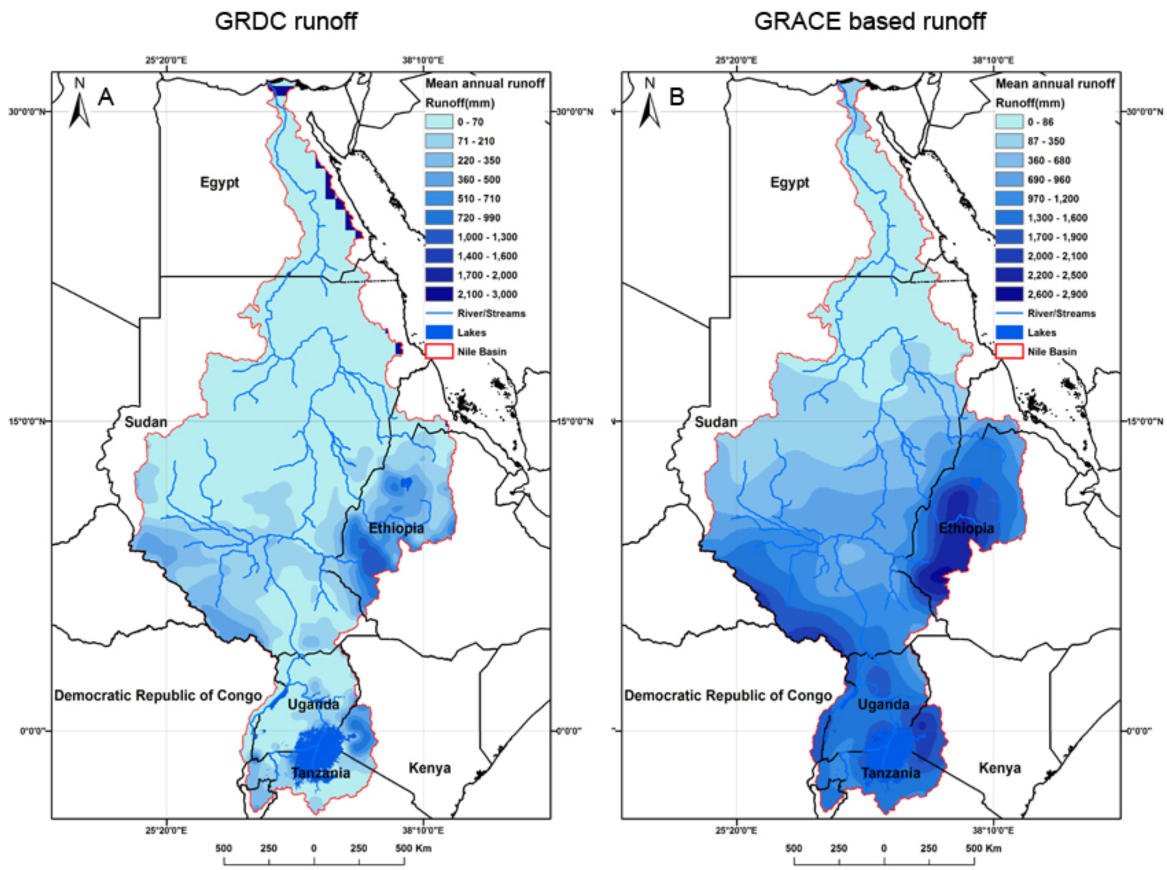

Figure 3.11 Mean annual surface runoff simulated and GRDC data sets (2002-2013).

The surface runoff elasticity to precipitation based on the Budyko relationship were estimated for each climate zone. Based on the Budyko relation between the aridity index and the evaporative index each climate zone plotted in a distinct space under Budyko curve (figure 3.12). The tropical-subtropical zone located over the energy-limited zone, where this zone characterized by potentially high rates of water-yield. The semiarid zone however it receives significant rate of surface water, the high rates of evapotranspiration causes substantial loss of water to the atmosphere that make this climate zone as moisture/water-constrained zone. The arid zone displayed very water-limited zone due to the limited supply of water and the high temperature rates that rises the rates of potential evapotranspiration. The arid zone displayed very low responsivity/resistance, since the deviation in the evaporative index is very high. The basin average showed an over-all water-limited state. This mainly attributed to that majority of the Nile Basin fall in semiarid-arid zone with limited water yield potentiality.

It can be concluded that in the absence of any change in potential evaporation, the surface runoff is solely determined by change in precipitation, which is clear for the tropical-subtropical zone. Conversely, in the absence of change in precipitation, the surface runoff is mainly governed by the changes in the change in potential evaporation. Therefore, and due to the high temperature rates over the semiarid and arid zones, the surface runoff is mainly controlled by the change in potential evaporation. Additionally, the coefficient β, the sensitivity index that measures the degree of changes under the Budyko space is proportionally correlated with the aridity index (i.e. increases in the aridity index implies increases in dryness conditions).

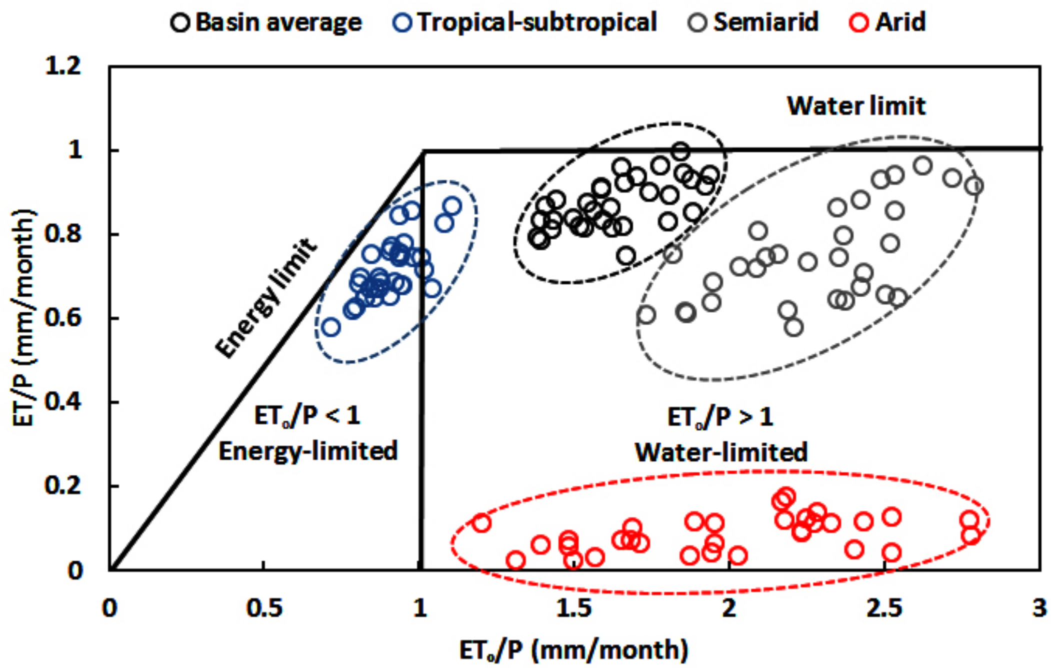

Figure 3.12 Distribution of different climate zone under the Budyko space

Figure 3.12, shows the relationship between the potential ET_o, and ET normalized by precipitation and the response of each climate zone to the precipitation and temperature changes. For instance, the Tropical-subtropical climate shows high potential of water yields, where this zone displayed a consistent water supply, except few years of transition to the water limited stage. The semiarid zone, however, it characterized by high potential of water yield, most of the water-yield loss due to high evaporation. The arid climate zone exposed to high temperature rate and insufficient amount of precipitation. The average of the Nile Basin displayed a water-limited state due to the basin uneven climate distributions.

Trajectory under Budyko space

Based on the Budyko curve, the data classified into dry and wet period and five years moving average were calculated. Equation 3 used to calculate the surface runoff elasticity to precipitation. The degree of changes under Budyko space (coefficient β), calculated using equation 5. For tropical-subtropical zone, the surface runoff elasticity can be measured using equation 7, runoff elasticity to potential (ET_o) and temperature are calculated using equations 8 and 9 respectively. Table 3.2 Summarizes the results of each climate region across the Nile Basin: the surface runoff coefficient $(\boldsymbol{Q/P})$, the surface runoff elasticity to precipitation (ε_p), the surface runoff elasticity to potential (ET_o), $(\boldsymbol{\varepsilon_{ET_\circ}})$, and the surface runoff elasticity to temperature $(\boldsymbol{\varepsilon_T})$. The results based on the listed methodology in section 2.2.

Table 3.2 Summary of the runoff elasticity in each climate zone across the Basin

Region	$\boldsymbol{Q/P}$	$\boldsymbol{\varepsilon_p}$	$\boldsymbol{\varepsilon_{ET_\circ} = -\beta}$	$\boldsymbol{\varepsilon_T}$
Tropical-Subtropical	0.65	1.96	-0.52	-0.31
Semiarid	0.19	0.62	-0.77	-0.46
Arid	0.0064	0.29	-1.70	-1.02
Basin average	0.34	0.83	-0.92	-0.55

Meanwhile, the surface runoff elasticity determines the ability of the system to restore its water-yield conditions under changing climates. For instance, the subtropical-tropical zone showed the surface runoff elasticity to precipitation is 1.96 this means at 10 percent increase of precipitation, the surface runoff over the tropical-subtropical zone expected to increase by about 20 percent. Subsequently, when the temperature decreases by -0.3°C, the surface runoff will recovered by about 3 percent. The rate of changes in the Budyko space showed less change for the tropical-subtropical zone compared by the semiarid and arid zone. For instance, the tropical-subtropical zone is 0.52, the changes in the semiarid is 0.77 and the rate for the semiarid zone has a high rate of changes of about 1.70. The high rate of changes for the semiarid and arid zone are related to the high rates of aridity index.

Mostly, the calculated surface off elasticity to precipitation that greater than 1 describes an elastic system/basin, in which the water-yield is high and able to resilient to climate change, basins with elasticity under 1 describes inelastic system/basin that non-resilient to climate change. The full details about the expected percentage of recovery and deterioration for each climate zone at the current climate condition and according to the RCP scenarios represented in table 3.3.

Table 3.3 Percentage of changes in surface runoff to precipitation and temperature.

Region	Current		Projected	
	(ε_p) at +10% (P)	(ε_T) -0.5°C (T)	RCP 2.6 (+14%)	RCP 5.8 (-15%)
			ε_p	ε_p
Tropical-Subtropical	20%	3%	28%	-30%
Semiarid	6%	4%	8%	-9%
Arid	3%	10%	4%	-4%
Basin average	8%	6%	11%	-12%

3.5 Summary and conclusion

Anecdotal evidence showed that the Nile Basin would experience increase in temperature and a wide temporal variability in precipitation due to climate change. Overall, the Nile river flows are very sensitive to the changes in the precipitation and temperature. Understand the fluctuation of the Nile flow is essential to enhance the adaptive capacity for future threats. For large part across the basin, the warming trend in temperature intensifies the movement toward extreme events such as floods and droughts. In spite of such intimidations, the riparian nations are still hurdled by the insufficient empirical data and the lack of the mutual corporation for adaptive measures. Climate change manifests primarily through changes in average temperature and precipitation, the most important drivers of the water cycle.

This paper discussed the potential impact of the continuing warming trend and precipitation variability on the Nile River flow. The Nile Basin is characterized by varied terrain and the temporal variability of climate. The basin divided into three major climate regimes based on the amount of precipitation and temperature: tropical-subtropical, semiarid, and arid zone. Meanwhile, the basin upstream countries lie over tropical-subtropical condition and receive sufficient and almost consistent amount of precipitation. The downstream nations experience drier conditions and suffer insufficient water supplies. Based on Budyko curve and the mathematical formulation introduced by (Arora, 2002; Pike, 1964), the percentage of changes in surface runoff to the changes in precipitation and temperature were illustrated. The tropical-subtropical region displays high elasticity, where under the current climate condition this region seems to be resilient to changing climates. Meanwhile, the semiarid and arid zones have low elasticity under the current climate conditions.

According to the projected climate scenarios under the RCP2.6, the tropical-subtropical region displays high runoff flow resistant to the climate under the projection increase in precipitation. Conversely, under the worse scenario of RCP 5.8, the subtropical and tropical region become highly vulnerable to the precipitation deficit. The riparian are encourage working in a mutual adaptive policies to future possible changes.

Acknowledgement

The first author thanks the Institute for Study of Human Flourishing, University of Oklahoma for providing the research fund for this study in form of a PhD dissertation fellowship to the first author. Thanks goes to the Advanced Radar Research Center (ARRC), and the Hydrometrology and Remote Sensing Laboratory (HyDROS) lab at University of Oklahoma, USA for providing the research facilities, workspace and the equipment to accomplish this research.

Thanks goes to the data centers that made remote sensing and reanalysis data sets be available and downloadable: The Goddard Earth Science Data and Information Service Centers (GES DISCs), the Climatic Research Unit at the University of East Anglia, the National Oceanic and Atmospheric Administration, Global Precipitation Climatological Center, and the Global Runoff Data Centre.

3.6 References

Allen, R.G., Pereira, L.S., Raes, D. and Smith, M., 1998. Crop evapotranspiration - Guidelines for computing crop water requirements. FAO - Food and Agriculture Organization of the United Nations, Rome.

Arora, V.K., 2002. The use of the aridity index to assess climate change effect on annual runoff. Journal of Hydrology 265 164–177.

Budyko, M.I., 1974. Climate and life. Academic Press, Orlando, FL.

Camberlin, P., 2009. Nile Basin Climates. In: H.J. Dumont (Editor), The Nile : Origin, Environments, Limnology and Human Use. Springer, Monographiae Biologicae, pp. 307-333.

Collins, R., 2002. The Nile. Yale University Press/ New Haven and London.

Conway, D., 2005. From headwater tributaries to international river: Observing and adapting to climate variability and change in the Nile basin. Global Environmental Change, 15(2): 99-114.

Creed, I.F., Spargo, A.T., Jones, J.A., Buttle, J.M., Adams, M.B., Beall, F.D., Booth, E.G., Campbell, J.L., Clow, D., Elder, K., Green, M.B., Grimm, N.B., Miniat, C., Ramlal, P., Saha, A., Sebestyen, S., Spittlehouse, D., Sterling, S., Williams, M.W., Winkler, R. and Yao, H., 2014. Changing forest water yields in response to climate warming: results from long-term experimental watershed sites across North America. Glob Chang Biol, 20(10): 3191-208.

CRU, 2015. Climate Research Unite Data.

Di Baldassarre, G., Elshamy, M., van Griensven, A., Soliman, E., Kigobe, M., Ndomba, P., Mutemi, J., Mutua, F., Moges, S., Xuan, Y., Solomatine, D. and Uhlenbrook, S., 2011. Future hydrology and climate in the River Nile basin: a review. Hydrological Sciences Journal, 56(2): 199-211.

Eltahir, E.A.B., 1996. El Niño and the Natural Variability in the Flow of the Nile River. Water Resources Research, 32(1): 131-137.

Fekete, B., Vörösmarty, C. and Grabs, W., 2002. Global composite runoff fields on observed river discharge and simulated water balances Water System Analysis Group,University of New Hampshire, and Global Runoff Data Centre. , Koblenz, Germany: Federal Institute of Hydrology (BfG), 2002.

Gleick, P.H., 1991. The vulnerability of runoff in the Nile basin to climatic changes. The Environmental Professional, 13: 66-73.

Grijsen, J.G., Tarhule, A., Brown, C., Ghile, Y.B., Taner, Talbi- Jordan, A., N, H., Guero, A., Y, R., Kone, S., Coulibaly, B. and Harshadeep, N., 2013. Climate Risk Assessment for Water Resources Development in the Niger River Basin Part II: Runoff Elasticity and Probabilistic Analysis.

Hargreaves, G. and Samani, Z., 1985. Reference crop evapotranspiration from temperature. Appl Engine Agric, 1(2): 96–99.

Hargreaves, G. and Samni, Z., 1982 Estimation of potential evapotranspiration. Journal of Irrigation and Drainage Division, Proceedings of the American Society of Civil Engineers 108: 223-230.

Hasan, E., Khan, S.I. and Hong, Y., 2015. Investigation of potential sea level rise impact on the Nile Delta, Egypt using digital elevation models. Environ Monit Assess, 187(10): 649.

Hassenforder, E. and Noury, B., 2015. Managing Transboundary River Basins: Chaper 7. River Basin Management in the Twenty-first Century. Taylor & Francis Group, LLC.

IPCC, 2014. Climate Change 2014: Synthesis Report. Contribution of Working Groups I, II and III to the Fifth Assessment Report of the Intergovernmental Panel on Climate Change, IPCC, Geneva, Switzerland.

Karyabwite, D.R., 2000 Water Sharing in the Nile River Valley, UNEP/DEWA/GRID, Geneva.

Lynas, M., 2008. Six Degrees: Our Future on a Hotter Planet. National Geographic.

NIS, 2012. Climate Change and its Implications for the Nile Region:Chapter 8.

Pike, J.G., 1964. The estimation of annual runoff from meteorological data in a tropical climate. Journal of Hydrology, Amsterdam, 2: 116–123.

Schneider, U., Becker, A., Meyer-Christoffer, A., Ziese, M. and Rudolf, B., 2011. Global Precipitation Analysis Products of the GPCC, Deutscher Wetterdienst, Offenbach a. M., Germany.

Swenson, S. and Wahr, J., 2006. Post-processing removal of correlated errors in GRACE data. Geophysical Research Letters, 33(8).

Syed, T.H., Famiglietti, J.S., Rodell, M., Chen, J. and Wilson, C.R., 2008. Analysis of terrestrial water storage changes from GRACE and GLDAS. Water Resources Research, 44(2): n/a-n/a.

van der Velde, Y., Vercauteren, N., Jaramillo, F., Dekker, S.C., Destouni, G. and Lyon, S.W., 2014. Exploring hydroclimatic change disparity via the Budyko framework. Hydrological Processes, 28(13): 4110-4118.

Zaroug, M.A.H., Eltahir, E.A.B. and Giorgi, F., 2014. Droughts and floods over the upper catchment of the Blue Nile and their connections to the timing of El Niño and La Niña events. Hydrology and Earth System Sciences, 18(3): 1239-1249.

Zhang, K., Kimball, J.S., Nemani, R.R. and Running, S.W., 2010. A continuous satellite-derived global record of land surface evapotranspiration from 1983 to 2006. Water Resources Research, 46(9): n/a-n/a.

Chapter 4: Investigation of potential sea level rise impact on the Nile Delta, Egypt using digital elevation models

Abstract

In this study, the future impact of Sea Level Rise (SLR) on the Nile Delta region in Egypt is assessed by evaluating the elevations of two freely available Digital Elevation Models (DEMs): the SRTM and the ASTER-GDEM-V2. The SLR is a significant worldwide dilemma that has been triggered by recent climatic changes. In Egypt, the Nile Delta is projected to face SLR of 1m by the end of the 21th century. In order to provide a more accurate assessment of the future SLR impact on Nile Deltas' land and population, this study corrected the DEM's elevations by using linear regression model with ground elevations from GPS survey. The information for the land cover types and future population numbers were derived from the Moderate Resolution Imaging Spectroradiometer (MODIS) land cover and the Gridded Population of the Worlds (GPWv3) datasets respectively. The DEM's vertical accuracies were assessed using GPS measurements and the uncertainty analysis revealed that the SRTM-DEM has positive bias of 2.5m, while the ASTER-GDEM-V2 showed a positive bias of 0.8m. The future inundated land cover areas and the affected population were illustrated based on two SLR scenarios of 0.5m and 1m. The SRTM DEM data indicated that 1m SLR will affect about 3,900 km^2 of cropland, 1,280 km^2 of vegetation, 205 km^2 of wetland, 146 km^2 of urban areas and cause more than 6 million people to lose their houses. The overall vulnerability assessment using ASTER-GDEM-V2 indicated that the influence of SLR will be intense and confined along the coastal areas. For instance, the data indicated that 1m SLR will

inundate about 580 Km^2 (6 percent) of the total land cover areas and approximately 887 thousand people will be relocated. Accordingly, the uncertainty analysis of the DEM's elevations revealed that the ASTER-GDEM-V2 dataset product was considered the best to determine the future impact of SLR on the Nile Delta region.

Keywords: SRTM DEM, ASTER-GDEM, Sea Level Rise, Climate Changes, and Nile Delta Egypt.

4.1 Introduction

The Nile Delta is one of the world's largest river deltas, located in North Egypt (figure 4.1). Before the High Dam construction in the Aswan area of southern Egypt, the Nile River emptied its sediment loads into the Mediterranean Sea. In addition, the Nile River provided the Delta soil which contained natural nutrients and mineral supplies that enriched the fertile soil and made the Delta an important agricultural region. The Delta's shoreline is occupied by three large brackish lakes: Idku, Burullus, and Manzala, which make up about twenty five percent of the wetland area where intensive fishing farms are located (El Raey, 1999). Moreover, major economic projects are situated along the coastal area, including recreational venues, new cities and housing communities, two major trading seaports, and an international highway. In terms of population density, the Nile Delta is a densely populated region with averages of 1,000 persons/km², form about 40 million people of the Egyptian population.

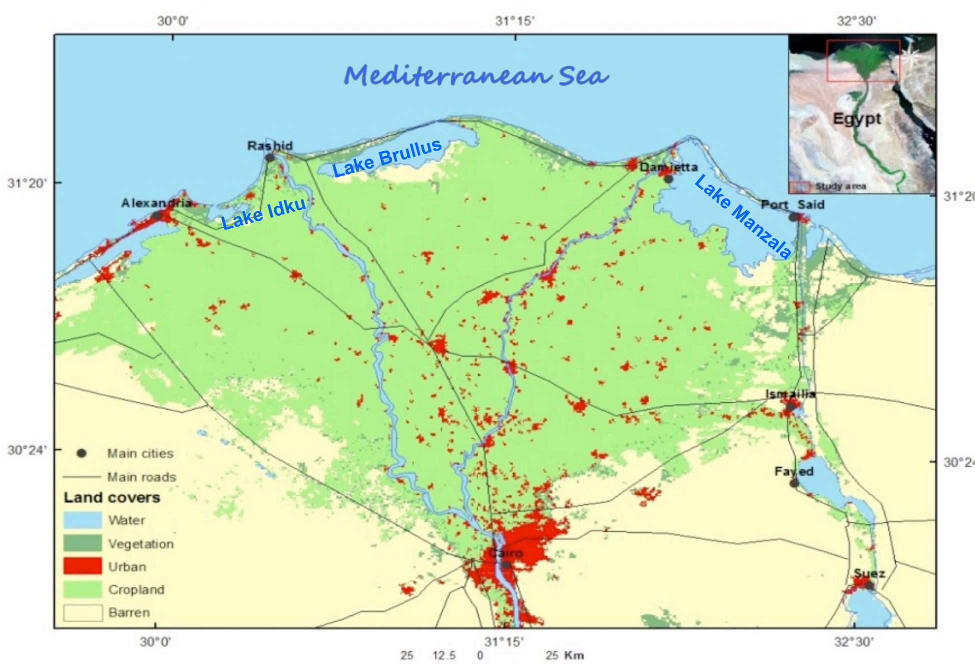

Figure 4.1 Land cover types from MODIS data of Nile Delta, Egypt.

The Nile Delta suffers from several problems: particularly high population growth, a strong trend towards urbanization, saltwater intrusion, and shoreline erosion (El Raey, 2010). The coastal area of the Nile Delta has a long history of sediment erosion that has been increased substantially since the building of the High Dam (El Raey, 2010; Stanley, 1996). Furthermore, the coastal areas are expected to face SLR in the range of 0.5m and 1m by the end of the 21st century due to climatic changes (Gornitz, 1991; IPCC, 2001; Rosetta, 2010). Many parts of the Nile Deltas' costal area are located in low elevation zones (figure 4.2), which in the future will be exposed to the risk of inundation caused by SLR (El Raey, 1999).

Figure 4.2 Heavy rainfalls accumulation in low elevation areas along Nile Delta shoreline. Photos taken after heavy rainfalls in year 2010 near New Damietta beach.

Several studies have revealed that more than 40 percent of the Nile Delta will be prone to the risk of inundation as a result of SLR by year 2050 (Agrawala et al., 2004; Bohannon, 2010; Brown et al., 2011; Dasgupta et al., 2007; El Raey, 1997; El Raey, 2010; FitzGerald et al., 2008; Hereher, 2010; Snoussi et al., 2008). These studies have concluded that 0.5m of SLR could result in the loss of approximately 1,800 km^2 of agricultural land and 12,000 km^2 of urban areas, with more than 3 million people who will be in need of relocation (Agrawala et al., 2004; El Raey, 2010; FitzGerald et al., 2008). It is estimated that at 1m of SLR, the expected loss will be approximately 4,500 km^2 of agricultural land, 25,000 km^2 of urban area, 24,000 km^2 of wetland, and the inundation risk will threaten a significant portion of the population (El Raey, 2010; FitzGerald et al., 2008).

In regards to SLR vulnerability assessment, the above estimates are substantially high, and some previous work based their estimates on inadequate sources of elevation, especially the uncorrected version of SRTM dataset (Blankespoor et al., 2012; Dasgupta et al., 2007; Dasgupta et al., 2009; Hereher, 2010; Simonett, 2012). Obviously, incorporating inadequate elevations in SLR analysis will add more uncertanities to the estimates. Therefore, to provide the Nile Delta's coastal community with the most accurate estimates regarding to SRL impacts, ground-controlled elevations should be incorporated with the analyzed digital elevation data.

Digital Elevation Models (DEMs) are 3D representations of the terrain's elevations that can be generated using GPS measurements, contour elevations, and onboard sensors. The Shuttle Radar Topographic Mission (SRTM) based DEM, and Advanced Spaceborne Thermal Emission and Reflection Radiometer Global DEM (ASTER-GDEM) datasets are among the most important and freely available DEM products that provide valuable information about the Earth's surface configuration. The SRTM data is available in two main resolutions; 1 arc-second (~30m) resolution for the United States and the 3 arc-sec (~90m) for global use (SRTM-DEM, 2006). Recently, the original SRTM 90m resolution data was downscaled and is being released as enhanced elevations data at 30m for the entire globe (JPL, 2014). The SRTM used dual radar antennas to acquire interferometry radar digital topographic data (SRTM-DEM, 2006). The ASTER-GDEM data is 1 arc-second (30m) resolution, and has two main versions: ASTER-GDEM-V-1 and V-2. The ASTER-GDEM-V-2 data is much improved from the previous version, because it removes some of the common DEM errors such as sinks and artifacts (ASTER-GDEM, 2011). The ASTER-DEM was generated using stereo-pair images of Band 3, the nadir (3N) band and the back-looking (3B) band, both collected by the ASTER instrument onboard the Terra mission (ASTER-GDEM, 2011).

The above mentioned DEM datasets are extensively employed in numerous hydrologic and engineering applications, where the DEM is usually used to derive the information about the slope aspects, drainage identification, watershed delineation, flow accumulation, and flow direction (Jenson, 1991; Maidment, 2002; Martz and Garbrecht, 1992; Moore et al., 1991; Wise, 2000; Wu et al., 2008). In recent applications, the digital elevation data has been an integral part of the downscaling techniques and radiometric correction of most satellite observations. In the current research, we are investigating the application of the DEMs elevation to study the impact of SLR on the Nile Delta region.

Indeed, the Nile Delta is an area of the world that lacks the detailed ground truth data and monitoring stations. Despite the economic importance of the Nile Delta, it could be considered as one of the most data-poor regions regarding to the available information. Moreover, if some ground information has been recorded, the institutional bureaucracies hinder the acquisition of such datasets. Therefore, the only alternative source for qualitative surface data on the Nile Delta is through remote sensing and DEMs. As the SLR problem along the Nile Delta through the 21th century is imminent, and in order to have better perspective about its impacts we should employ the most validated elevations from DEMs as well as the available ground observations.

In this research, elevation acts as the main parameter in order to determine the SLR impact on the Nile Delta region. Elevation is made the central feature because the Nile Delta is located in a fairly stable tectonic region (Meshref, 1990), with a low land subsidence rates that ranges between approximately 6mm per year to 8mm per year (Becker and Sultan, 2009; Stanley, 2005). Similarly, this region rarely experiences any catastrophically large storm surge waves that are generated by frequent Tsunami earthquake events (Yalciner et al., 2014). The average size of storm surge heights is only 0.6m during the winter season (Dasgupta et al., 2009; Radwan and El-Geziry, 2013).

The current work provides a glimpse of the SLR impacts on the coastal communities based on the most adequate DEM datasets with the highest possible ground resolution along with GPS survey. The Moderate Resolution Imaging Spectroradiometer (MODIS), Land Use Land Cover (LULC) data, and socioeconomic Gridded Population of the Worlds (GPWv3) products are utilized to determine the future SRL influences on both the coastal land areas and populations. The main objectives of this research are: elaborating the importance of the ground validation in order to extract the right information from remote sensing data, and to accurately determined the impact of SLR. In addition, this research displays how uncorrected elevation can mislead the final SLR results and reveals how the spatial resolution of the two different DEM products yields different results when the same analysis is applied.

The current paper is organized as follows: Section 1.1 defines the study area location. Section 2 details the datasets as well as the methodology employed. The results are described in sections 3, followed by a conclusion in section 4.

4.2. Study Area

The study area is located along the Nile Delta shoreline that extends from west to east by approximately about 500 km. The study area is bounded from south to north by latitudes 30.08° and 30.20° and from east to west by longitudes 30.8° and 31.10° respectively (figure 1). The shoreline is occupied by three major lakes and a number of agricultural farms and dispersed vegetation cover. The surface profile along the shoreline area from the west to east reveals that the maximum elevation is about 9m along the sand dune piles at the entrance of El-Brullus city, while the minimum elevation is of about -2.5m along the northern lakes (Geocontext, 2010).

4.3. Data and Methodology

The datasets that are used in this research are two DEM datasets: the 3 arc-second SRTM data with approximately 90m ground resolution and the 1 arc-second ASTER-GDEM-V2 data with approximately 30m ground resolution. The 90m SRTM data is from the latest updated version 4, which was released in August 2008. The data is freely available at http://srtm.csi.cgiar.org/. For the ASTER-GDEM-V2, the data was release for public use in August 2011 and can be downloaded at: http://gdex.cr.usgs.gov/gdex/.

The Global Positioning System (GPS) elevation points were collected to evaluate the accuracy of the DEM datasets. A portable hand-held GPS unit was used for elevation survey. The datasets were collected using a Garmin GPS-72H device. The reported accuracy of such device is up to 10 foot. The designed GPS survey occurred in August 2014, and it covers a length of about 200 km along the coastal area. The survey consisted of about 9 main stops, with a total number of 394 points. The collected points were confined to the international coastal road and the nearby barren lands (figure 4.3).

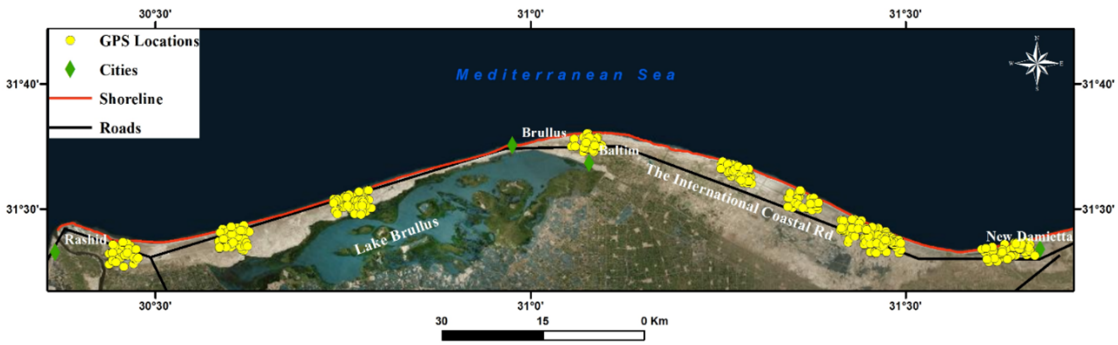

Figure 4.3 GPS locations along the Nile Delta shoreline.

Additionally, The MODIS Land Cover Type product (short name: MCD12Q1) was used to extract the land cover information on the coastal area. MCD12Q1 is a standard MODIS Land Cover product which provides five global land cover classification systems; the data is available at http://glcf.umd.edu/data/lc/. The selected Land Cover classification system is the type-I classification that was developed by the International Geosphere Biosphere Programme (IGBP) and contains 17 land cover classes. The spatial resolution of this dataset is 500m, and it was chosen because it has the most representative classes found on the Nile Delta region.

The Delta's population information is derived from two main sources: the Gridded Population of the World version3 (GPWv3) datasets and the census data from the Egyptian Central Agency for Public Mobilization and Statistics (CAPMAS) (CAPMAS, 2014). The GPWv3 data include gridded population counts and population densities. The data is available from Socioeconomic Data and Applications Center (SEDAC), Columbia University via the http://sedac.ciesin.columbia.edu/data/set/nagdc-population-landscape-climate-estimates-v3 (SEDAC, 2013).

DEM's Elevation Errors

DEMs are inevitably subjected to errors that can be inherited during either data acquisition or interpolation (Reuter et al., 2009). The DEM's errors are autocorrelated, which means that the amount of the error is highly correlated between neighborhood pixels due to the spatially dependent nature of the elevation entities (Xuejun and Lu, 2008). Additionally, if these errors' effects are not eliminated, it could be propagated to further analysis adding more uncertainties to the results (Band, 1986; Ehlschlaeger, 1998). The accuracy of the DEMs' derived parameters is primarily dependent on both their vertical and horizontal resolutions (Oksanen and Sarjakoski, 2005; Zandbergen, 2011). Several studies have investigated the vertical and the horizontal accuracies of different DEM products (AL-Harbi S. D., 2007; Chirico, 2004; Gerald and Ben, 2012; Guth, 2010; Nikolakopoulos et al., 2006; Sefercik, 2007; Suwandana et al., 2012). It can be concluded that the errors varied among different DEM products according to the nature of the study region and the land covers type (Guth, 2010). In addition, it is very important to choose the correct DEM scale for particular applications (Akbari et al., 2015).

In many instances, the lack of ground truth points makes the systematic evaluation of these errors difficult. Several methods can be implemented to determine the DEM's elevation errors. For example, the elevations can be represented using two independent DEM datasets, then compared to determine the residual differences in elevation values over stable terrain (Burrough et al., 1998; Nuth and Kaab, 2011). Similarly, performing detailed statistics to measure the degree of data correlation can help to investigate how the DEMs data are significantly different (Nikolakopoulos et al., 2006).

In order to evaluate the DEM's elevations, several evaluation points were sampled from the two DEMs in correspondence to the actual GPS locations. The elevations from the two DEMs were correlated together and evaluated according to (Equation 4.1) to determine whether the DEMs mean difference is significant or not. The Pearson's correlation analysis was performed between the DEMs and GPS points. Additionally, *F*- and *t*-tests were applied to determine the relationship between the DEMs variances (Equations 4.2 and 4.3). The vertical accuracies of the DEMs were estimated using reference elevations from the GPS, and being represented by the Mean Error (ME) term (Equations 4.4). A linear regression fitting between the DEM datasets and the GPS reference elevations is performed to eliminate the DEM errors and to adjust the digital elevation data according to the same benchmarks. All of statistical analyses were accomplished using the R-statistical package and various Excel functions.

$$\varepsilon = \sqrt{\frac{\sigma_1^2}{n1} + \frac{\sigma_2^2}{n2}} \tag{4.1}$$

Where ε is the elevation mean difference and σ_1 and σ_2 are the DEM standard deviation, $n1$ and $n2$ are the size of samples.

$$F = \frac{MS_B}{MS_w} \tag{4.2}$$

Where MS_B is the mean square between the datasets and the MS_W is the mean square within the datasets.

$$t = \frac{\overline{y}1-\overline{y}2}{Sp\sqrt{\left(\frac{1}{n1}\right)+\left(\frac{1}{n2}\right)}} \quad (4.3)$$

Where $\overline{y}1$ and $\overline{y}2$ are the datasets' means, S_p is the datasets' pooled variance, and n1 and n2 are the sample sizes.

$$ME = \frac{\sum_{i}^{j}(Zele-Zdem)}{N} \quad (4.4)$$

Where Z_{ele} represents the elevation from obseravtions and Z_{dem} represents the elevation from the DEM datasets, N sample size.

SLR Analysis

The SLR analysis was performed in three major steps. First, the DEMs were brought to uniform ground resolution by scaling the ASTER-GDEM up and aggregating it into the 90m resolution of SRTM. The resampled method which was utilized was the Nearest Neighborhood resample technique, which served to preserve the values of the newly aggregated ASTER-GDEM (Nikolakopoulos et al., 2006). The second step taken was the interpolation of the DEM's missing values, and execution of data smoothing by applying a low pass spatial filter of 3x3 moving cells. The low pass filter smooths the data by reducing the local variation between the extreme values, and also removes data noise. Finally, the elevation was corrected by applying a linear regression fitting model between the DEMs and the reference elevations from the GPS survey. Figure 4.4 shows the entire SLR workflow.

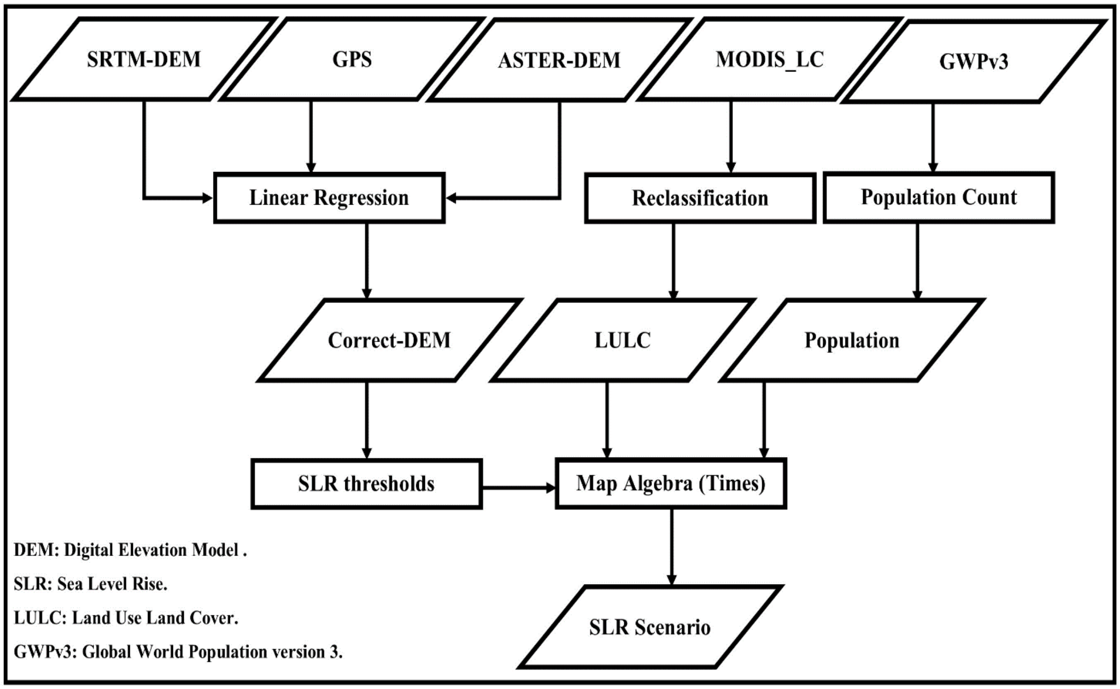

Figure 4.4 Schematic chart of the workflow.

The SLR analysis can be summarized as follows:

1- The future SLR vulnerability assessments were performed by utilizing the bathtub technique (Leon et al., 2014; Poulter and Halpin, 2008) on both DEM datasets. This method uses a deterministic line separating the flooded area from the dry land. ArcGIS software provides a Kriging probability function in which the bathtub method was applied by using specific SLR thresholds of 0.5m, and 1m according to the expected SLR values to identify the inundated pixels. The resulting images are binary datasets of (0,1) that differentiates the flooded pixels from the dry land pixels.

2- The MODIS land cover types dataset with 17 classes were reclassified and merged into 5 main classes. This was accomplished by combining the 5 forest classes, the 2 savanna, the 2 shrublands, and the vegetation mosaic and grassland classes into one class called green vegetation. The ice and snow class is considered unclassified because they do not existed in the study area due to the climatology of the region. The remaining four of the classes are water, cropland, urban, and wetland (table 4.1).

3- The GPWv3 gridded population density data and population count are obtained in ASCII format and converted into raster datasets at the same spatial resolution as the SRTM data. The population count attributes are built using information from the Central Agency for Public Mobilization and Statistics CAPMAS (CAPMAS, 2014). The total number of population counted per pixel grid according to the available population information from CAPMAS as well as the future population for year 2100 were determined using the reported population growth factor of 1.9 percent/year by (CAPMAS, 2014).

4- Spatial analysis was performed to determine the SLR impact on land and population using the multiplication function in the Map Algebra extension in the ArcGIS software. The binary images representing different SLR scenarios are multiplied by the reclassified MODIS LULC data and the future population count.

Table 4.1 Reclassification of IGBP MODIS Land Cover Type-1 classes.

Value	Original Classification	Reclassification
0	Water	Water
1	Evergreen Needleleaf forest	
2	Evergreen Broadleaf forest	
3	Deciduous Needleleaf forest	
4	Deciduous Broadleaf forest	
5	Mixed forest	
6	Closed shrublands	
7	Open shrublands	Vegetation
8	Woody savannas	
9	Savannas	
10	Grasslands	
15	Vegetation mosaic	
16	Barren or sparsely vegetated	
11	Permanent wetlands	Wetland
12	Croplands	Croplands
13	Urban and built-up	Urban
14	Snow and ice	Unclassified
254	Unclassified	
255	Fill Value	

4.4 Results and Discussion

Based on the sampled elevation points, several statistical analyses were performed to measure the degree of data correlation and the significant difference between the elevation means. The samples were restricted to the flat and barren areas on the coastal zone, because it would be difficult and beyond the ability of this study to conduct a GPS survey that covers the entire Delta region for validation. The statistical results revealed that the mean difference between the elevation values from the two DEMs is about 2.2m, according to equation (1). Although, the DEMs scatterplot (figure 4.5A) showed a positive correlation with a coefficient (R^2) of 85 percent, there is a systematic offset between the two DEMs elevations of about -4.18m. The P-values resulting from test statistics using F- and t-tests (equations 2&3) showed significantly different means between the DEMs elevations (table 4.2). The correlations between the GPS values and DEM datasets indicated a positive correlation with R^2 of 88 percent with SRTM, and 97 percent with ASTER data. The offset between the SRTM and GPS data is approximately 2.6m and about 0.8m with regards to the ASTER-GDEM data (figure 4.5B). The ME analysis revealed that the SRTM data has ME value of 2.18m, while the ASTER-GDEM-V2 data has a ME value of -0.69m. The statistics provided in table 2 concluded that the two DEM datasets have significant mean differences, which explained the systematic bias between the DEM's elevations. Thus, to adjust the digital elevations, a linear regression model was performed based on the GPS elevations.

Table 4.2 Statistical results of the two DEMs datasets

Statistics	*ASTER*	*SRTM*
Mean	80.60	112.71
Variance	17248.02	21158.36
P(F<=f) one-tail	0.0019	
P(T<=t) one-tail	1.66E-6	
ME	-0. 69	2.18

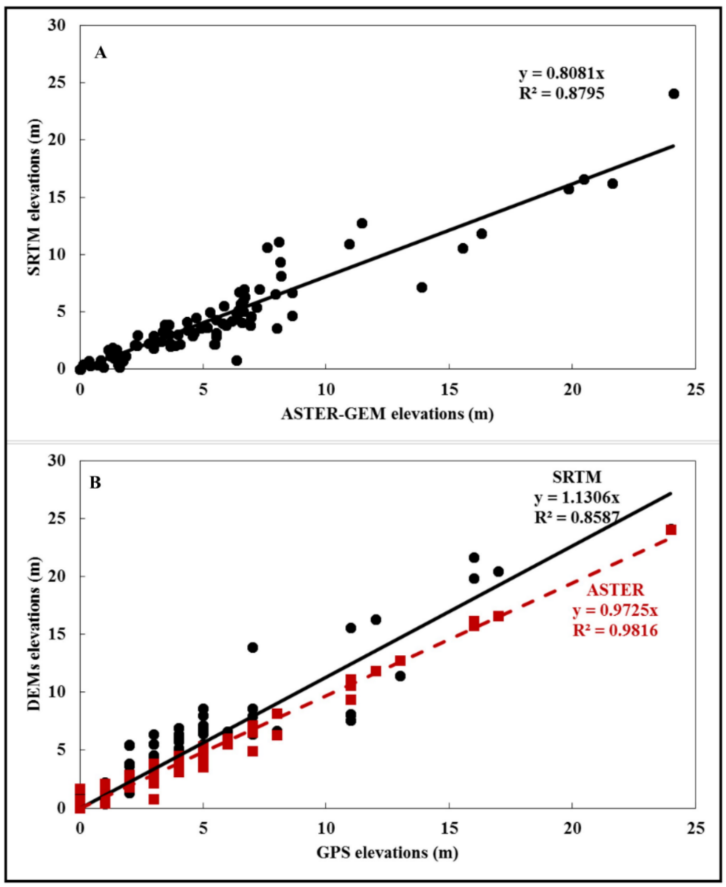

Figure 4.5 Correlation between the DEMs and GPS elevations points. A) SRTM and ASTER-GDEM correlation. B) SRTM/ASTER-DEM and GPS elevations Correlation. Total number of sample points (N= 390 points).

Figure 4.6 shows the representation of the elevation values from the original DEM datasets; figure 4.6A indicates how the original SRTM has uniformly distributed elevation values that gradually increase when moving from the shoreline in the north toward the land in the south. In contrast, figure 4.6B shows that the ASTER-GDEM-V2 recorded more elevations that are less uniformly distributed across the study area.

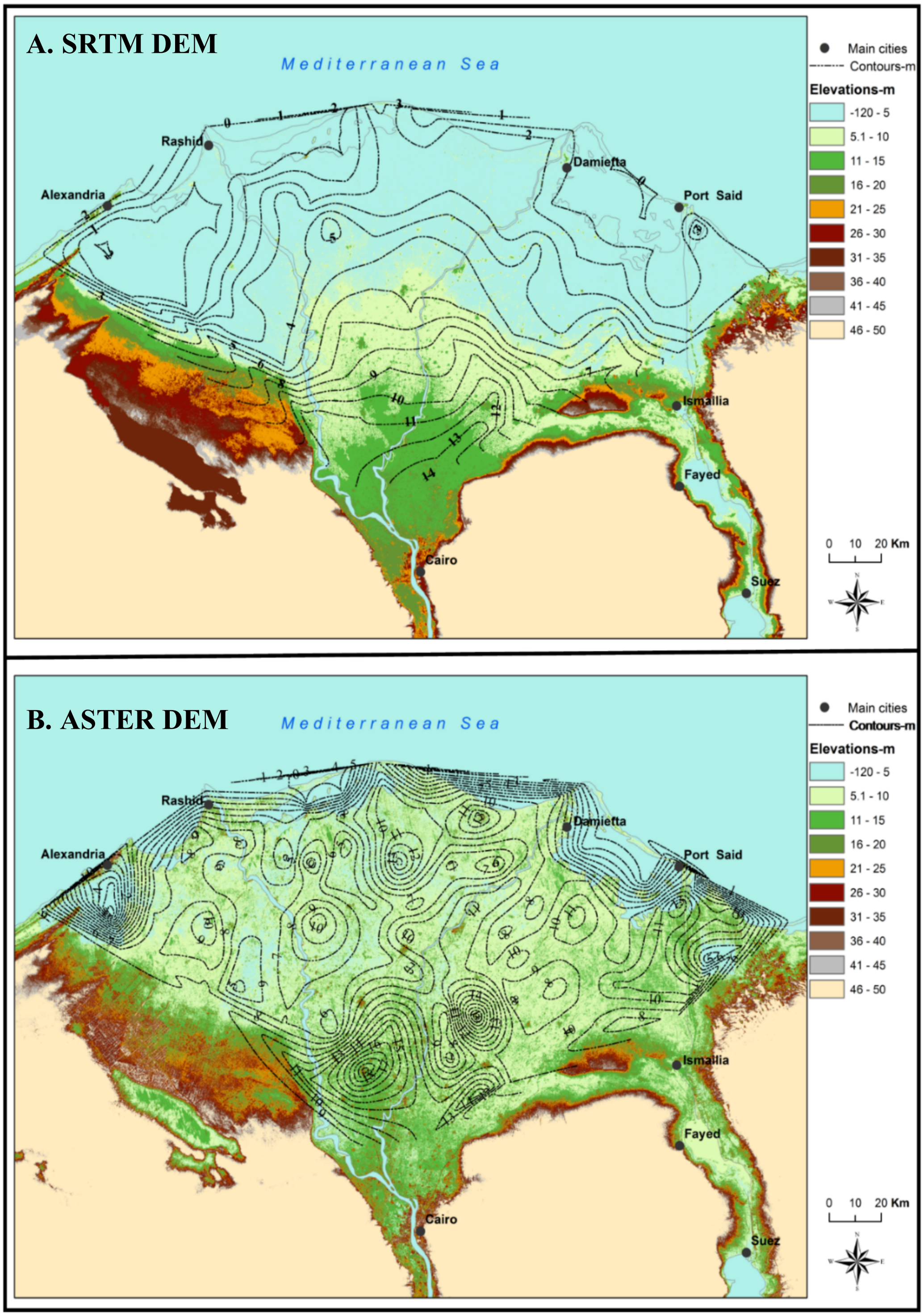

Figure 4.6 Contouring of original DEMs using interval 1 meter. A) The SRTM-DEM showed more homogenous elevations that increase from the north to south, while ASTER-GDEM-V2, B) recorded more elevation points and showing less uniform elevation distribution.

In addition, to evaluate the merged/reclassified MODIS classes from the original LULC datasets, numbers of training values were provided from the ground survey. To assess the classification accuracy, we used the post classification technique for accuracy assessment in the ENVI 5.0 digital image processing software package. The classification overall accuracy is 96.22 percent and the kappa coefficient (κ) is 0.93. The kappa (κ) coefficient measures the agreement between classification and ground truth pixels; a kappa value of 1 represents perfect agreement, while a value of 0 represents no agreement (ENVI, 2008).

SRTM-based SLR

The original SRTM data analysis indicated that at the 0.5m-based SLR scenario indicated that potential affected number of population would be about 3 million people. Approximately 600 km^2 of vegetation, 98 km^2 of wetland, 1800 km^2 of cropland, and 70 km^2 of urban area will be under threat. The 1m SLR, an estimated 6 million people would be at risk of inundation and displacement. The expected LULC loss would be more than 1,200 km^2 of vegetation, 204 km^2 of wetland, 4,000 km^2 of cropland, and 145 km^2 of urban area (table 4.3: SRTM section).

Table 4.3 The total areas (Km2) of projected land cover types vulnerable to SLR at 0.5m and 1m SLR scenarios using original DEM datasets

Affected cover	SRTM		ASTER-DEM-V2	
	0.5 m	**1 m**	**0.5 m**	**1 m**
Vegetation	610	1,272	81	169
Wetland	98	205	17	36
Cropland	1,885	3,928	157	328
Urban	70	146	26	55
2100 Population	3,058,227	6,116,454	580,539	1,209,457

The adjusted SRTM data indicated, however, that at 0.5m SLR the affected land cover would be 98 km^2 of vegetation, 14 km^2 wetlands, 804 km^2 of cropland, and 22 km^2 of urban area. The 1m SLR threshold, the total number of affected population would be about 4 million people. The LULC loss will be approximately 205 km^2 of vegetation, 30 km^2 wetlands, 1,600 km^2 of cropland, and 47 km^2 of urban area (table 4.4: SRTM section). For both the original and adjusted DEM datasets, as the threshold's values increased, the projected land cover loss and number of population affected also increased.

ASTER-GDEM-based SLR

The original ASTER-GDEM-V2 data analysis showed significantly different results when compared to the original and the adjusted SRTM DEM datasets' results. At 0.5m SLR, an estimated 580 thousand people will face the dangers of inundation and be displaced, and about 280 km^2 of the total LULC will be destroyed (table 4.3: ASTER section). The SLR results are significantly different when the same analysis is performed using the adjusted ASTER-GDEM-V2 data. At 1m SLR, an estimated 887 thousand people will be at risk of inundation and displacement and about 100 km^2 of vegetation, 16 km^2 wetland, 402 km^2 cropland, and 47 km^2 of urban area land would be destroyed. Table 4.4 summarizes the total projected damage and the affected population in the study area using the adjusted DEM datasets.

Table 4.4 The total areas (Km^2) of projected land cover types vulnerable to SLR at 0.5m and 1m SLR scenarios using corrected DEM datasets

Affected cover	SRTM		ASTER-DEM-V2	
	0.5 m	**1 m**	**0.5 m**	**1 m**
Vegetation	98	205	57	119
Wetland	14.4	30	7.8	16
Cropland	804	1,675	192	402
Urban	22.5	47	14.5	47
2100 Population	2,166,987	4,514,558	426,159	887,832

The two original DEM datasets showed distinctly different results in terms of the areas vulnerable to SLR impact when the same analysis steps are applied. Figure 4.7 displayed the projected vulnerable areas using the original SRTM-DEM. It can be clearly seen that the amount of vulnerable land cover will be potentially high when relying on the original SRTM data. On the other hand, the biased corrected ASTER datasets displayed completely different SLR results (figure 4.8). Table 4.5 summarized the total percentage of vulnerable land cove types at 1m SLR scenario using the corrected DEMs. The combined average of the total LULC loss is approximately 13 percent and the inland inundation will be approximately 8 km landward.

Table 4.5 The percentage of vulnerable Land cover (LC) areas to 1m SLR scenarios using edited DEM datasets.

Classes	% Total LC area	% LC at the coast area	Vulnerable LC% using SRTM	Vulnerable LC% using ASTER
Vegetation	2856	1,790	11.45%	6.62%
Wetland	247	237	12.66%	6.64%
Cropland	21,888	7,206	23.24%	5.58%
Urban	1,935	393	12.09%	11.99%
Total	26,928	9,628	20.27%	6.06%

The difference in SLR impact results regarding the LULC types can be related primarily to the spatial resolution and the vertical accuracy of the DEMs. The SRTM data has more aggregated pixel elevations, which displays uniformly along the entire Nile Delta as shown in figure 4.6A. Up-scaling of the 30m ASTER data into 90m did not produce much difference in the newly aggregated ASTER, which did not resemble the original SRTM. This means that the 90m SRTM data contains more aggregated elevation values than the 30m ASTER data. In contrast, the ASTER-DEM-V2 data incorporates more detailed elevation values that produce much higher quality elevation points without voids (artifacts) or anomalies. Additionally, the SRTM elevations data might contain numerous voids and other spurious points over large water bodies, due to the low accuracy of the SRTM's backscattered radar beam over these and other irregular surfaces. For example, the projected inundated areas around Manzala, Brullus and Idku lakes based on the SRTM analysis (figure 4.7) are relatively larger than the corresponding inundated areas based on the analysis of ASTER data (figure 4.8). Also, the existence of the sparse vegetation, and irregular surfaces in the same areas could influence the quality of the SRTM DEM's data as well.

The DEM errors substantially affected the data analysis (Oksanen, 2006; Oksanen and Sarjakoski, 2005; Zandbergen, 2011). The comparison of the vertical resolution of the SRTM data and ASTER-GDEM-V2 data was accomplished by calculating the elevations mean difference, and the DEMs' vertical accuracy was representing by the ME. The mean difference analysis and the correlation statistics reveal how much the results differ. Additionally, the SLR impact based on the SRTM dataset was overestimated, while the ASTER dataset gave more realistic results. Moreover, the adjusted data showed that the SRTM-DEM had less vertical accuracy than the ASTER-GDEM-V2 data. Performing the correlation statistics and the linear regression fitting using the GPS reference elevation values relatively enhanced the DEMs elevations. Therefore, according to the uncertainty analysis, the ASTER-GDEM-V2 dataset is considered the best product to determine the SLR impact on the Nile Delta, and it displayed more realistic expectations (figure 4.8).

In the meantime, this methodology may still encounter some limitation due to the DEMs horizontal and vertical resolutions. Thus far, the available literatures about SLR impact on the Nile Delta revealed high SLR impact on that region. The current results showed that using higher resolution datasets indicated lesser impact. Even more, this SLR impact will be restricted only to portion of the coastal areas behind the shoreline. The findings of our study can be supported by (Jelínek et al., 2009) work, which determined the impact of probable Tsunami waves on Alexandria city west of the Nile Delta. The researchers in that study indicated two main vulnerability scenarios: a "medium" scenario of a 5m run-up and a "worst-case" scenario of a 9m run-up where the vulnerability would be high (Jelínek et al., 2009). This study primarily supports our finding that using ASTER-GDEM-V2 datasets indicated a less vulnerable area. Our estimate provides more details about the coastal communities' future under SLR conditions.

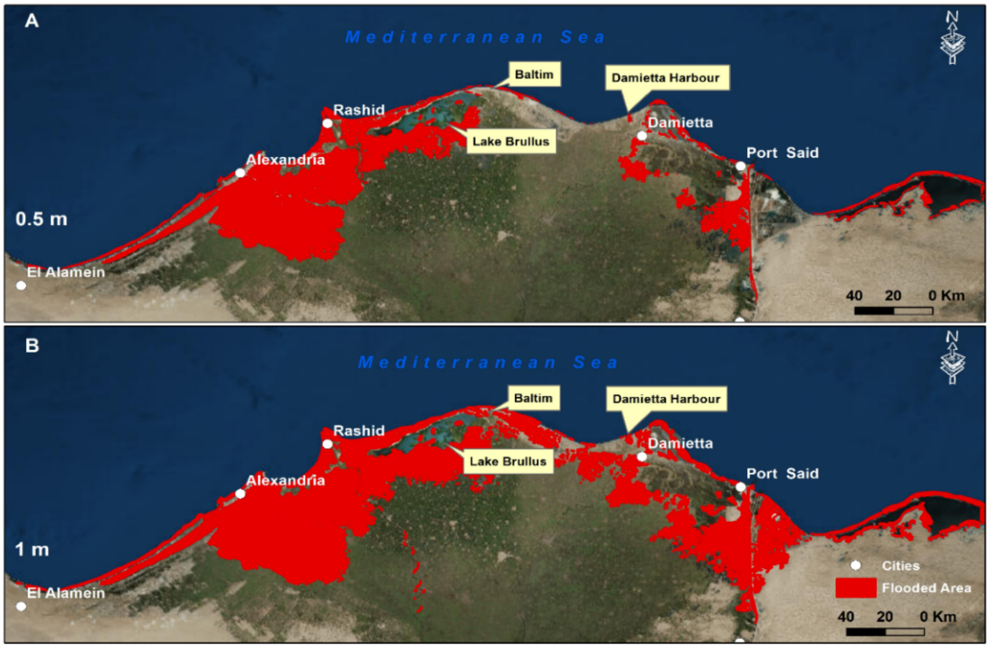

Figure 4.7 Overestimated SLR impact on the Nile Delta's coastal area using uncorrected SRTM-DEM dataset, A) showing the 0.5m SLR and B) the 1m SLR scenarios respectively.

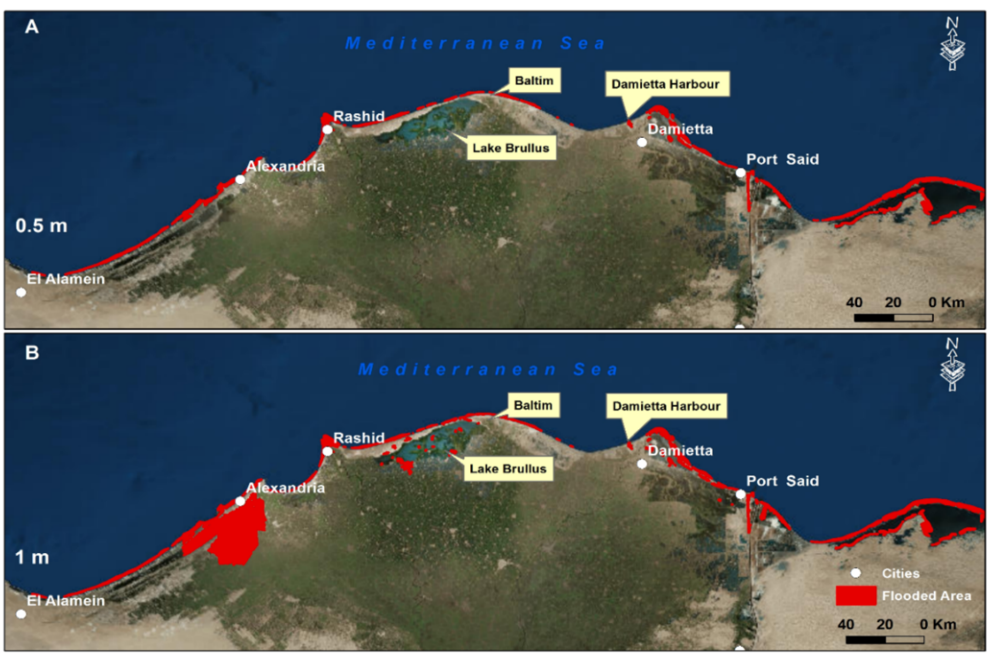

Figure 4.8 Expected future SLR impact on the Nile Delta's coastal area using corrected ASTER-DEM dataset, A) showing the 0.5m SLR and B) the 1m SLR scenarios respectively.

We believe that the current results might still possess some uncertainties due the lack of detailed DEM data. However, comparing the current study findings with the published literatures indicates how the previous works exaggerated the estimates regarding the amount of land inundation as a result of the future SLR on Nile Delta. We are presenting new conclusions about the SLR impact by using the highest resolution data available and providing more reliable information in a data-poor region. Although, the SLR problem is considered as one of the biggest issues worldwide, the geologic setting of the Nile Delta will contribute to minimize the impact over the coastal areas.

4.5 Conclusion

The SRTM and ASTER-GDEM-V2 elevation data are the most commonly used DEM datasets in many hydrologic applications. These two DEMs are used to determine the SLR impact on Nile Delta region. DEMs are subjected to inherent errors that could affect the quality of the data analysis. Several GPS measurements were collected to evaluate and adjust the DEMs' elevations. Two major SLR scenarios with threshold values of 0.5m and 1m were applied to the two DEM datasets before and after bias removal. The original and the corrected DEMs were integrated with the MODIS land cover types and gridded population datasets for SLR impact estimation on Nile Delta land and population.

Statistical analyses were performed and linear regression used to correct the DEMs data. The SRTM and ASTER-GDEM-V2 DEM-based comparison showed substantially different SLR impact results on the Nile Delta land and population. Using the original SRTM DEM data, the expected SLR impact will be significant, while, the original ASTER-GDEM-V2 DEM data revealed that the inundation will affect small portion of the coastal area. The removal of the DEM data sets' biases helped to determine the errors associated with those calculations and to obtain more consistent and reasonable SLR impact estimates. The adjusted SRTM datasets indicated that about 21% of the total land cover areas would be inundated due to SLR impact. On the other hand, the ASTER-GDEM based SLR analysis showed that about 6.6 % percent of the total land cover types will be affected due to SLR. The difference between the two DEM datasets' resolutions and the nature of the backscattered radar beams are the main factors for revealing quite different results about SLR impact in the Nile Delta region.

This study added more in depth analysis about SLR impact on the low-lying coastal areas of the Nile Delta. Future work can consider more detailed datasets using the Unmanned Aerial Vehicle (UAV) survey or employing high-resolution LiDAR-based DEM, once these become available for the Delta region; such detailed datasets can add overall value to the understanding of SLR impacts on such a data-poor region. The current research provides practical insight of the future SLR impacts on the coastal communities, which can be extrapolated to include the whole Mediterranean coast. These estimates on land area and at risk population are valuable and essential for future risk mitigation and preparedness for the communities along the Nile delta coastal areas.

Acknowledgements

The first author acknowledges the Mission sector of the Egyptian Ministry of Higher Education and Scientific research for providing the financial support to conduct this research in the United States of America through a PhD scholarship. The Advanced Radar Research Center (ARRC) group and the Hydrometrology and Remote Sensing Laboratory (HyDROS) research group at the University of Oklahoma for providing the research facilities for this work. We would like to thank Kayla L. Brandt for the English correction and the Manuscript editing. Thanks goes to Ms. Jenny Bailey for the manuscript proof reading and her fruitful comments that added more value to this work. We would like to thank the two anonymous reviewers for their valuable suggestions and constructive comments that improved the overall quality our manuscript.

The DEM datasets and MODIS LULC products are from the Land Processes Distributed Active Archive Center (LP DAAC). The gridded population maps are acquired from SEDAC.

4.6 References

Agrawala, S., Moehner, A., El Raey, M., Conway, D., Van Aalst, M., Hagenstad, M. and Smith, J., 2004. Development And Climate Change In Egypt: Focus On Coastal Resources And The Nile.

Akbari, A., Ramli, N.I.B. and Kong, N.S., 2015. Application of Public Domain Satellite-Based DEMs in Natural Hazard Modeling. International Journal of Environmental Science and Development, 7(2).

AL-Harbi S. D., K.T., 2007. The accuracy of a DEM derived from ASTER data using differential GPS measurements, ISPRS Hannover Workshop 2007. ISPRS.

ASTER-GDEM, 2011. ASTER Global Digital Elevation Model Version 2 – Summary of Validation Results. NASA LPDAAC & JPL, pp. 1-27.

Band, L.E., 1986. Topographic partition of watersheds with digital elevation models. Water Resources Research, 22(1): 15-24.

Becker, R.H. and Sultan, M., 2009. Land subsidence in the Nile Delta: inferences from radar interferometry. The Holocene 19: 949–954.

Blankespoor, B., Dasgupta, S. and Laplante, B., 2012. Sea-Level Rise and Coastal Wetlands Impacts and Costs. Policy Research Working Paper 6277.

Bohannon, J., 2010. Climate change. The Nile Delta's sinking future. Science, 327(5972): 1444-7.

Brown, S., Abiy S. Kebede, a. and Nicholls, R.J., 2011. Sea-Level Rise and Impacts in Africa, 2000 to 2100, University of Southampton, UK.

Burrough, P., McDonnell, R. and Burrough, P., 1998. Principles of geographical information systems. Oxford University Press, Oxford.

CAPMAS, 2014. Central Agency for Public Mobilization and Statistics.

Chirico, P.G., 2004. An Evaluation of SRTM, ASTER, and Contour-Based DEMS in the Caribbean region, URISA Caribbean GIS Conference.

Dasgupta, S., Laplante, B., Meinsner, C. and Wheeler, D.a.Y., J., 2007. The Impact of Sea Level Rise on Developing Countries: A Comparative Analysis. Climate Change, 93(3-4): 379-388.

Dasgupta, S., Laplante, B., Murray, S. and Wheeler, D., 2009. Sea-Level Rise and Storm Surges A Comparative Analysis of Impacts in Developing Countries. Policy Research Working Paper 4901.

Ehlschlaeger, C.R., 1998. The Stochastic Simulation Approach: Tools for Representing Spatial Application Uncertainty, University of California, Santa Barbara.

El Raey, M., 1997. Vulnerability assessment of the coastal zone of the Nile delta of Egypt, to the impacts of sea level rise. Ocean & Coastal Manaoemen, 37(1): 29-40.

El Raey, M., 1999. Egypt: Coastal zone development and climate change: Impact of climate change on Egypt.

El Raey, M., 2010. Impacts and Implications of Climate Change for the Coastal Zones of Egypt. In: David Michel and Amit Pandya (Editors). The Henry L. Stimson Center, Washington, DC, pp. 31-50.

ENVI, 2008. User’s Guide. ENVI on-line software user’s manual, ITT Visual Information Solutions.

FitzGerald, D.M., Fenster, M.S., Argow, B.A. and Buynevich, I.V., 2008. Coastal Impacts Due to Sea-Level Rise. Annual Review of Earth and Planetary Sciences, 36(1): 601-647.

Geocontext, 2010. Nile Delta shoreline profile.

Gerald, F. and Ben, M., 2012. Comparison of SRTM and ASTER Derived Digital Elevation Models over Two Regions in Ghana – Implications for Hydrological and Environmental Modeling. Studies on Environmental and Applied Geomorphology.

Gornitz, V., 1991. Global coastal hazards from future sea level rise. Glob. Planet. Change, 89: 379-98.

Guth, P.L., 2010. Geomorphometric Comparison Of ASTER GDEM And SRTM, ASPRS/CaGIS. ASPRS, Orlando, Florida.

Hereher, M.E., 2010. Vulnerability of the Nile Delta to sea level rise: an assessment using remote sensing. Geomatics, Natural Hazards and Risk, 1(4): 315-321.

IPCC, 2001. The Scientific basis. Contribution of Working Group I to the Third Assessment Report of the Intergovernmental Panel on Climate Change, Cambridge University Press, Cambridge, United Kingdom and New York, NY, USA. 881pp.

Jelínek, R.b., Eckert, S., Zeug, G. and Krausmann, E., 2009. Tsunami Vulnerability and Risk Analysis Applied to the City of Alexandria, Egypt, Institute for the Protection and Security of the Citizen. Italy.

Jenson, S.K., 1991. Applications of hydrologic information automatically extracted from digital elevation models. Hydrological processes, 5(1): 31-44.

JPL, 2014. SRTM, U.S. Releases Enhanced Shuttle Land Elevation Data.

Leon, J.X., Heuvelink, G.B.M. and Phinn, S.R., 2014. Incorporating DEM Uncertainty in Coastal Inundation Mapping. PLoS ONE 9 (9:e108727).

Maidment, D.R., 2002. Arc Hydro: GIS for Water Resources. Environmental Systems Research Institute, Inc., Redlands, California.

Martz, L.W. and Garbrecht, J., 1992. Numerical definition of drainage network and subcatchment areas from digital elevation models. Computers & Geosciences, 18(6): 747-761.

Meshref, W.M., 1990. Tectonic Framework. In: Said R (ed.) The Geology of Egypt, Rotterdam, Netherlands: 381-389.

Moore, I.D., Grayson, R. and Ladson, A., 1991. Digital terrain modelling: a review of hydrological, geomorphological, and biological applications. Hydrological processes, 5(1): 3-30.

Nikolakopoulos, K.G., Kamaratakis, E.K. and Chrysoulakis, N., 2006. SRTM vs ASTER elevation products. Comparison for two regions in Crete, Greece. International Journal of Remote Sensing, 27(21): 4819-4838.

Nuth, C. and Kaab, A., 2011. Co-registration and bias corrections of satellite elevation data sets for quantifying glacier thickness change. The Cryosphere, 5: 271-290.

Oksanen, J., 2006. Digital elevation model error in terrain analysis, University of Helsinki, Finlad, 369 pp.

Oksanen, J. and Sarjakoski, T., 2005. Error propagation of DEM-based surface derivatives. Computers & Geosciences, 31(8): 1015-1027.

Poulter, B. and Halpin, P.N., 2008. Raster modelling of coastal flooding from sea‐level rise. International Journal of Geographical Information Science, 22(2): 167-182.

Radwan, A.A. and El-Geziry, T.M., 2013. Some Statistical Characteristics of Surges at Alexandria, Egypt. JKAU: Mar. Sci, 24(2): 31-38.

Reuter, H.I., Hengl, T., Gessler, P. and Soille, P., 2009. Preparation of DEMs for Geomorphometric Analysis. In: Tomislav H, Hannes IR, editors. Geomorphometry: Concepts, Software, Applications: Elsevier: 87-120.

Rosetta, 2010. Egypt's Nile Delta falls prey to climate change. Al Arabiya News.

SEDAC, 2013. Gridded Population of the World (GPW), V3. http://sedac.ciesin.columbia.edu/data/set/nagdc-population-landscape-climate-estimates-v3 .

Sefercik, U., Jacobsen, K., Oruc, M., Marangoz, A., 2007. Comparison of Spot, SRTM and ASTER DEMS, ISPRS Hannover Workshop 2007. ISPRS

Simonett, O., 2012. Potential impact of sea level rise: Nile Delta, UNEP/GRID; G. Sestini, Florence; Remote Sensing Center, Cairo; DIERCKE Weltwirtschaftsatlas.

Snoussi, M., Ouchani, T. and Niazi, S., 2008. Vulnerability assessment of the impact of sea-level rise and flooding on the Moroccan coast: The case of the Mediterranean eastern zone. Estuarine, Coastal and Shelf Science, 77(2): 206-213.

SRTM-DEM, 2006. Shuttle Radar Topography Mission DTED Level 1 (3-arc second) documentation. NASA/LPDAAC and USGS/EROS, pp. 1-8.

Stanley, D.J., 1996. Nile Delta: extreme case of sediment entrapment. Journal of Marine Geology, 129: 189-195.

Stanley, J.D., 2005. Submergence and burial of ancient coastal sites on the subsiding Nile delta margin, Egypt. Méditerranée, 104: 64-73.

Suwandana, E., Kawamura, K., Sakuno, Y., Kustiyanto, E. and Raharjo, B., 2012. Evaluation of ASTER GDEM2 in Comparison with GDEM1, SRTM DEM and

Topographic-Map-Derived DEM Using Inundation Area Analysis and RTK-dGPS Data. Remote Sensing, 4(12): 2419-2431.

Wise, S., 2000. Assessing the quality for hydrological applications of digital elevation models derived from contours. Hydrological processes, 14(11‐12): 1909-1929.

Wu, S., Li, J. and Huang, G., 2008. A study on DEM-derived primary topographic attributes for hydrologic applications: Sensitivity to elevation data resolution. Applied Geography, 28(3): 210-223.

Xuejun, L. and Lu, B., 2008. Accuracy Assessment of DEM Slope Algorithms Related to Spatial Autocorrelation of DEM Errors. In: Q. Zhou, B. Lees and G.-a. Tang (Editors), Advances in Digital Terrain Analysis. Lecture Notes in Geoinformation and Cartography. Springer-Verlag Berlin Heidelberg, pp. 307-322.

Yalciner, A.C., Zaytsev, A., Aytore, B., Heidarzadeh, M., Kian, R. and Imamura, F., 2014. A Possible Submarine Landslide and Associated Tsunami at the Northwest Nile Delta, Mediterranean Sea. Oceanography, 27(2): 68-75.

Zandbergen, P.A., 2011. Error Propagation Modeling for Terrain Analysis using Dynamic Simulation Tools in ArcGIS Modelbuilder. Geomorphometry.org.

Chapter 5: Estimating the Terrestrial Water Storage with Multiscale Remote Sensing and Model Reanalysis in the Nile River Basin

Abstract

The hydrologic utility of Remote Sensing and Reanalysis (RSRA) datasets has proved problematic in data-poor regions especially the Nile River Basin (NRB). This study seeks to provide an alternative approach to circumvent this problem by using Multi-Regression Analysis (MRA) to: 1- Estimate the uncertainties of the RSRA with the NASA's Gravity Recovery and Climate Experiment (GRACE) data sets. 2- Reconstruct the Terrestrial Water Storage (TWS) anomalies from GRACE data and extend the estimates to the past +30-years for the water-climate nexus study. While the TWS has been simulated for long time using Land Surface Models (LSMs) data, the proposed methodology enhances the TWS reconstruction though increasing the R2 from 0.47 of the conventional water balance approach to above 80 percent. Multiple RSRA data has been blended as a training variables to our MRA model. The results show the combination of precipitation information from the TRMM research product, the MODIS Land Surface Temperatures (LST) and Vegetation indices can simulate the TWS anomalies with R2 as high as 0.93. The hydrologic information from the reanalysis data provided by Climate Research Unite (CRU), the National Center for Environmental Predication (NCEP), and the Global Land Data Assimilation Systems (GLDAS) predicted the GRACE TWS anomalies with R2 above 0.80. The best combination involves the water/energy balance components with the LST and vegetation indices and generates where the TWS has been simulated with R2 of 0.96. Using the training data set, we extend the TWS over the NRB

to the past +30-years; The historic TWS time-series has been compared with the El Niño Southern Oscillation (ENSO) records to define he severe historic flooding and drought events over the basin.

Keywords: GRACE, Multi-regression Analysis, Total Water Storage, Nile River Basin.

5.1 Introduction

The Nile River Basin (NRB) is one of the largest river basins worldwide. It covers an area of about 3.4 million Km^2, and it is the lifeline for more than 300 million people in 11 African nations (Collins, 2002; Erlich, 2000; NBI, 2010). The Nile Basin has complex terrains with large latitudinal extent and varied climates and land covers. The basin has two main hydrologic systems (figure 5.1): the Blue Nile in the East and the White Nile in the Southwest, which are connected together near Khartoum City in Sudan to form the Nile River crossing through all the Egyptian territory (Collins, 2002). The basin climate is mainly affected by the El-Nino Southern Oscillation (ENSO), which makes the Intercontinental Tropical Climate Zone (ITCZ) fluctuate across Africa (Camberlin, 2009; Eltahir, 1996). The ENSO impedes rain to reach the Ethiopian hills, resulting in a decreased amount of rainfall (Eltahir, 1996). On contrary, the La Nina event is linked to dramatic rainfall that causes the Nile floods (NIS, 2012a; UNEP, 2013).

The climate across the basin varies from South to North and ranges from tropical, subtropical, semiarid, arid and Mediterranean. These climates affect the distribution of precipitation, and temperature, which affect the rates of actual and potential evapotranspiration across the basin (figure 5.2). Each climate regime has a unique contribution to the Nile waters; the downstream countries lie in arid to semiarid regions, where the annual rainfall rates range between 150-400 mm/y. This mainly limits the downstream countries' share of the Nile water. On the other hand, most of the upstream countries, except Kenya, receive high amounts of rainfall annually (> 1000 mm/y) providing the Nile with large amounts of water (Hassenforder and Noury, 2015;

Karyabwite, 2000). The NRB is characterized by higher temperature in the arid and semiarid region compared to the tropical and subtropical zones (Camberlin, 2009).

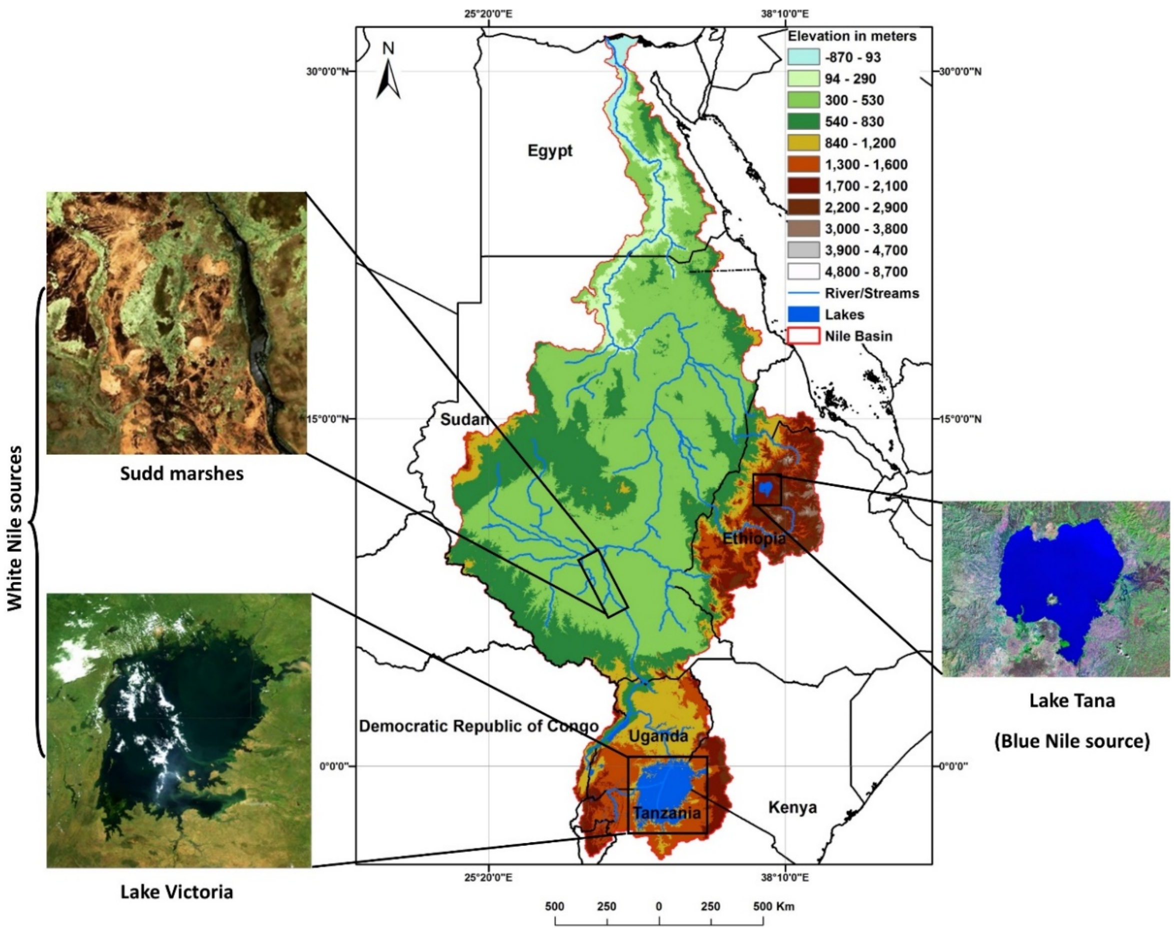

Figure 5.1 Nile River Basin elevations, snapshots of the major hydrological systems over the basin, data from Landsat ETM+.

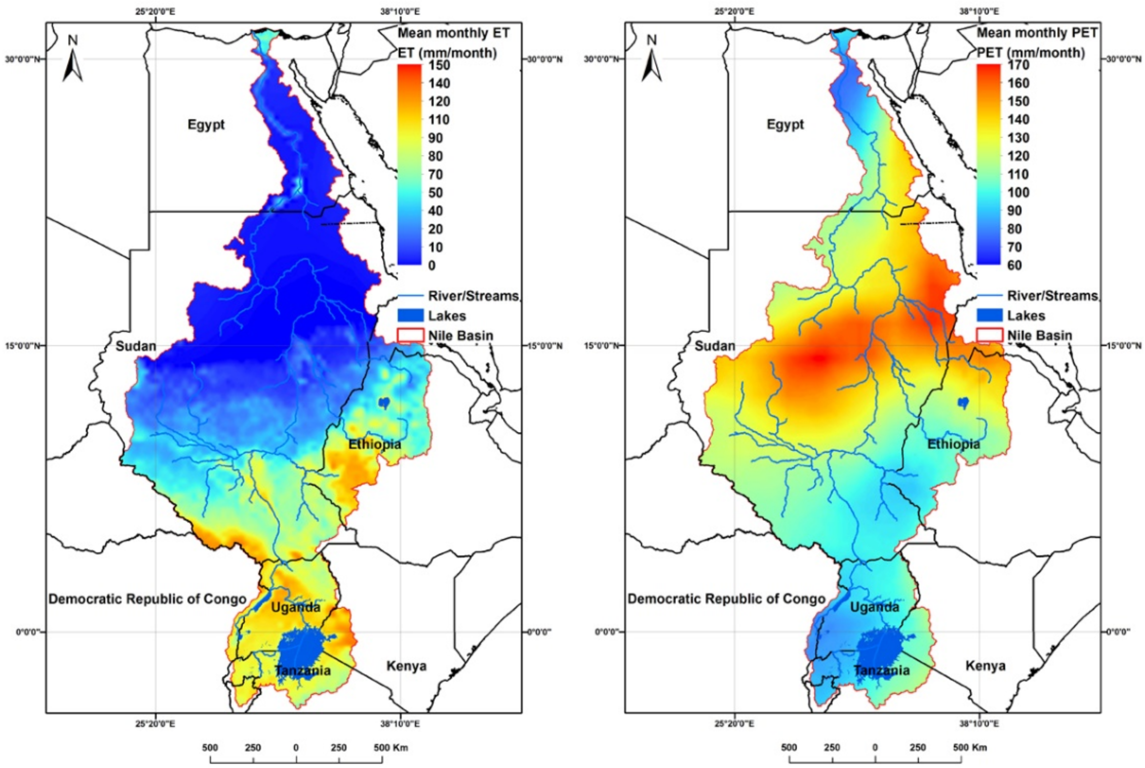

Figure 5.2 Mean monthly actual and potential evapotranspiration of the Nile Basin.

In general, increasing Land Surface Temperature (LST) raises the evaporation rates while causing less surface runoff. This results in less water reaching the Nile, moving the basin to a more moisture-constrained region (NIS, 2012a).

To understand the waters future along the NRB under the current changing climate, reliable and sufficient ground information are needed. The available gauging stations are extremely sparse with poor temporal and spatial coverage (Shahin, 2003) leaving most parts along the basin uncovered with *in situ* data. However, and due to the institutional bureaucracies, the access to the observation data is difficult. The riparian countries in NRB are challenged by their infirm relationships and lack of information sharing policies. Therefore, the satellite technologies and the released model reanalysis datasets are the main alternative proxies and global wide sources for valuable physical measurements and real-time observations for poor and ungauged basins.

Meanwhile, the hydrologic based estimates that are derived from remote sensing and reanalysis (RSRA) data require rigorous inputs of ground observations for accurate evaluation and implementation. Since the satellite based and reanalysis datasets inherit uncertainties and errors that can hinder their hydrologic applications, validation is practically the most inherent challenge especially when ground parameters are missing or insufficient. Therefore, a novel multi-Parameters Regression Approach (MRA) is developed to investigate how the derived hydrologic information from RSRA can be used for water-climate nexus studies in a context where no significant and sufficient ground observations are available.

NASA's Gravity Recovery and Climate Experiment (GRACE) satellite mission estimates the distribution of water over land surfaces and its temporal variations (Wahr,

2004) since its launch in 2002. GRACE helps in tracking the fresh water availability, groundwater fluctuation and understanding the water cycle (Ahmed et al., 2011; Bastiaanssen et al., 2014; Becker et al., 2010; Cao et al., 2015; Hasan et al., 2015b). GRACE records the Total Water Storage (TWS) anomalies as the variation in the Equivalent Water Thickness (EWT) which is the sum of all water stored in different forms of land's reservoir (Chambers, 2007).

The main objective of this study is to reconstruct the historical records of the Total Water Storage (TWS) across the NRB by using multi-inputs of RSRA datasets. Another objective is to quantify the uncertainties of the hydrologic variables derived from the RSRA data. A conventional approach to simulate TWS makes use of Land Surface Model (LSM) simulations and the water balance Equation (5.1):

$$\Delta TWS = P - ET - R + \varepsilon \tag{5.1}$$

Where P (precipitation), ET (evapotranspiration) and R (surface runoff) are outputs of the LSM. The ε is an error term which is not usually accounted for, especially in ungauged regions. A representative example is provided with the Global Land Data Assimilation System (GLDAS) (figure 5.3). While the overall agreement between the simulated and the observed TWS is good ($R^2 = 0.48$), the extreme values are not well reproduced as the TWS anomalies inferred from the LSM outputs tend to overestimate the lower anomalies (< -30 mm/month) and underestimate the anomalies over 60 mm/month. The proposed approach focuses on enhancing the TWS estimation to ultimately build more reliable TWS estimates.

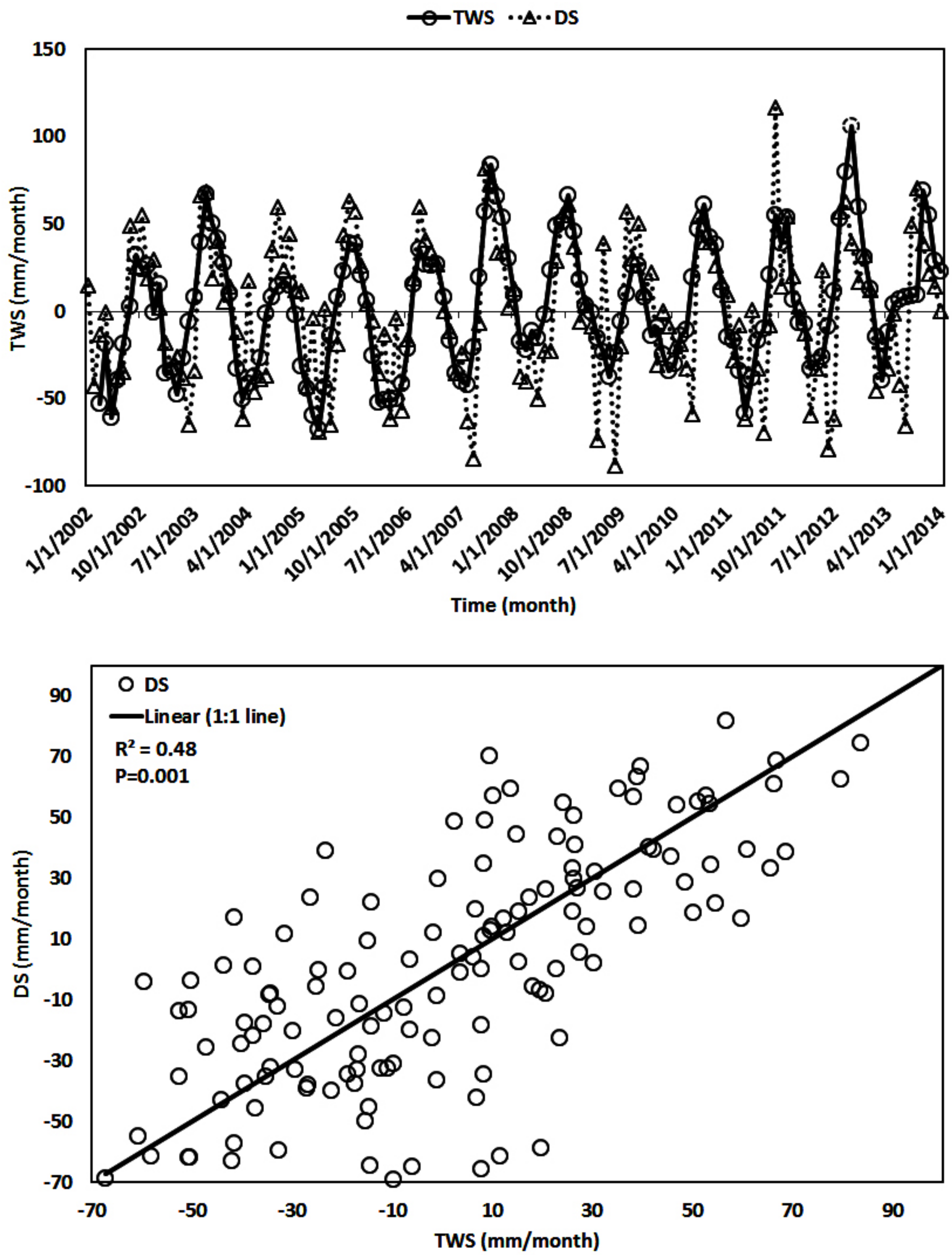

Figure 5.3 Estimation of TWS anomalies using the conventional water balance approach, left panel show the time series of the Modeled and TWS from GRACE, the right panel display the coloration results.

5.2 Materials and Datasets

Remote sensing systems/onboard satellite platforms monitor the Earth's dynamics at regular temporal intervals using selective absorption and reflectance of light (Jensen, 2007). Ultimately, remote sensing is becoming the norm to provide tremendous physical measurements about Earth's surface. Model reanalysis provide other inclusive records of Earth's climate over historical decades (Reanalysis Wiki, 2015). Despite the recent advances in the onboard satellite data and the climatic models, our understanding of the water balance for the data-poor regions remains limited. In this study, we utilized multisensory RSRA data at the basin scale to model TWS over the NRB; the following sections describe the datasets.

Remote sensing data

GRACE

GRACE data are collected, processed using the spherical harmonic solution, and made available through three mission partners; the University of Texas Center for Space Research (CSR), the Geo Forschungs Zentrum (GFZ) Potsdam, and the Jet Propulsion Laboratory (JPL). Recently, another solution of gravity field of GRACE data was released as the mass concentration blocks or GRACE mascons (Watkins et al., 2015). The GRACE data are given at the monthly scale and over a 1° grid. The accuracy of the recovered water mass variations from GRACE data increases with the increasing size of the monitored basin (Wahr et al., 2006). The observation covers the period between March 2002 and February 2015. In this research, GRACE Release 05 Level 2 (RL05) data processed by the three centers are obtained through the GRACE Tellus at http://grace.jpl.nasa.gov/data/get-data/monthly-mass-grids-land/.

MODIS datasets

The Moderate Resolution Imaging Spectroradiometer (MODIS) satellite provides a continuous observation of the Earth's surface. In the current research, several MODIS products were implemented: the MODIS temperature grids (short name: MOD11C1) are used for the Land Surface Temperature (LST) average in Kelvin for daytime and nighttime observations. The vegetation information is extracted from the MODIS Vegetation Index (VI) (MOD13), which includes the Normalized Difference Vegetation Index (NDVI), the Enhanced Vegetation Index (EVI) and the Leaf Area Index (LAI) from the MOD15A2 datasets. These MODIS data are at monthly scale with 1-km resolution, and made available by the Goddard Earth Science Data and Information Service Centers (GES DISCs).

TRMM data

The Tropical Rainfall Measuring Mission (TRMM) is a joint mission between US and Japan launched in 1997 to provide 3-hourly to daily surface quantitative measurements and comprehensive four-dimensional distribution of rainfall and latent heating over tropics and sub-tropics regions (GSFC, 2011). The monthly research product TRMM-3B43 of 0.25° grids are utilized in this study.

Model reanalysis data

A model reanalysis dataset is a comprehensive data record extended over several decades or longer to monitor the changes in weather and climate over the entire globe. Reanalysis data were developed using observations and numerical modelling to give insight into the past climate and enable the comparison with the current conditions (Reanalysis Wiki, 2015). In this research, the model reanalysis data focus on several hydrological variables such as air Temperature (Tair), Precipitation (PRE), Actual Evapotranspiration (AET), Potential Evapotranspiration (PET), Surface Runoff (SR), Soil Moisture (SM), Palmer Severity Drought Index (PSDI), Latent Heat Flux (LHF), Sensible Heat Flux (SHF), and Soil Heat (SH). The data are acquired from number of data centers such as the Climatic Research Unit (CRU) at the University of East Angelia (UEA), the Global Land Data Assimilation System (GLDAS), the Physical Science Division (PSD) at National Oceanic and Atmospheric Administration (NOAA). The following section provides information about the utilized model reanalysis datasets.

Climate Research Unit (CRU)

CRU model reanalysis time series are monthly temporal datasets recording the climate variation over the last century. The data are calculated at high-resolution (0.5°x0.5°) based on more than 4000 weather stations around the world (CRU, 2015). The data provide several climate variables such as precipitation, air temperature, potential evapotranspiration, the PSDI Index, and the wet day frequency. We acquired the monthly mean CRU time series data version 3.21 datasets for the period 1901-2013. The data are available at http://www.cru.uea.ac.uk/data.

Global land data assimilation system (GLDAS)

GLDAS provides a wide range of hydrologic and energy flux information (e.g. surface runoff, soil moisture, surface temperature, latent heat, and sensible heat) (Rui, 2011). GLDAS parameters are generated from four land surface models (LSMs): the Community Land Model (CLM), Mosaic, Noah, and the Variable Infiltration Capacity (VIC). The data are available at global scale with high resolutions ranging from 0.25° to 1°, through temporal averaging of 3-hourly to monthly products. The datasets cover a time-period from January 1979 to present. The GLDAS data can be accessed via the GES DISCs at http://disc.gsfc.nasa.gov/hydrology.

Physical Science Division (PSD)

PSD at the National Oceanic and Atmospheric Administration (NOAA) offers a collection of model reanalysis datasets, which are collected from different observations such as radar, satellite, and ground stations to assimilate the historical climatic conditions. The utilized PSD reanalysis data are the NCEP/NCAR reanalysis I (available through http://www.esrl.noaa.gov/psd/data/gridded/reanalysis/). The data include the climate information of the period from 1948 to present.

Gauged corrected data

The NRB is lacking the *in-situ* observation and is considered as one of the data-poor regions. The instrumented climate and gauging stations along the basin are quite few, and the data sharing and accessing between the riparian countries is too limited. The following section describes the implemented gauge corrected datasets.

The Global Precipitation Climatological Center (GPCC)

The Global Precipitation Climate Center (GPCC) dataset at the Deutscher Wetterdienst, Germany is a global analysis of monthly gauged-corrected precipitation products (Schneider et al., 2011). The gridded GPCC products are available at spatial resolutions of 0.5° x 0.5°, latitude by longitude, and are freely downloadable via the Deutscher Wetterdienst portal at http://gpcc.dwd.de. The GPCC provides long-term monthly precipitation datasets from 1901 to 2015. Precipitation analysis addresses the need to assess climate change and its impacts over all spatial scales. In the current research, we utilized the 0.5° full data product version 6. Figure 5.4 compares the precipitation products from RSRA (sections 2.1 and 2.2) against GPCC. All products underestimate precipitation accumulation greater than 50 mm/month relative to GPCC. The VIC estimates display a significant conditional bias with overestimation of light/moderate precipitation accumulations (below 40 mm/month) and underestimation of higher accumulations. Among all products the TRMM precipitation displays the highest correlation with the GPCC data (R^2=0.99). It is expected since GPCC is used as inputs in the TRMM-3B43 product. The simulated precipitation from CRU and NCEP data display good correlation with the GPCC data (R^2=0.80), the precipitation estimates from the three GLDAS models (CLM, Mosaic, and Noah) have similar R^2 of 0.83. VIC precipitation estimates display the lowest correlation (R^2=0.57) in relation to the aforementioned conditional bias.

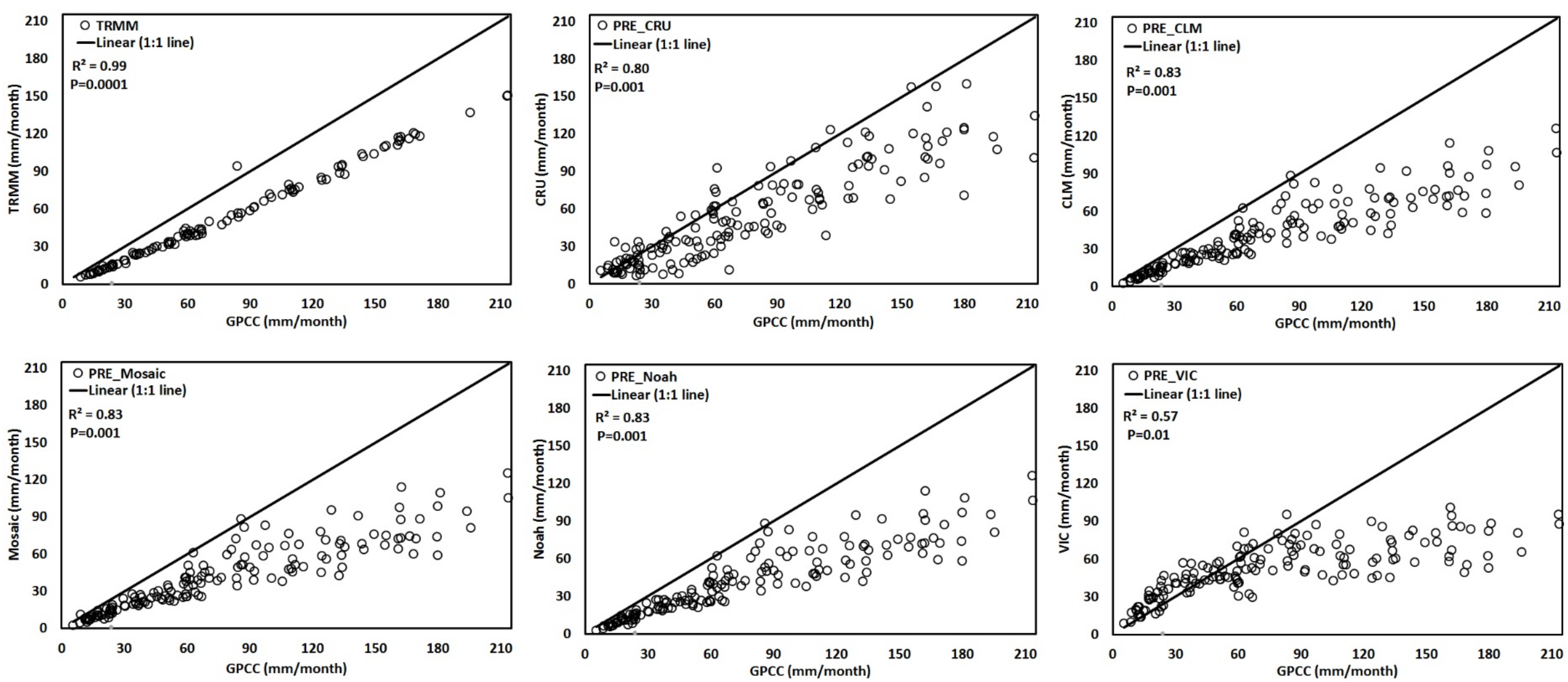

Figure 5.4 Correlations of gauge-corrected precipitation data with different precipitation products from satellite, reanalysis and LSM.

The Global Runoff Data Centre (GRDC)

The Global Runoff Data Centre (GRDC) is an international archive of long-term surface runoff data up to 200 years old. It stores and provides river discharge data collected at daily/monthly intervals from more than 9,000 stations in 160 countries. The GRDC operates under the auspices of the World Meteorological Organization (WMO) and is hosted by the German Federal Institute of Hydrology (Bundesanstalt für Gewässerkunde or BfG), the data are available through the link at http://www.bafg.de/GRDC/EN/Home/homepage_node.html. The GRDC data were utilized to evaluate the performance of the simulated surface runoff products from the four GLDAS models (figure 5.5). Accordingly, the surface runoff from Noah and Mosaic models show better consistency with the observed data compared to CLM (significant overestimation) and VIC data (increasing overestimation with time).

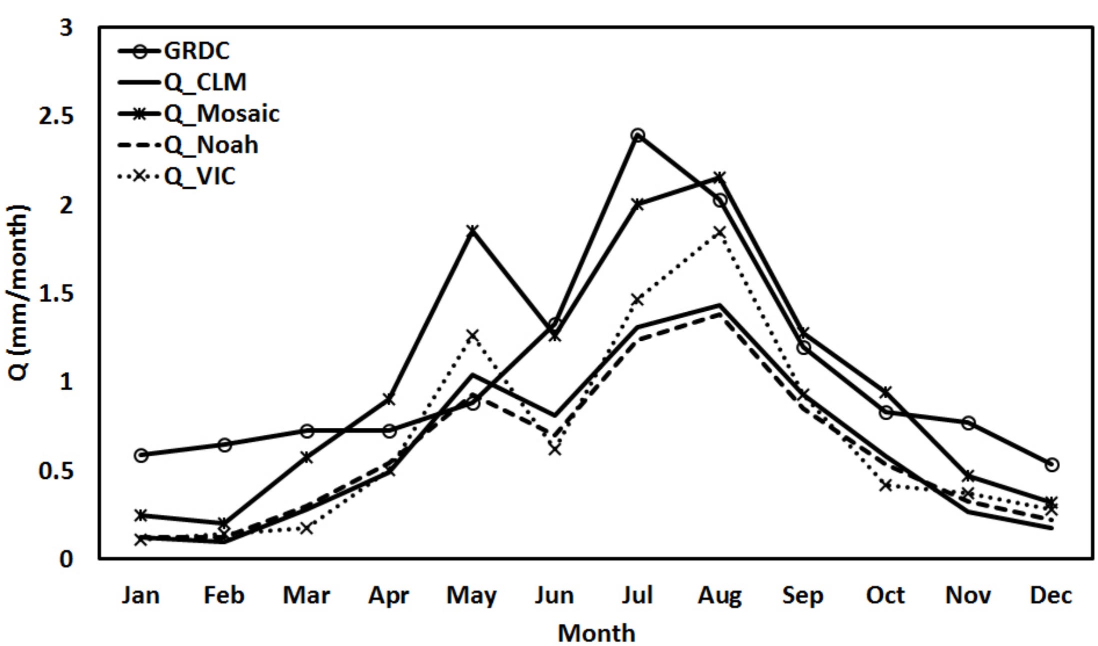

Figure 5.5 Time series of annual surface runoff from GRDC observation and surface run off from the four GLDAS models.

Corrected ET/PET products

Monthly archive of gauge corrected ET/PET at 0.25° to 1° global grid resolution over the period 1980-current are available at the Hydrometeorology and RemOte Sensing (HyDROS) lab archive (Zhang et al., 2010). These monthly ET shows very good agreements with the measurements from flux towers. Figure 5.6 shows the performance of the GLDAS prediction of evapotranspiration relative to the gauge corrected ET data. All models show underestimation relative to the reference. The correlations indicate that the Mosaic and Noah models have the best performance with R^2 = 0.77 and 0.86, respectively. The ET from CLM model has R^2 = 0.67, while the VIC model shows a lower correlation (R^2 = 0.72).

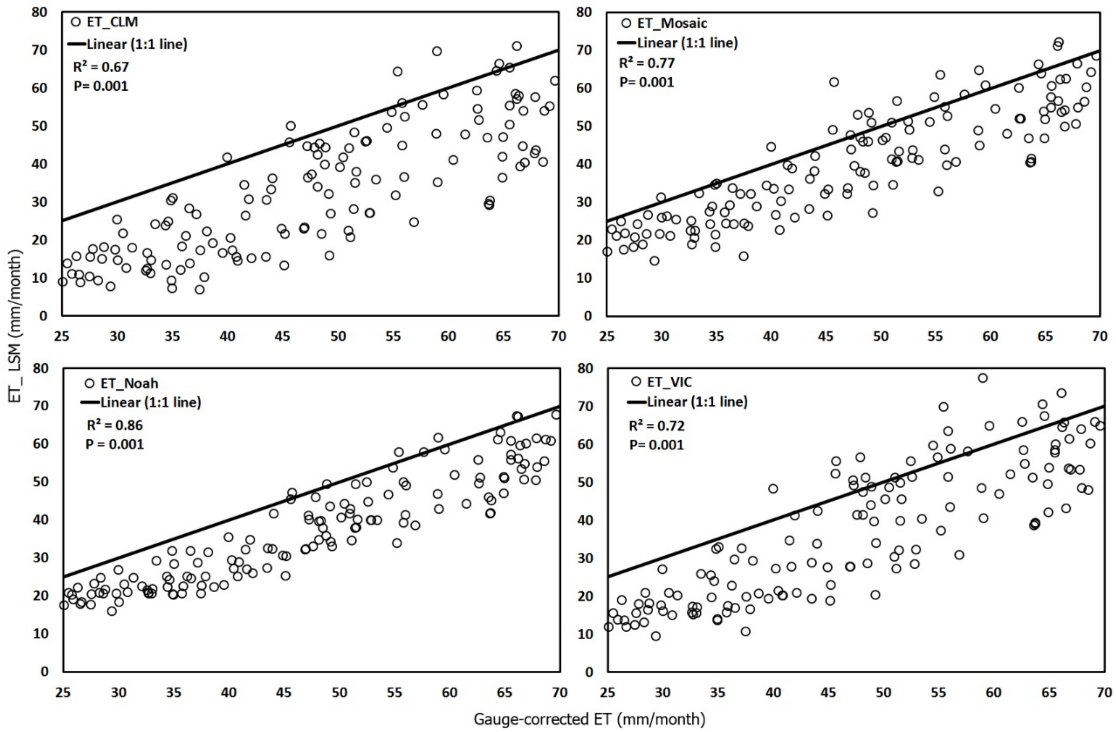

Figure 5.6 Correlations of gauged corrected ET dataset and ET estimates from GLDAS land surface model data.

Global Climate Historical Network-Monthly (GCHN-M) data

The GCHN-M database is an integrated summary of the temperature records from land surface stations across the globe. The temperature data from GCHN-M are compared with the reanalysis in figure 5.7. The CRU data is highly correlated ($R^2 = 0.84$), the NCEP data have ($R^2 = 0.77$), while among the GLDAS models again, CLM and Mosaic show the highest correlation (R^2 of about 0.70). Noah and VIC data show less agreement with GCHN-M data as shown by their correlation (R^2 below 0.61).

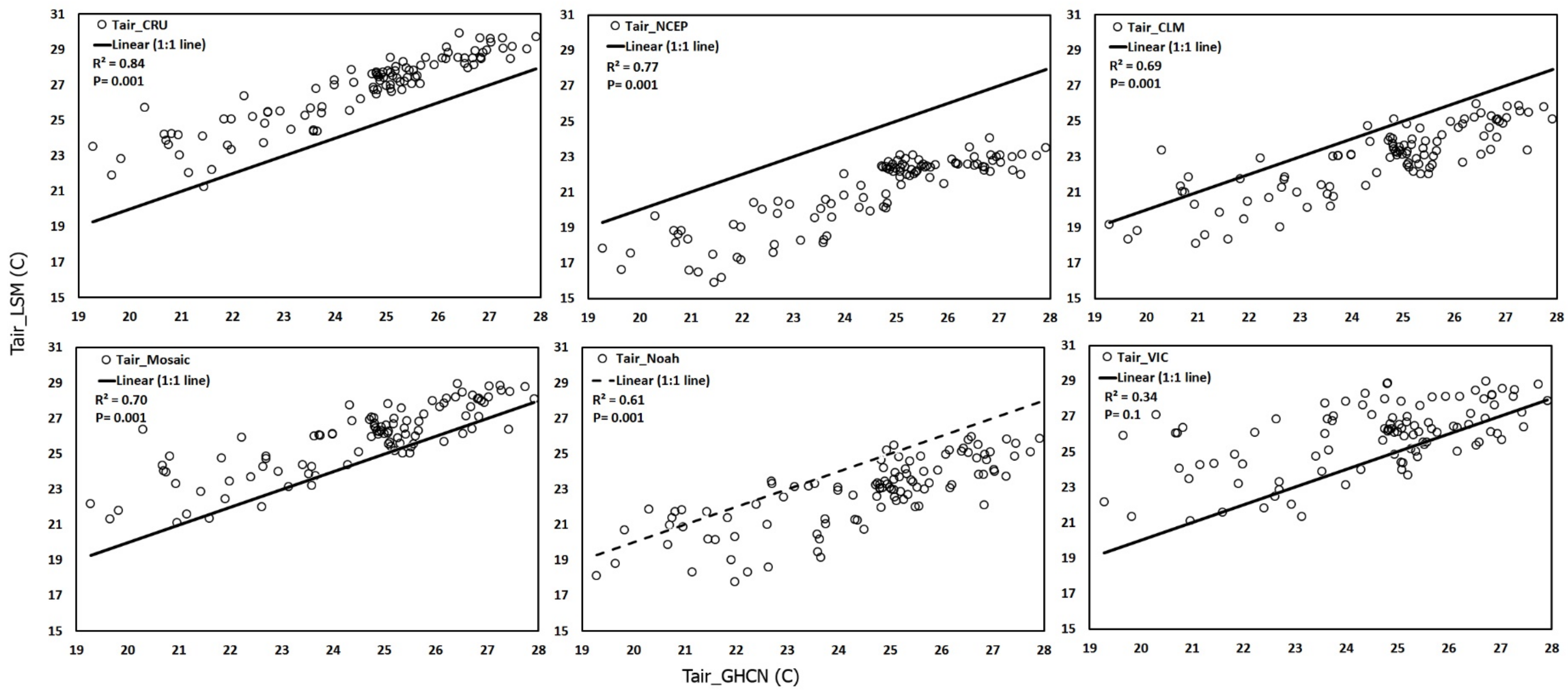

Figure 5.7 Correlations of GHCN-Tair dataset and other Tair from RSRA data.

5.3 Procedure and methodology

Data preparation

The GRACE spherical harmonics data obtained from the CSR are scaled and factorized according to the methodology of (Landerer and Swenson, 2012). The data are destriped and smoothed using Gaussian filter of 300m to remove noisy short-wavelength spectral coefficients according to (Swenson and Wahr, 2006; Wahr et al., 2006). MODIS products are utilized to derive monthly grids of LST, VI, and LAI (as indictors for vegetation land-covers). The selected timeframe of the RSRA data covers the GRACE period of record (2002-2015). Zonal statistics were performed at the basin scale to summarize the relative monthly estimates of the hydrologic variables from the RSRA data in terms of the minimum, maximum, range, mean, standard deviation, and sum.

Eight variable pools have been created following the water balance basis to study the hydrologic utility of RSRA data (Table 5.1), and are designed upon their data sources (figure 5.8). A model is derived from each pool to reconstruct the GRACE TWS anomalies and identify the most explanatory variables.

The first model builds upon the remote sensing data: the PRE information from TRMM data is combined with MODIS LST, VI, and LAI. This model includes one of the best precipitation product (Figure 4), energy, and landcover (LC) information to model the TWS. Reanalysis data from CRU, NCEP, and GLDAS datasets are grouped to form subsets 2 to 7. They have their own biases and uncertainties as shown in previous sections. The CRU data (subset 2) contains information about PRE, PET, Tair, and PDSI. This subset tests the combination of water-energy fluxes and drought information to model the TWS. The NCEP data (subset 3) include information about PRE, AET, PET, and Tair.

The model build on this subset uses water-energy parameters as predictors for the TWS. The four LSMs from GLDAS data (subset 4 to 7) involve most of the water balance components such as PRE, ET, and SR. These variables are combined with the Tair to build four different models to simulate the TWS. As shown earlier, the CLM pool (subset 4) overestimates runoff and underestimates precipitation, ET, and Tair. The Mosaic pool (subset 5) underestimates precipitation while the Noah pool (subset 6) underestimates precipitation, ET, and Tair. The VIC pool (subset 7) presents a conditional bias on precipitation, overestimates runoff, and underestimate ET, and presents a poor correlation with GHCN Tair. These disagreements with observations may limit the ability of models derived from these data pools to reproduce the TWS anomalies. Finally, a compiled pool (subset 8) gathers the water-energy fluxes and LC information with gauge corrected PRE and ET, and SR from Noah plus the LHF estimates. This model will test the potential of using the water/energy balance parameters with LC to model the TWS.

Table 5.1 Statistical summary and correlations between TWS_{GRACE} and hydrological variables from multi-sensory and reanalysis data.

Model	Paras	AIC	LRT	Pr(Chi)
(1) TWS_{RS} ~ (NDVI) + (EVI) + (LST) + (LAI) + (TRMM)	(NDVI)	1106.6	64.08	4.023e-13 ***
	(EVI)	1081.1	38.58	8.498e-08 ***
	(LST)	1056.2	13.73	0.008213 **
	(LAI)	1053.2	10.69	0.030230 *
	(TRMM)	1056.4	13.91	0.007593 **
(2) TWS_{CRU} ~ (PRE) + (PET) + (Tair) + (DI)	(PRE)	794.36	50.12	3.409e-10 ***
	(PET)	873.46	129.22	< 2.2e-16 ***
	(Tair)	787.84	43.59	7.787e-09 ***
	(DI)	837.69	93.45	< 2.2e-16 ***
(3) TWS_{NCEP} ~ (PRE) + (AET) + (PET) + (Tair)	(AET)	912.63	52.12	1.302e-10 ***
	(PET)	896.77	36.26	2.554e-07 ***
	(Tair)	895.18	34.67	5.430e-07 ***
(4) TWS_{CLM} ~ (ET) + (PRE) + (SR) + (Tair)	(ET)	1437.8	64.67	3.021e-13 ***
	(PRE)	1396.2	23.08	0.0001219 ***
	(SR)	1384.7	11.58	0.0208042 *
	(Tair)	1413.6	40.41	3.553e-08 ***
(5) TWS_{Mosaic} ~ (ET) + (PRE) + (SR) + (Tair)	(ET)	1487.1	122.47	< 2.2e-16 ***
	(PRE)	1385.5	20.85	0.0003387 ***
	(SR)	1423.0	58.35	6.452e-12 ***
(6) TWS_{Noah} ~ (ET) + (PRE) + (SR) + (Tair)	(ET)	1486.5	142.60	< 2.2e-16 ***
	(PRE)	1371.5	27.53	1.556e-05 ***
	(SR)	1370.9	26.99	2.000e-05 ***
	(Tair)	1370.6	26.69	2.297e-05 ***
(7) TWS_{VIC} ~ (ET) + (PRE) + (SR) + (Tair)	(PRE)	1353.0	11.51	0.02137 *
	(SR)	1399.3	57.78	8.490e-12 ***
	(Tair)	1409.3	67.77	6.707e-14 ***
(8) TWS_{EB} ~ (ET) + (PRE) + (SR) + (LC) + (LHF)	(ET)	1271.5	25.53	< 1.2e-16 ***
	(PRE)	1270.9	23.99	<1.556e-05 ***
	(SR)	1270.6	24.69	2.197e-05 ***
	(LC)	1357.7	22.19	0.0001841 ***
	(LHF)	1454.9	119.31	< 2.2e-16 ***

Significant codes: 0 ‘***’, 0.001 ‘**’ ,0.01 ‘*’ ,0.05 ‘.’, 0.1 ‘ ’ 1.

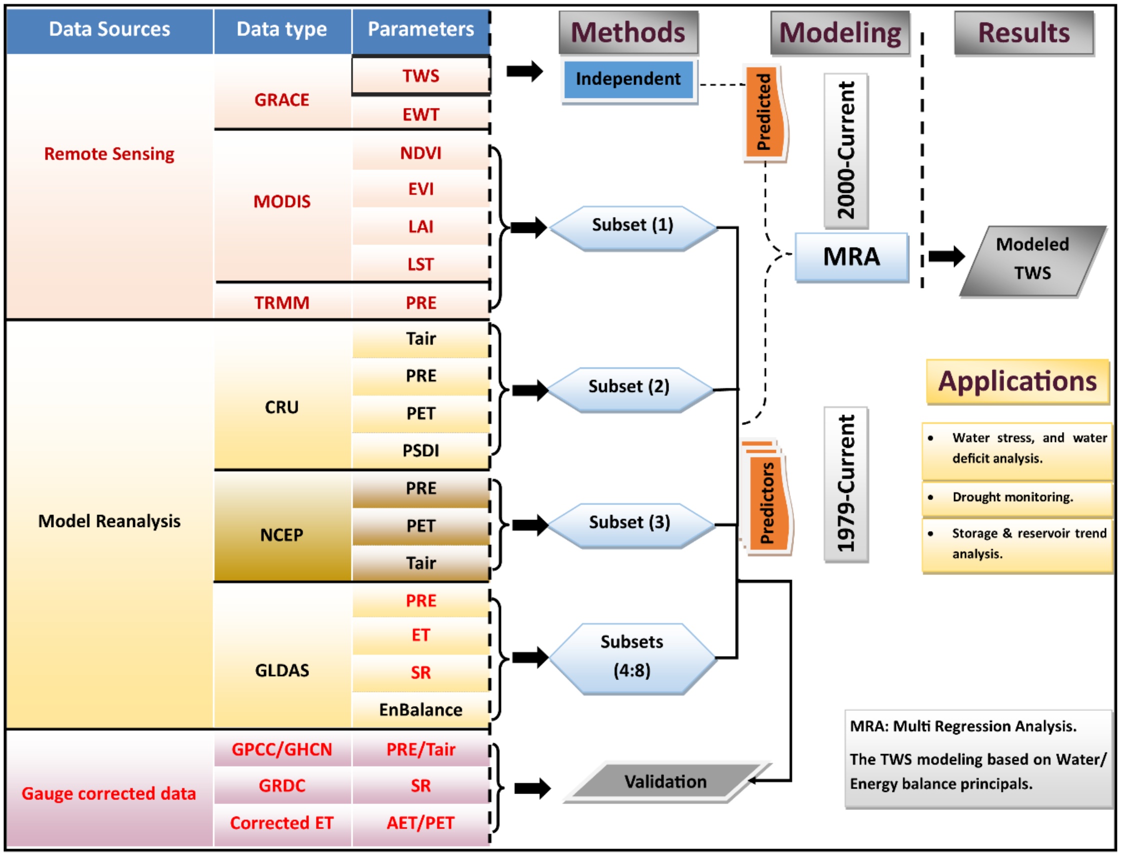

Figure 5.8 Data sources and schematic workflow to derive the Total Water Storage (TWS). Each subset is correspondent to one of the inputted models.

TWS statistical modeling

RSRA datasets have uncertainties and potentially limited information content to retrieve the GRACE TWS anomalies. Therefore, TWS anomalies conditional distributions are fitted using multiple regressive explanatory predictors. The probabilistic conditional distribution fitting was performed using the Generalized Additive Models for Location, Scale, and Shape approach (GAMLSS) (Rigby and Stasinopoulos, 2005), which allows a flexible fitting with multiple parameters. The GAMLSS model can cope with nonlinear relationships between the predicted and predictor variables, and considers the nonlinearity in the location and the heteroskedasticity in the scale as functions of the explanatory variable. The following assumptions are made: (1) TWS is a random variable following a known distribution with density $f\,(TWS|\mu,\sigma)$ conditional on the parameters (μ,σ); and (2) the observed TWS values are mutually independent given the parameter vector (μ,σ). GAMLSS is best fitted using the (Stasinopoulos and Rigby, 2007) package in R Development (R Core Team, 2012).

To simplify and distinguish between systematic trends and (random) uncertainties, conditional densities with the first two moments as parameters are considered: the location μ (mean) describing systematic trends and the scale σ (standard deviation) representing uncertainties. A number of conditional two-parameter models were tested and the goodness of fit was checked with the Akaike Information Criterion (AIC) for each of the semi-parametric density fits. The normal distribution was found to be the most appropriate according to Equation 5.2:

$$f(TWS|\mu,\sigma) = \frac{1}{\sqrt{2\pi}\sigma}\, e^{-\frac{(TWS-\mu)^2}{2\sigma^2}} \qquad (5.2).$$

Note that for a given conditional distribution of the response variable, the conditional quantiles can be expressed as a function of the location and scale. After selecting the distribution family, an iterative procedure trying several combinations of explanatory variables is followed to refine the structure of the model. Each distribution parameter is modeled as a function of the explanatory variables using link functions (Akantziliotou et al., 2002; Stasinopoulos and Rigby, 2007). The model selection is carried out by checking the significance of the fitting improvement in terms of information criteria such as the Akaike Information Criterion (AIC), the Schwarz Bayesian Criterion (SBC), and the generalized AIC. Forward, backward, and step-wise procedures were applied to select the meaningful explanatory variables showing strong predictive association with the TWS anomaly, supervised by diagnostic plots to check the fitting performance (Stasinopoulos and Rigby 2007). Penalized splines are used to fit the trends for each parameter for their flexibility to model complex nonlinear relationships.

Since all of the incorporated parameters should be highly independent from each other, some of the input variables can be dropped if they show similar significance and are highly correlated with other input variables. The statistical analysis retained from the hydrological variables is showed in Table 5.1.

5.4 Result and discussion

NRB hydrological variability

RSRA data record the monthly mean variations of different hydrologic variables on the NRB from 2002-2015. Figure 9 shows twelve years of TWS cycles from four GRACE averaged anomalies solutions. At the basin scale, the four GRACE data products show very similar pattern. We selected the CRS for the analysis in the remaining of the study. The illustration shows considerable year-to-year variability with significant anomaly peaks. For instances, the TWS peaks around August at about +80 mm, while a minimum around -60 mm is usually reached in January. Generally, the average peak occurs in August, peaks for individual year occur between May and October, while the minimums occur between November and April.

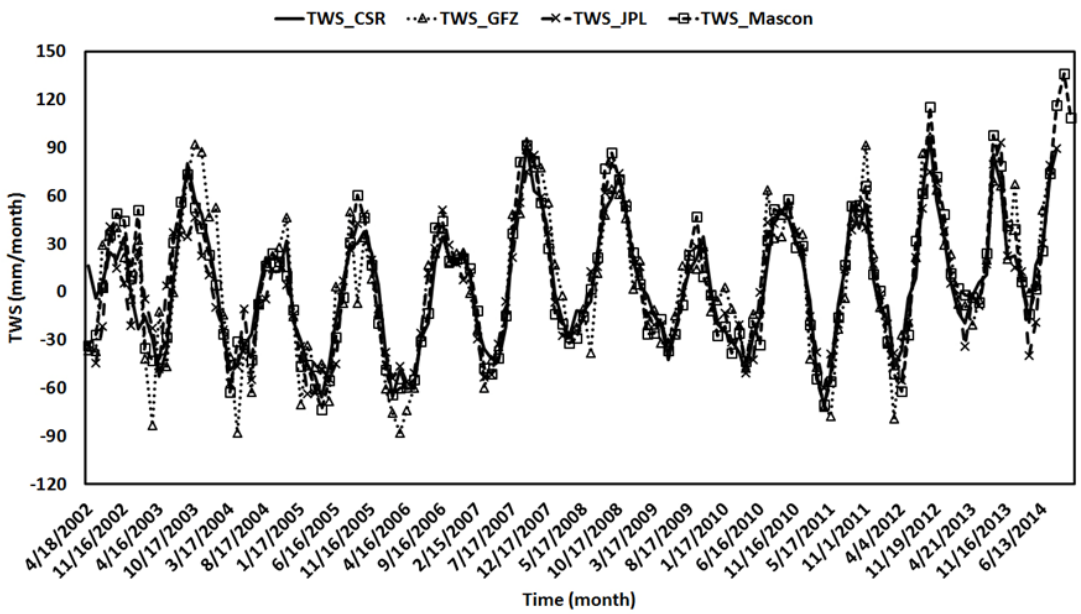

Figure 5.9 Time series of the normalized monthly regional average TWS from different four GRACE products covering the period from 2002-2015.

The monthly mean estimates of hydrologic variables on the NRB from the RSRA are indicated in figure 5.10. The rainy season starts in May and ends after October, and the maximum precipitation peak is usually during August (figure 5.10A). Regarding the temperature data (figure 5.10B), the minimum LST and air temperature display the same annual variations and trends with different magnitudes; the air temperature has a maximum monthly average of 29°C during May, and a minimum of 18°C during January. The LST anomalies are used to determine the variations in the Nile water volume and to understand the interaction between the climate and surface water in the region. The monthly mean ET indicates that the maximum ET is about 70 mm during August, and the minimum-recorded ET is about 10 mm in January (figure 5.10C). As shown in Figure 4, the various surface runoff products show considerable variability. The surface runoff is closely linked to the occurrence of precipitation events; the maximum surface runoff is usually reached during August and declines substantially in January (figure 5.10D). Generally, the data indicate an alternance of wet and dry phases during the year. The temporal and the seasonal variation of the vegetation is linked to the rainy season. In terms of spatial distribution the green biomass is concentrated on the southern and eastern parts of the NRB where there are sufficient rainfalls. The vegetation in the northern part of the basin is located around the main flood plain of the Nile River and along the Delta.

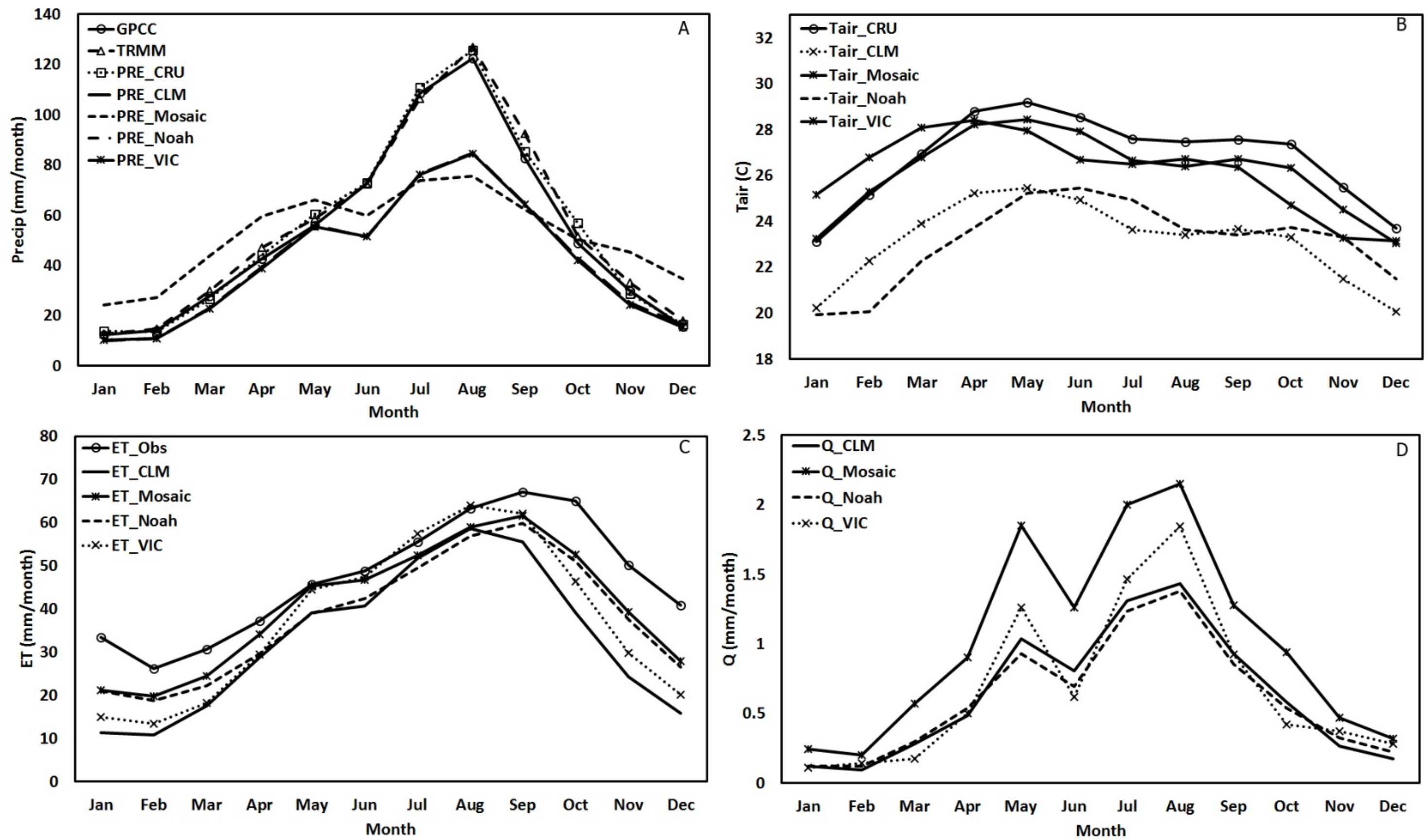

Figure 5.10 Time series of monthly basin-average variations of (a) precipitation, (b) land surface temperature, (c) evapotranspiration, and (d) surface runoff.

Statistical model output

The TWS analysis with the multivariate GAMLSS statistical approach reveals that some explanatory climatic variables have stronger predictive association with the TWS anomaly than others. Table 5.1 summarizes the relationship between the TWS and the explanatory variables according to the chi-square test. Deterministic prediction of the TWS anomaly was performed using the modeled locations, μ, which allows a comparison with the TWS that is observed by GRACE. Since the models are conditionally unbiased by design, the correlation is a more appropriate criterion than the bias to assess the models agreement with the observed TWS. Through the correlation results, we can infer the hydrologic performance of the input datasets. The predictions of deterministic TWS anomalies display good consistency with the GRACE estimates correlation, R^2, ranging from 0.79 to 0.96 (see figure 5.11). Table 5.2 summaries the statistical results of the modeled TWS anomalies using the MRA and the conventional water balance approach with repsect to the GRACE TWS. The MRA bias and Root Mean Square Error (RMSE) are generally lower in magnitude than the conventional approach and the correlation is systematically higher.

The model (1) using remote sensing TRMM and MODIS data (LST, VI, and LAI) shows the second best performance in terms of correlation ($R^2 = 0.93$). The higher RMSE (0.32) relative to the conventional approach (0.19) is linked to the underestimation (bias –3.83 mm while -2.33 mm with the conventional approach). The good correlation is attributed to the higher accuracy of the monthly TRMM precipitation research product. Additionally, the LST, VI, and LAI indices from MODIS provide information content to monitor the climatic influences on water and vegetation cover. Note that the vegetation indices (NDVI and EVI) are highly significant explanatory variables to model the TWS. The LST is a key parameter to understand the land surface processes, heat budget and energy balance, and the terrestrial vegetation that is a very sensitive indicator to climatic and anthropogenic influences. Model (2) from the CRU data and model (3) using the NCEP datasets show more pronounced underestimation (-6.51 mm and -6.32 mm respectively) with very good correlation (R^2 is 0.86 and 0.88 respectively). The PRE, ET, and PSDI have high significance to model the TWS anomaly. The CRU and NCEP data are derived from gauge corrected datasets. The GLDAS-based LSM models (4 to 7) show more moderate performances with correlation R^2 ranging from 0.79 to 0.86, but lower RMSE ranging from 0.4 mm to 0.15 mm/month associated with lower magnitude in the bias. Among these models, the Noah LSM displays the highest correlation and the lowest absolute bias (-0.43 mm/month). This result is consistent with the performances of the Noah runoff and ET relative to the other GLDAS models (see figures 5.5 and 5.6).

Table 5.2 Statistical summary of the modeled TWS anomalies using multi-sensory and reanalysis data.

Model	**Mean (mm/month)**	**Bias (mm/month)**	**RMSE (mm/month)**	**R^2**
1. TWS_{RS}	0.03	-3.83	0.32	0.93
2. TWS_{CRU}	-2.65	-6.51	0.54	0.86
3. TWS_{NCEP}	-2.46	-6.32	0.53	0.88
4. TWS_{CLM}	5.08	1.22	0.10	0.79
5. TWS_{Moasic}	5.12	1.25	0.10	0.82
6. TWS_{Noah}	3.43	-0.43	0.04	0.86
7. TWS_{VIC}	5.70	1.84	0.15	0.83
8. TWS_{EB}	4.76	0.90	0.07	0.96
$TWS_{P\text{-}ET\text{-}R}$	0.18	-2.33	0.19	0.56

It is important to point out that using gauged corrected datasets contributes to the improvement of the modeling of TWS, by providing higher information content. For instance, the gauge corrected data for precipitation (TRMM/GPCC) and ET, and SR from Noah model along with the energy balance components have a higher hydrologic performance as forcing variables to predict the TWS. Model (8) combines parameters from the water/and energy balance such as PRE, ET, SR, VI, LHF to simulate the TWS estimates. This model incorporates gauged corrected variables, especially precipitation and evapotranspiration, with surface runoff components from the Noah model. The correlation statistics (figure 5.11) indicate that it provides the best modeled TWS with a high coefficient of determination (R^2 = 0.96) associated with a very good RMSE (0.07 mm/month) and smallest bias (0.9 mm).

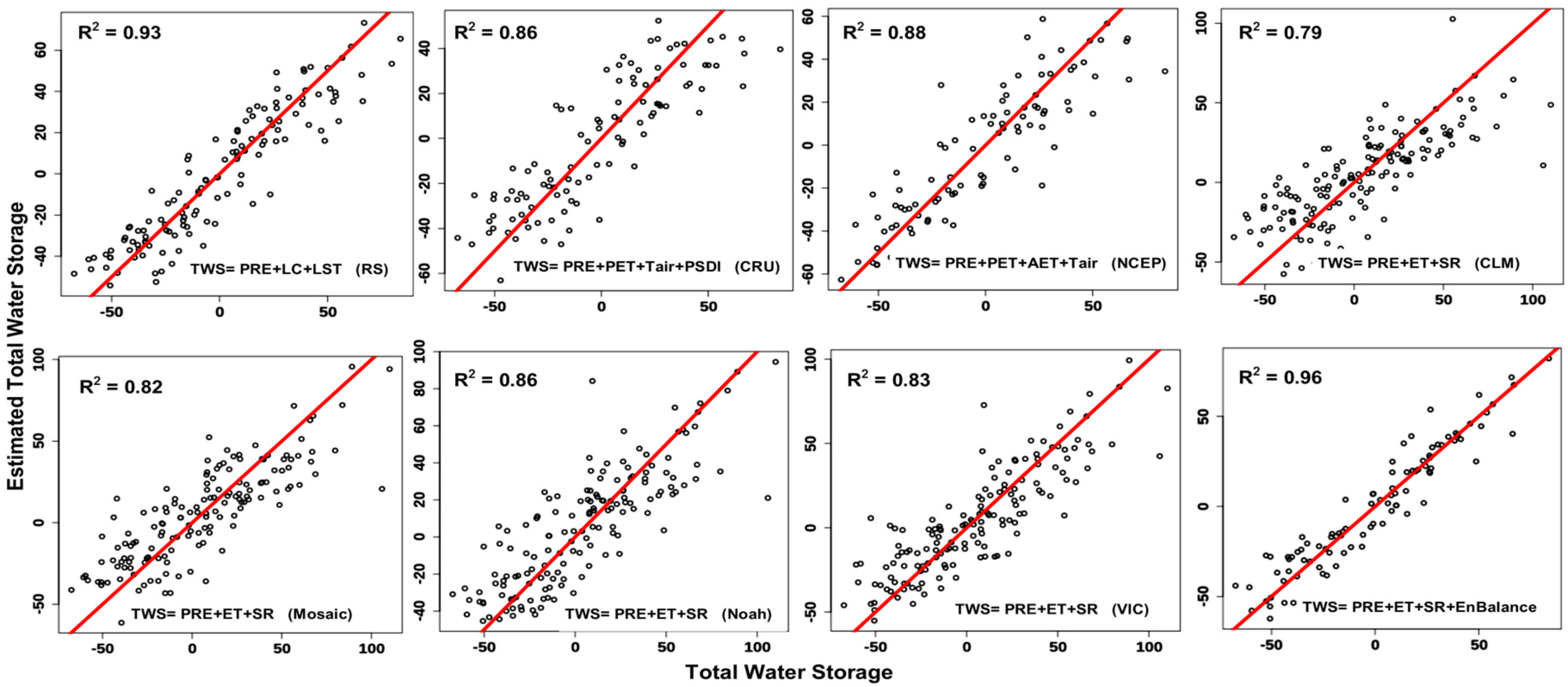

Figure 5.11 Correlation of the modeled TWS and the TWS from GRACE based anomalies.

Finally, figure 5.12 shows the full time series for the observed GRACE TWS and the modeled TWS using the MRA approach. The time series display high consistency between the resulted TWS and the data from the GRACE satellites. The selection of the input parameters that are linked to the water/energy balance components, or that have direct influence to one or more of their parameters, enhance the TWS models. The current results explained and validated the hydrologic variables of RSRA to estimate the TWS. The predicted TWS from the RSRA data give the promise to conduct a follow up research to build historical estimates of TWS across the transboundary river basins, even prior to the launch of the GRACE mission.

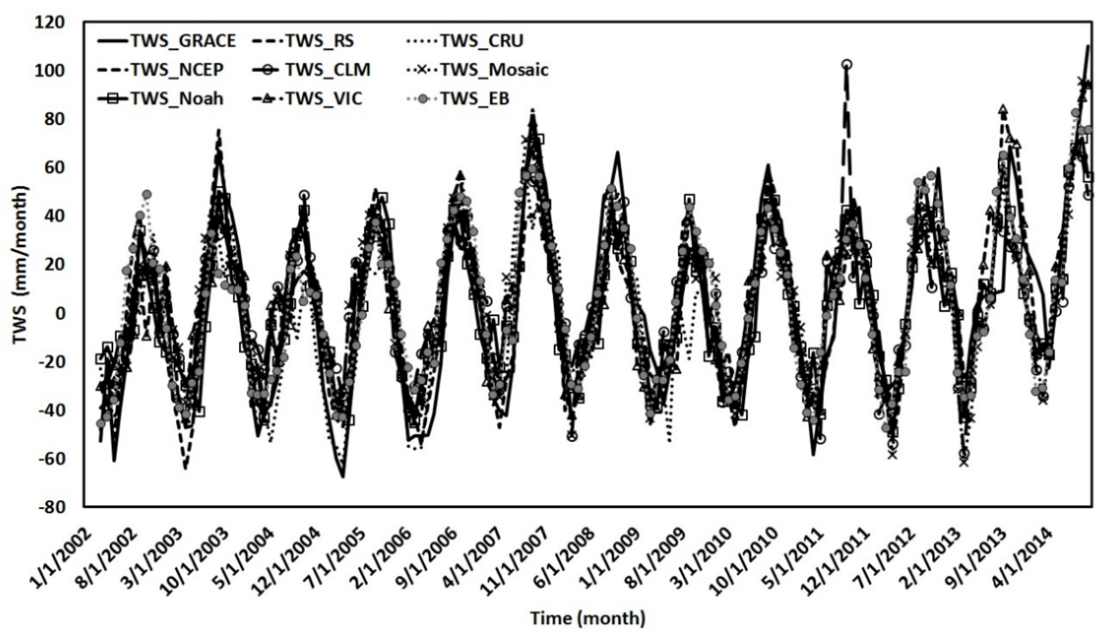

Figure 5.12 Time series of the modeled monthly basin-average TWS and observation of TWS from GRACE satellite.

5.5 Hydroclimate risk assessment

To understand how El-Nino Southern Oscillation (ENSO) could affect the TWS records. Based on the aforementioned methodology the TWS was simulated based on the training period from 2002-2015. This approach first aims to reconstruct the historical records of TWS from 1950-2009 (figure 5.13).

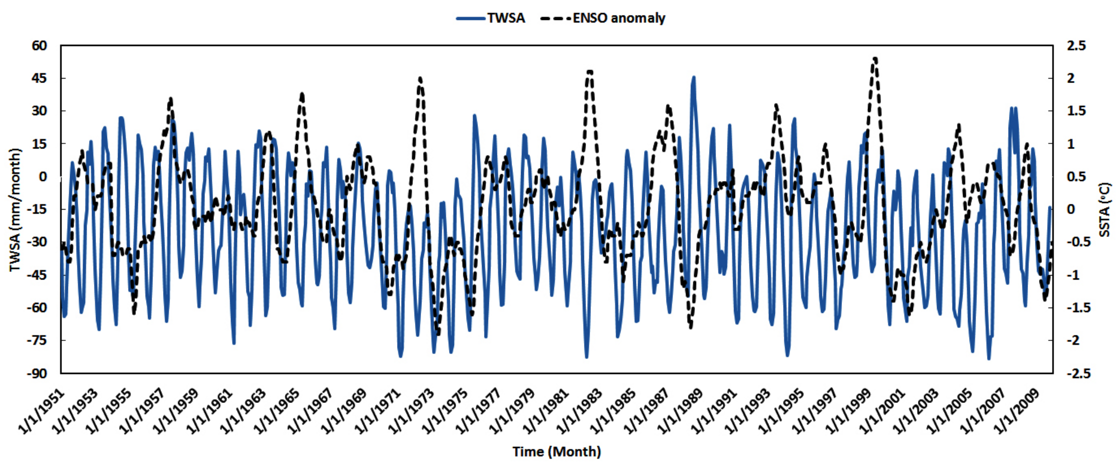

Figure 5.13 The temporal variation of the TWS (blue line) and the ENSO variation (dotted line) over Nile River Basin.

The correlation between TWS and the ENSO records indicated that, the positive ENSO, which corresponding to El Nino event is associated with dramatic decline in the TWS. Meanwhile, the negative ENSO anomaly, that corresponding to the La Nina event is mainly associated with a positive recovery to the TWS (figure 5.14). Meanwhile, during the dry periods the El Niño impedes rain to reach the Ethiopian hills, resulting in a decreased amount of rainfall (Eltahir, 1996). On contrary, the and the La Niña event demonstrated dramatic rainfall that causes the Nile flood (NIS, 2012a; UNEP, 2013). According to the current results, the Nile Basin have been affected by drier condition over the period from 1950-2009. The annual changing in precipitation and sea surface temperature pattern significantly affects the Nile water.

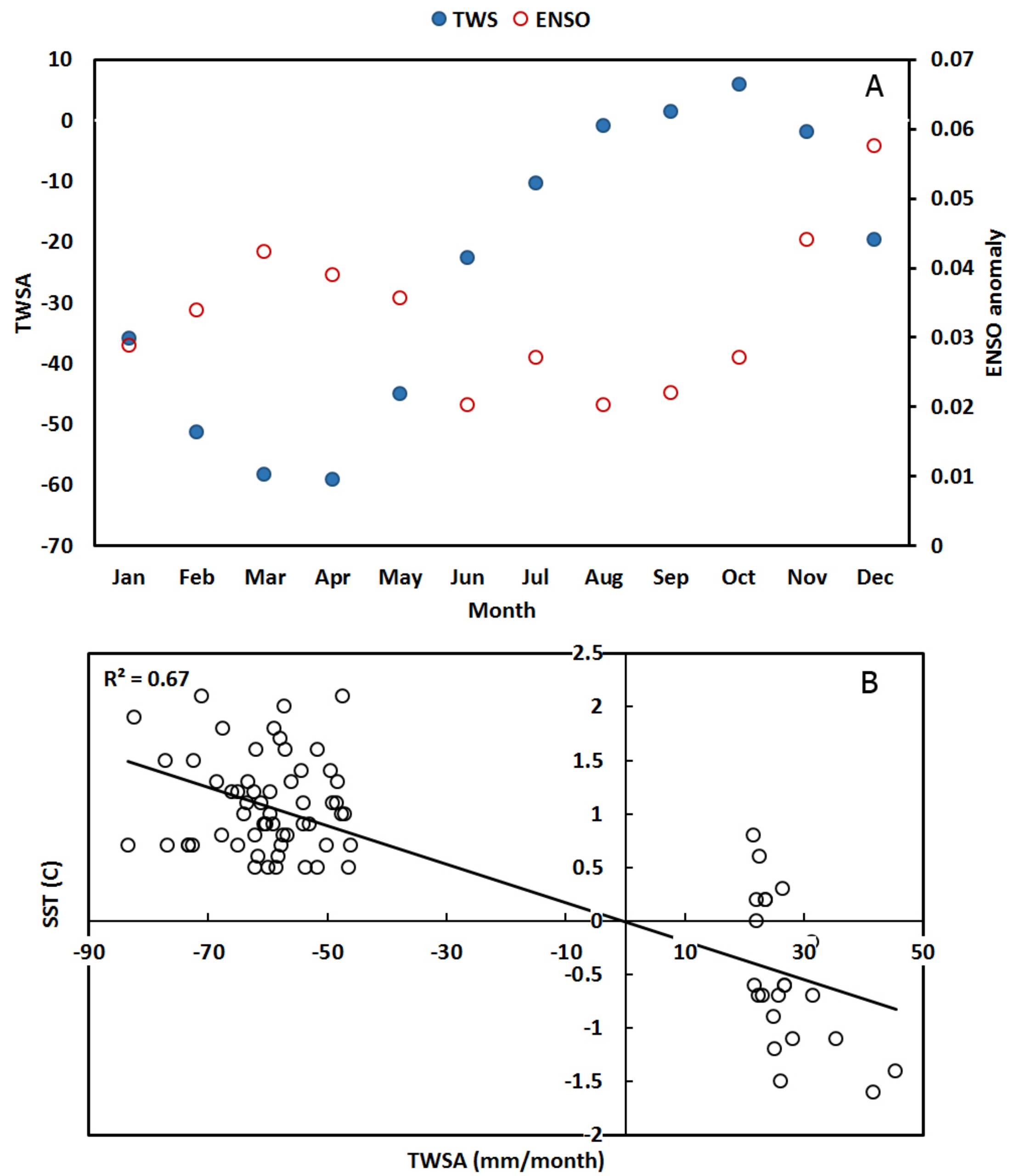

Figure 5.14 The relation between TWS variation and ENSO anomaly, (A) shows their monthly variations, (B) shows the correlation between TWS and ENSO signals.

5.6 Summary, Conclusion and Future Work

The NRB is one of the largest river basins in the world that suffers insufficient *in-situ* data for climatic information. The human and climate variables are considered as key changes for the environmental instabilities in the region. Across the NRB, the seasonal cycles show that the maximum precipitation occurs during Summer and the minimum in Fall. The TWS variation is consistent with the precipitation and runoff anomalies during the wet and dry periods. During the wet season, the green biomass is relatively abundant, with higher VI values.

With sparse climate monitoring stations in the region, RSA data are invaluable for water resources trend detection and climate impacts in the NRB region. These datasets are, however, inheriting numerous errors and carry uncertainties that require further quantification and validation. The current research shows new insights to validate the hydrologic utilities of RSRA data in absence or insufficient inputs of ground observations. The MRA framework was used to model the TWS anomalies from the GRACE mission from 2002 to 2015 and to test the hydrologic information of the RSRA.

The results indicate that:

1- The MRA approach outperforms the traditional LSMs based water balance approach to estimate the TWS anomalies.

2- combinations of water/energy balance components with land surface temperature and vegetation information simulate better results of the TWS anomalies.

3- TRMM and MODIS (land-cover, land surface temperatures, and Vegetation indices) are the next most important parameters to simulate the TWS anomalies.

4- The hydrologic information from the reanalysis data such as CRU, NCEP, and the GLDAS are valuable sources to model the GRACE TWS anomalies.

This work provides a new method to use the RSRA information for reliable hydrologic applications that help the society at large in the NRB. This approach is transferable to similar basins. In addition, the datasets and the methodology can be adapted to extend the TWS estimation to the past 30+ years and provide new records for TWS prior to the launch of the GRACE satellites. Ultimately, it will contribute in studying the drought frequencies and water deficit periods, as well as understanding the state of water in transboundary basins under the changing climate.

Acknowledgement

The first author thanks the Egyptian Mission sector in the Ministry of Higher Education and Scientific Research for providing the research fund to conduct this study in the form of a PhD scholarship to the first author. Thanks goes to the Advanced Radar Research Center (ARRC), and the Hydrometrology and Remote Sensing Laboratory (HyDROS) lab at University of Oklahoma, USA for providing the research facilities, workspace and the equipment to accomplish this research.

Thanks goes to the data centers that made RSRA datasets available and downloadable: the Goddard Earth Science Data and Information Service Centers (GES DISCs), the Climatic Research Unit at the University of East Anglia, the National Oceanic and Atmospheric Administration, Global Precipitation Climatological Center, and the Global Runoff Data Centre.

We would like to thank Stasinopoulos, Rigby, Akantziliotou, and Ruckdeschel for making the GAMLSS (Stasinopoulos and Rigby, 2007) freely available in R (R Core Team, 2012).

5.6 References

Agrawala, S., Moehner, A., El Raey, M., Conway, D., Van Aalst, M., Hagenstad, M. and Smith, J., 2004. Development And Climate Change In Egypt: Focus On Coastal Resources And The Nile.

Ahmed, M., Sultan, M., Wahr, J. and Yan, E., 2014. The use of GRACE data to monitor natural and anthropogenic induced variations in water availability across Africa. Earth-Science Reviews, 136: 289-300.

Ahmed, M., Sultan, M., Wahr, J., Yan, E., Milewski, A., Sauck, W., Becker, R. and Welton, B., 2011. Integration of GRACE (Gravity Recovery and Climate Experiment) data with traditional data sets for a better understanding of the time-dependent water partitioning in African watersheds. Geology, 39(5): 479-482.

Akantziliotou, C., Rigby, R. and Stasinopoulos, D., 2002. The R implementation of generalized additive models for location, scale and shape, Statistical modelling in Society: Proceedings of the 17th International Workshop on statistical modelling. Statistical Modelling Society, pp. 75-83.

Akbari, A., Ramli, N.I.B. and Kong, N.S., 2015. Application of Public Domain Satellite-Based DEMs in Natural Hazard Modeling. International Journal of Environmental Science and Development, 7(2).

AL-Harbi S. D., K.T., 2007. The accuracy of a DEM derived from ASTER data using differential GPS measurements, ISPRS Hannover Workshop 2007. ISPRS.

Alemu, H., Senay, G.B., Kaptue, A.T. and Kovalskyy, V., 2014. Evapotranspiration Variability and Its Association with Vegetation Dynamics in the Nile Basin, 2002–2011. Remote Sensing, 6: 5885-5908.

Allen, R.G., Pereira, L.S., Raes, D. and Smith, M., 1998. Crop evapotranspiration - Guidelines for computing crop water requirements. FAO - Food and Agriculture Organization of the United Nations, Rome.

Arora, V.K., 2002. The use of the aridity index to assess climate change effect on annual runoff. Journal of Hydrology 265 164–177.

ASTER-GDEM, 2011. ASTER Global Digital Elevation Model Version 2 – Summary of Validation Results. NASA LPDAAC & JPL, pp. 1-27.

Band, L.E., 1986. Topographic partition of watersheds with digital elevation models. Water Resources Research, 22(1): 15-24.

Barrett, S., 1994. Conflict and Cooperation in Managing International Water Resources, CSERGE Working Paper WM 94-04. Centre for Social and Economic Research on the Global Environment University College London and University of East Anglia.

Bastiaanssen, W., Karimi, P., Rebelo, L.-M., Duan, Z., Senay, G., Muttuwatte, L. and Smakhtin, V., 2014. Earth Observation Based Assessment of the Water Production and Water Consumption of Nile Basin Agro-Ecosystems. Remote Sensing, 6(11): 10306-10334.

Becker, M., Llovel, W., Cazenave, A., Güntner, A. and Crétaux, J.-F., 2010. Recent hydrological behavior of the East African great lakes region inferred from

GRACE, satellite altimetry and rainfall observations. Comptes Rendus Geoscience, 342(3): 223-233.

Becker, R.H. and Sultan, M., 2009. Land subsidence in the Nile Delta: inferences from radar interferometry. The Holocene 19: 949–954.

Beyene, T., Lettenmaier, D.P. and Kabat, P., 2009. Hydrologic impacts of climate change on the Nile River Basin: implications of the 2007 IPCC scenarios. Climatic Change, 100(3-4): 433-461.

Blankespoor, B., Dasgupta, S. and Laplante, B., 2012. Sea-Level Rise and Coastal Wetlands Impacts and Costs. Policy Research Working Paper 6277.

Bohannon, J., 2010. Climate change. The Nile Delta's sinking future. Science, 327(5972): 1444-7.

Brown, S., Abiy S. Kebede, a. and Nicholls, R.J., 2011. Sea-Level Rise and Impacts in Africa, 2000 to 2100, University of Southampton, UK.

Budyko, M.I., 1974. Climate and life. Academic Press, Orlando, FL.

Burrough, P., McDonnell, R. and Burrough, P., 1998. Principles of geographical information systems. Oxford University Press, Oxford.

Camberlin, P., 2009. Nile Basin Climates. In: H.J. Dumont (Editor), The Nile : Origin, Environments, Limnology and Human Use. Springer, Monographiae Biologicae, pp. 307-333.

Cao, Y., Nan, Z. and Cheng, G., 2015. GRACE Gravity Satellite Observations of Terrestrial Water Storage Changes for Drought Characterization in the Arid Land of Northwestern China. Remote Sensing, 7(1): 1021-1047.

CAPMAS, 2014. Central Agency for Public Mobilization and Statistics.

Chambers, D.P., 2007. Converting Release-04 Gravity Coefficients into Maps of Equivalent Water Thickness.

Chirico, P.G., 2004. An Evaluation of SRTM, ASTER, and Contour-Based DEMS in the Caribbean region, URISA Caribbean GIS Conference.

Collins, R., 2002. The Nile. Yale University Press/ New Haven and London.

Conway, D., 2005. From headwater tributaries to international river: Observing and adapting to climate variability and change in the Nile basin. Global Environmental Change, 15(2): 99-114.

Creed, I.F., Spargo, A.T., Jones, J.A., Buttle, J.M., Adams, M.B., Beall, F.D., Booth, E.G., Campbell, J.L., Clow, D., Elder, K., Green, M.B., Grimm, N.B., Miniat, C., Ramlal, P., Saha, A., Sebestyen, S., Spittlehouse, D., Sterling, S., Williams, M.W., Winkler, R. and Yao, H., 2014. Changing forest water yields in response to climate warming: results from long-term experimental watershed sites across North America. Glob Chang Biol, 20(10): 3191-208.

CRU, 2015. Climate Research Unite Data.

Dasgupta, S., Laplante, B., Meinsner, C. and Wheeler, D.a.Y., J., 2007. The Impact of Sea Level Rise on Developing Countries: A Comparative Analysis. Climate Change, 93(3-4): 379-388.

Dasgupta, S., Laplante, B., Murray, S. and Wheeler, D., 2009. Sea-Level Rise and Storm Surges A Comparative Analysis of Impacts in Developing Countries. Policy Research Working Paper 4901.

DFO, 2012. Dartmouth Flood Observatory

Di Baldassarre, G., Elshamy, M., van Griensven, A., Soliman, E., Kigobe, M., Ndomba, P., Mutemi, J., Mutua, F., Moges, S., Xuan, Y., Solomatine, D. and Uhlenbrook, S., 2011. Future hydrology and climate in the River Nile basin: a review. Hydrological Sciences Journal, 56(2): 199-211.

Ehlschlaeger, C.R., 1998. The Stochastic Simulation Approach: Tools for Representing Spatial Application Uncertainty, University of California, Santa Barbara.

El Raey, M., 1997. Vulnerability assessment of the coastal zone of the Nile delta of Egypt, to the impacts of sea level rise. Ocean & Coastal Manaoemen, 37(1): 29-40.

El Raey, M., 1999. Egypt: Coastal zone development and climate change: Impact of climate change on Egypt.

El Raey, M., 2010. Impacts and Implications of Climate Change for the Coastal Zones of Egypt. In: David Michel and Amit Pandya (Editors). The Henry L. Stimson Center, Washington, DC, pp. 31-50.

El-Fadel, M., El-Sayegh, Y., El-Fadl, K. and Khorbotly, D., 2003. The Nile River Basin: A Case Study in Surface Water Conflict Resolution. Journal of Natural Resourorces Life Science Education 32: 107-117.

El-Quosy, D.E., 2009. Fresh Water In: M.K. Tolba and N.W. Saab (Editors), In Impact of Climate Change on Arab Countries Arab Forum for Environment and Development, Beirut.

Eltahir, E.A.B., 1996. El Niño and the Natural Variability in the Flow of the Nile River. Water Resources Research, 32(1): 131-137.

ENVI, 2008. User's Guide. ENVI on-line software user's manual, ITT Visual Information Solutions.

Erian, W., Katlan, B., Ouldbedy, B., Awad, H., Zaghtity, E. and Ibrahim, S., 2012. Agriculture Drought in Africa Mediterranean and Middle East, Geneva, Switzerland.

Erlich, H., 2000. The Nile: Histories, Cultures, Myths. Lynne Rienner, Boulder, Colorado.

Fekete, B., Vörösmarty, C. and Grabs, W., 2002. Global composite runoff fields on observed river discharge and simulated water balances Water System Analysis Group,University of New Hampshire, and Global Runoff Data Centre. , Koblenz, Germany: Federal Institute of Hydrology (BfG), 2002.

FitzGerald, D.M., Fenster, M.S., Argow, B.A. and Buynevich, I.V., 2008. Coastal Impacts Due to Sea-Level Rise. Annual Review of Earth and Planetary Sciences, 36(1): 601-647.

Flickr, 2008. Nilometer.

Flickr, 2009. Nilometer on Elephantine.

Geocontext, 2010. Nile Delta shoreline profile.

Gerald, F. and Ben, M., 2012. Comparison of SRTM and ASTER Derived Digital Elevation Models over Two Regions in Ghana – Implications for Hydrological and Environmental Modeling. Studies on Environmental and Applied Geomorphology.

Gleick, P.H., 1991. The vulnerability of runoff in the Nile basin to climatic changes. The Environmental Professional, 13: 66-73.

Gornitz, V., 1991. Global coastal hazards from future sea level rise. Glob. Planet. Change, 89: 379-98.

GRDC, 2015. Long-Term Mean Monthly Discharges and Annual Characteristics of GRDC Stations. GRDC center.

Grijsen, J.G., Tarhule, A., Brown, C., Ghile, Y.B., Taner, Talbi- Jordan, A., N, H., Guero, A., Y, R., Kone, S., Coulibaly, B. and Harshadeep, N., 2013. Climate Risk Assessment for Water Resources Development in the Niger River Basin Part II: Runoff Elasticity and Probabilistic Analysis.

GSFC, 2011. Tropical Rainfall Measuring Mission Office. Goddard Space Flight Center.

Guth, P.L., 2010. Geomorphometric Comparison Of ASTER GDEM And SRTM, ASPRS/CaGIS. ASPRS, Orlando, Florida.

Hargreaves, G. and Samani, Z., 1985. Reference crop evapotranspiration from temperature. Appl Engine Agric, 1(2): 96–99.

Hargreaves, G. and Samni, Z., 1982 Estimation of potential evapotranspiration. Journal of Irrigation and Drainage Division, Proceedings of the American Society of Civil

Engineers 108: 223-230.

Hasan, E., Khan, S.I. and Hong, Y., 2015a. Investigation of potential sea level rise impact on the Nile Delta, Egypt using digital elevation models. Environ Monit Assess, 187(10): 649.

Hasan, E., Kirstetter, P., Ke, Z. and Hong, Y., 2015b. The Challenges and Opportunities of Hydrologic Remote Sensing in Data-Poor Regions: Case Study of Nile River Basin, 2015 AGU Fall Meeting. AGU.

Hassenforder, E. and Noury, B., 2015. Managing Transboundary River Basins: Chaper 7. River Basin Management in the Twenty-first Century. Taylor & Francis Group, LLC.

Hereher, M.E., 2010. Vulnerability of the Nile Delta to sea level rise: an assessment using remote sensing. Geomatics, Natural Hazards and Risk, 1(4): 315-321.

Houborg, R., Rodell, M., Li, B., Reichle, R. and Zaitchik, B.F., 2012. Drought indicators based on model-assimilated Gravity Recovery and Climate Experiment (GRACE) terrestrial water storage observations. Water Resources Research, 48(7): n/a-n/a.

Hugh Turral, Jacob Burke and Faurès, J.-M., 2011. Climate change, water and food security, Itlay.

IPCC, 2014. Climate Change 2014: Synthesis Report. Contribution of Working Groups I, II and III to the Fifth Assessment Report of the Intergovernmental Panel on Climate Change, IPCC, Geneva, Switzerland.

IPCC, 2001. The Scientific basis. Contribution of Working Group I to the Third Assessment Report of the Intergovernmental Panel on Climate Change, Cambridge University Press, Cambridge, United Kingdom and New York, NY, USA. 881pp.

Jelínek, R.b., Eckert, S., Zeug, G. and Krausmann, E., 2009. Tsunami Vulnerability and Risk Analysis Applied to the City of Alexandria, Egypt, Institute for the Protection and Security of the Citizen. Italy.

Jensen, J.R., 2007. Remote Sensing of the Environment: An Earth Resource Perspective (2nd Edition). Prentice Hall; 2 edition (2007).

Jenson, S.K., 1991. Applications of hydrologic information automatically extracted from digital elevation models. Hydrological processes, 5(1): 31-44.

JPL, 2014. SRTM, U.S. Releases Enhanced Shuttle Land Elevation Data.

Karyabwite, D.R., 2000 Water Sharing in the Nile River Valley, UNEP/DEWA/GRID, Geneva.

Kebede, S., Travi, Y., Alemayehu, T. and Marc, V., 2006. Water balance of Lake Tana and its sensitivity to fluctuations in rainfall, Blue Nile basin, Ethiopia. Journal of Hydrology, 316(1-4): 233-247.

Kieyah, J., 2007. The 1929 Nile Waters Agreement: Legal and economic analysis. Available at: http://works.bepress.com/joseph_kieyah/1.

Landerer, F.W. and Swenson, S.C., 2012. Accuracy of scaled GRACE terrestrial water storage estimates. Water Resources Research, 48(4): n/a-n/a.

Leon, J.X., Heuvelink, G.B.M. and Phinn, S.R., 2014. Incorporating DEM Uncertainty in Coastal Inundation Mapping. PLoS ONE 9 (9:e108727).

Long, D., Scanlon, B.R., Longuevergne, L., Sun, A.Y., Fernando, D.N. and Save, H., 2013. GRACE satellite monitoring of large depletion in water storage in response to the 2011 drought in Texas. Geophysical Research Letters, 40(13): 3395-3401.

Long, D., Shen, Y., Sun, A., Hong, Y., Longuevergne, L., Yang, Y., Li, B. and Chen, L., 2014. Drought and flood monitoring for a large karst plateau in Southwest China using extended GRACE data. Remote Sensing of Environment, 155: 145-160.

Lott, F.C., P. A. Stott, D. M. Mitchell, N. Christidis, N. P. Gillett, L. Haimberger, J. Perlwitz and Thorne, P.W., 2013. Models versus radiosondes in the free atmosphere: A new detection and attribution analysis of temperature. Journal of Geophysical Research, 118: 2609-2619.

Lynas, M., 2008. Six Degrees: Our Future on a Hotter Planet. National Geographic.

Maidment, D.R., 2002. Arc Hydro: GIS for Water Resources. Environmental Systems Research Institute, Inc., Redlands, California.

Martz, L.W. and Garbrecht, J., 1992. Numerical definition of drainage network and subcatchment areas from digital elevation models. Computers & Geosciences, 18(6): 747-761.

Melesse, A.M., 2011. Nile River Basin: Hydrology, Climate and Water Use. Springer, Springer Dordrecht Heidelberg London New York.

Melesse, A.M., Abtew, W. and Setegn, S.G., 2014. Nile River Basin: Ecohydrological Challenges, Climate Change and Hydropolitics. Springer, Springer International Publishing Switzerland.

Meshref, W.M., 1990. Tectonic Framework. In: Said R (ed.) The Geology of Egypt, Rotterdam, Netherlands: 381-389.

Moges, S.A. and Gebremichael, M., 2014. Climate Change Impacts and Development-Based Adaptation Pathway to the Nile River Basin. In: A.M.M.e. al. (Editor), Nile River Basin. Springer International Publishing Switzerland.

Moore, I.D., Grayson, R. and Ladson, A., 1991. Digital terrain modelling: a review of hydrological, geomorphological, and biological applications. Hydrological processes, 5(1): 3-30.

NBI, 2010. Key facts about the Nile basin. Nile Basin Initiative (NBI), Entebbe. http://www.nilebasin.org/newsite/index. Accessed 19th December 2012.

NBI, 2012. State of River Nile Basin 2012. Nile Basin Initiative (NBI), Entebbe.

NBI, 2016. The Nile Basin Water Resources Atlas. NBI: Nile Basin Initiative

Niang, I., Ruppel, O.C., Abdrabo, M.A., Essel, A., Lennard, C., J. Padgham and Urquhart, P., 2014. Africa. In: Climate Change 2014: Impacts, Adaptation, and Vulnerability. Part B: Regional Aspects. Contribution of Working Group II to the Fifth Assessment Report of the Intergovernmental Panel on Climate Change. In: V.R. Barros, C.B. Field, D.J. Dokken, M.D. Mastrandrea, K.J. Mach, T.E. Bilir, M. Chatterjee, K.L. Ebi, Y.O. Estrada, R.C. Genova, B. Girma, E.S. Kissel, A.N. Levy, S. MacCracken, P.R. Mastrandrea and L.L. White (Editors). Cambridge University Press, Cambridge, United Kingdom and New York, NY, USA, pp. 1199-1265.

Nikolakopoulos, K.G., Kamaratakis, E.K. and Chrysoulakis, N., 2006. SRTM vs ASTER elevation products. Comparison for two regions in Crete, Greece. International Journal of Remote Sensing, 27(21): 4819-4838.

NIS, 2012a. Climate Change and its Implications for the Nile Region:Chapter 8.

NIS, 2012b. Nile Basin Evapotranspiration.

Nuth, C. and Kaab, A., 2011. Co-registration and bias corrections of satellite elevation data sets for quantifying glacier thickness change. The Cryosphere, 5: 271-290.

Oestigaard, T., 2009. Water, Culture and Identity: Comparing Past and Present Traditions in the Nile Basin Region. Nile Basin Research Programme. BRIC Press, Norway.

Oestigaard, T., 2010. Nile Issues, Small Streams from the Nile Basin Research Programme. Fountain Publishers, Kampala-Uganda.

Oksanen, J., 2006. Digital elevation model error in terrain analysis, University of Helsinki, Finlad, 369 pp.

Oksanen, J. and Sarjakoski, T., 2005. Error propagation of DEM-based surface derivatives. Computers & Geosciences, 31(8): 1015-1027.

Ollinger, S.V., 2010. Tansley review. Sources of variability in canopy reflectance and the convergent properties of plants. New Phytologist

Pike, J.G., 1964. The estimation of annual runoff from meteorological data in a tropical climate. Journal of Hydrology, Amsterdam, 2: 116–123.

Poulter, B. and Halpin, P.N., 2008. Raster modelling of coastal flooding from sea-level rise. International Journal of Geographical Information Science, 22(2): 167-182.

R Core Team, 2012. R: A Language and Environment for Statistical Computing, R Found. for Stat. Comput., Vienna, Austria. ISBN 3-900051- 07-0. [Available at http://www.r-project.org/.].

Radwan, A.A. and El-Geziry, T.M., 2013. Some Statistical Characteristics of Surges at Alexandria, Egypt. JKAU: Mar. Sci, 24(2): 31-38.

Reanalysis Wiki, 2015. Model Reanalysis Data.

Reuter, H.I., Hengl, T., Gessler, P. and Soille, P., 2009. Preparation of DEMs for Geomorphometric Analysis. In: Tomislav H, Hannes IR, editors. Geomorphometry: Concepts, Software, Applications: Elsevier: 87-120.

Rigby, R.A. and Stasinopoulos, D.M., 2005. Generalized additive models for location, scale and shape. Journal of the Royal Statistical Society, 54: 507-554.

Rosetta, 2010. Egypt's Nile Delta falls prey to climate change. Al Arabiya News.

Rui, H., 2011. Global Land Data Assimilation System Version 1 (GLDAS-1) Products: README Document.

Said, R., 1981. The geological evolution of the River Nile. Springerverleg.

Salama, R.B., 1987 The evolution of the River Nile. The buried saline rift lakes in Sudan. Journal African Earth Sciences 6(6): 899-913.

Salama, R.B., 1997. Rift basins of Sudan. African basins, Sedimentary basins of the World. 3. Elsevier, Amsterdam.

Schneider, U., Becker, A., Meyer-Christoffer, A., Ziese, M. and Rudolf, B., 2011. Global Precipitation Analysis Products of the GPCC, Deutscher Wetterdienst, Offenbach a. M., Germany.

SEDAC, 2013. Gridded Population of the World (GPW), V3. http://sedac.ciesin.columbia.edu/data/set/nagdc-population-landscape-climate-estimates-v3 .

Sefercik, U., Jacobsen, K., Oruc, M., Marangoz, A., 2007. Comparison of Spot, SRTM and ASTER DEMS, ISPRS Hannover Workshop 2007. ISPRS

Shahin, M., 2003. Hydrology and Water Resources of Africa. Kluwer Academic Publishers, New York, Boston, Dordrecht, London, Moscow.

Simonett, O., 2012. Potential impact of sea level rise: Nile Delta, UNEP/GRID; G. Sestini, Florence; Remote Sensing Center, Cairo; DIERCKE Weltwirtschaftsatlas.

Snoussi, M., Ouchani, T. and Niazi, S., 2008. Vulnerability assessment of the impact of sea-level rise and flooding on the Moroccan coast: The case of the Mediterranean eastern zone. Estuarine, Coastal and Shelf Science, 77(2): 206-213.

SRTM-DEM, 2006. Shuttle Radar Topography Mission DTED Level 1 (3-arc second) documentation. NASA/LPDAAC and USGS/EROS, pp. 1-8.

Stanley, D.J., 1996. Nile Delta: extreme case of sediment entrapment. Journal of Marine Geology, 129: 189-195.

Stanley, J.D., 2005. Submergence and burial of ancient coastal sites on the subsiding Nile delta margin, Egypt. Méditerranée, 104: 64-73.

Stasinopoulos, D.M. and Rigby, R.A., 2007. Generalized additive models for location scale and shape (GAMLSS) in R. Journal of Statistical Software, 10: 1-46.

Suwandana, E., Kawamura, K., Sakuno, Y., Kustiyanto, E. and Raharjo, B., 2012. Evaluation of ASTER GDEM2 in Comparison with GDEM1, SRTM DEM and Topographic-Map-Derived DEM Using Inundation Area Analysis and RTK-dGPS Data. Remote Sensing, 4(12): 2419-2431.

Swenson, S. and Wahr, J., 2006. Post-processing removal of correlated errors in GRACE data. Geophysical Research Letters, 33(8).

Syed, T.H., Famiglietti, J.S., Rodell, M., Chen, J. and Wilson, C.R., 2008. Analysis of terrestrial water storage changes from GRACE and GLDAS. Water Resources Research, 44(2): n/a-n/a.

UNEP, 2000. Water Sharing in the Nile River Valley, DEWA/GRID -Geneva.

UNEP, 2013. Adaptation to Climate-change Induced Water Stress in the Nile Basin A Vulnerability Assessment Report.

UNISDR, 2011. Global Assessment Report on Disaster Risk Reduction, Geneva, Switzerland: United Nations International Strategy for Disaster Reduction.

van der Velde, Y., Vercauteren, N., Jaramillo, F., Dekker, S.C., Destouni, G. and Lyon, S.W., 2014. Exploring hydroclimatic change disparity via the Budyko framework. Hydrological Processes, 28(13): 4110-4118.

Vijverberg, J., Sibbing, F.A. and Dejen, E., 2009. Lake Tana: Source of the Blue Nile. Nile: Origin, Environments, Limnology and Human Use. Springer Science + Business Media B.V. 2009.

Wahr, J., 2004. Time-variable gravity from GRACE: First results. Geophysical Research Letters, 31(11).

Wahr, J., Swenson, S. and Velicogna, I., 2006. Accuracy of GRACE mass estimates. Geophysical Research Letters, 33(6).

Watkins, M.M., Wiese, D.N., Yuan, D.-N., Boening, C. and Landerer, F.W., 2015. Improved methods for observing Earth's time variable mass distribution with GRACE using spherical cap mascons. Journal of Geophysical Research: Solid Earth, 120(4): 2648-2671.

Wise, S., 2000. Assessing the quality for hydrological applications of digital elevation models derived from contours. Hydrological processes, 14(11-12): 1909-1929.

Wu, S., Li, J. and Huang, G., 2008. A study on DEM-derived primary topographic attributes for hydrologic applications: Sensitivity to elevation data resolution. Applied Geography, 28(3): 210-223.

Xuejun, L. and Lu, B., 2008. Accuracy Assessment of DEM Slope Algorithms Related to Spatial Autocorrelation of DEM Errors. In: Q. Zhou, B. Lees and G.-a. Tang (Editors), Advances in Digital Terrain Analysis. Lecture Notes in Geoinformation and Cartography. Springer-Verlag Berlin Heidelberg, pp. 307-322.

Yalciner, A.C., Zaytsev, A., Aytore, B., Heidarzadeh, M., Kian, R. and Imamura, F., 2014. A Possible Submarine Landslide and Associated Tsunami at the Northwest Nile Delta, Mediterranean Sea. Oceanography, 27(2): 68-75.

Zandbergen, P.A., 2011. Error Propagation Modeling for Terrain Analysis using Dynamic Simulation Tools in ArcGIS Modelbuilder. Geomorphometry.org.

Zaroug, M.A.H., Eltahir, E.A.B. and Giorgi, F., 2014. Droughts and floods over the upper catchment of the Blue Nile and their connections to the timing of El Niño and La Niña events. Hydrology and Earth System Sciences, 18(3): 1239-1249.

Zhang, K., Kimball, J.S., Nemani, R.R. and Running, S.W., 2010. A continuous satellite-derived global record of land surface evapotranspiration from 1983 to 2006. Water Resources Research, 46(9): n/a-n/a.

Chapter 6: Summary and Conclusion

The Nile River Basin is one of major transboundary river basin that hosts variety of cultures, terrains and climates. The basin consists of two major hydrological systems that provide the Nile with its essential water supply, the White and Blue River Basin. The Blue Nile Basin furnish the Nile with more than 76 percent of the water supply and the sediments. Yet the impact of the climate changes on the Nile Basin is less understood due to the lake of the systematic hydrological observation data. The Nile Basin is challenged by complex hydrologic system and uneven climate conditions. The fluctuation of the Intertropical Climate Zone (ITCZ) causes either ample of precipitation and severe flooding or imped the rainfalls and prevailing of the drought conditions. The basin population growing dramatically and causes substantial pressure on the water resource, land and the agriculture productivity. The infirm relations between the riparian nations, especially the upstream and the downstream nations, hinder the developing of mutual adaptive policies to mitigate the climate issues and better use the basin water resources.

To date, the gap to implement operational ground station to collect hydrological observation is huge. However, the wealth of the hydrological observation from satellite, reanalysis and land surface model could fill such gap. The gridded observations are the main reliable source for the hydrological observation that could help to understand how the temporal and spatial variability of the basin climate could influence the basin water resources. The Gravity Recovery and Experiment Satellite (GRACE) offer unprecedented information about the overall storage changes. The gauge-corrected grids of the precipitation and evaporation are the main source to understand the water and energy fluxes. Precipitation minus evapotranspiration reveals an acceptable estimates of the surface water runoff.

The temporal variability in precipitation and temperature could influence the amount of the surface runoff. To best express how the basin water flow is resilient to the climate changes, the functional forms introduced by Arora (2002) and Pike (1964) were implemented to measure the surface runoff elasticity to precipitation, temperature and potential evapotranspiration over the tropical-subtropical climate zones. Meanwhile, relationship between actual evapotranspiration and potential evapotranspiration that normalized by the precipitation as depicted through Budyko Curve illustration. The Budyko curve utilized to understand the surface runoff elasticity to precipitation for the tropical-subtropical, semiarid and arid zone. The tropical-subtropical zone showed overall energy-limited conditions, where the water-yield is potentially at high rates. The semiarid zone however it receives significant amount of water, the high rates of evapotranspiration causes substantial loss of water to the atmosphere and make the zone as moisture-water-constrained zone. The arid zone displayed very limited water-yield condition with very high temperature and evapotranspiration rates. In terms of the resilient, the tropical-subtropical zones are considered more resilient under the current climate conditions compared with the semiarid and arid zones that displayed less responsivity to the climate conditions. For example, the runoff elasticity to precipitation for the tropical-subtropical zone showed at 10 percent increase in precipitation the runoff expected to increase by 20 percent. As gradually moved to the arid zone the runoff only will recove by 3 percent when the precipitation increased by 10 percent. The surface runoff is higly determined by temperature, so far as the temperature decreases, i.e. by (-

0.5°C), the tropical-subtropical zone will undergo to an increase in the surface runoff by 5 percent. Accordingly, the runoff elasticity to potential ET ranging from (-0.52 to -1.70) from the tropical-subtropical to the arid zone.

Meanwhile, according to the projected climate scenarios under the RCP2.6, the tropical-subtropical region displays high runoff flow resistant to the climate under the projection increase in precipitation. Conversely, under the worst scenario of RCP 5.8 showed that the subtropical and tropical region will become highly vulnerable to the precipitation deficit, where at decrease of precipitation by 15 percent, the surface runoff will diminish by 30 percent. The basin riparians are encouraging to mutually develop an adaptive policy to face the possible future changes.

Sea Level Rise (SLR) is another climate challenge to the downstream country, i.e. Egypt. The SLR on the Nile Delta region in Egypt is assessed by evaluating the elevations of two available Digital Elevation Models (DEMs): the SRTM and the ASTER-GDEM-V2. The Nile Delta is one of the world's largest river deltas, located in North Egypt. The Nile Delta is an area of the world that lacks the detailed ground truth data and monitoring stations. Despite the economic importance of the Nile Delta, it could be considered as one of the most data-poor regions regarding to the available information. It is believed that the Nile Delta is projected to face SLR of 1m by the end of the 21th century. In order to provide an accurate assessment of the future SLR impact on Nile Deltas' land and population, the DEM's elevations were corrected using linear regression model with ground elevations from GPS survey. The information for the land cover types and future population numbers were derived from the Moderate Resolution Imaging Spectroradiometer (MODIS) land cover and the Gridded Population of the Worlds

(GPWv3) datasets respectively. The future inundations were illustrated based on two SLR scenarios of 0.5m and 1m. For instances, at 0.5m SLR, an estimated 580 thousand people will face the dangers of inundation and be displaced, and about 280 km^2 of the total LULC will be destroyed. At 1m SLR, an estimated 887 thousand people will be at risk of inundation and displacement and about 100 km^2 of vegetation, 16 km^2 wetland, 402 km^2 cropland, and 47 km^2 of urban area land would be destroyed. The overall vulnerability assessments indicated that the influence of SLR would be intensified and confined along the coastal areas. The estimates of the land area and risked population are considered very valuable and essential for future risk mitigation and preparedness for the communities along the Nile delta coastal areas.

The hydrologic utility of Remote Sensing and Reanalysis (RSRA) datasets has proved to be problematic in data-poor regions due to the lack of ground truth observations. An alternative approach was developed to circumvent this problem by using Multi-Regression Analysis (MRA) to: 1- Estimate the uncertainties of the RSRA with the NASA's Gravity Recovery and Climate Experiment (GRACE) data sets. 2- Reconstruct the Terrestrial Water Storage (TWS) anomalies from GRACE data and extend the estimates to the past +30-years for the water-climate nexus study. While the TWS has been simulated for long time using Land Surface Models (LSMs) data, the proposed methodology enhances the TWS reconstruction though increasing the R2 from 0.47 of the conventional water balance approach to above 80 percent. The MRA framework was used to model the TWS anomalies from the GRACE mission from 2002 to 2015 and to test the hydrologic information of the RSRA.

The results indicate that:

1- The MRA approach outperforms the traditional LSMs based water balance approach to estimate the TWS anomalies.

2- Combination of water/energy balance components with land surface temperature and vegetation information simulate better results of the TWS anomalies.

3- TRMM and MODIS (land-cover, land surface temperatures, and Vegetation indices) are the next most important parameters to simulate the TWS anomalies.

4- The hydrologic information from the reanalysis data such as CRU, NCEP, and the GLDAS are valuable sources to model the GRACE TWS anomalies.

This work provides a new method to use the RSRA information for reliable hydrologic applications that help the society at large in the NRB. This approach is transferable to similar basins. In addition, the datasets and the methodology can be adapted to extend the TWS estimation to the past 30+ years and provide new records for TWS prior to the launch of the GRACE satellites. Ultimately, it will contribute in studying the drought frequencies and water deficit periods, as well as understanding the state of water in transboundary basins under the changing climate.